BESSY

Magnetism · Semiconductors · Superconductivity

Fundamental Physics · Material Sciences

Micro Engineering · Archeometry · Biology

Highlights 2002

Highlights2002

Highlights2002

Berliner Elektronenspeicherring-Gesellschaft für Synchrotronstrahlung m.b.H.

Contents

Published by:
Berliner Elektronenspeicherring-Gesellschaft
für Synchrotronstrahlung m.b.H. – BESSY

Albert-Einstein-Straße 15
12489 Berlin, Germany
phone +49 (0)30 / 6392 2999
fax +49 (0)30 / 6392 2990
www.bessy.de
info@bessy.de

Editors:
Gabriele André, Dr. Markus Sauerborn,
BESSY GmbH

Layout:
Stitz & Betz Kooperations GmbH, Berlin

Printing:
Druckhaus Berlin-Mitte GmbH

ISSN 1611-6127

Berliner Elektronenspeicherring-Gesellschaft für Synchrotronstrahlung m.b.H.

Member of the Leibniz-Association

1 Introduction

Dear users and friends,

the new version of our annual report, the BESSY Highlights, including a CD covering all the activities and publications for the year is now published for the second year. We were overwhelmed by the positive feedback on our first Highlights edition which ran out of print only after 6 months, and we feel encouraged to keep on informing you in this new style.

Last year witnessed a novelty for synchrotron radiation (SR) sources around the world – the generation of stable, broadband THz-radiation and its application in a unique experiment at BESSY. This achievement is a result of three years development on accelerator operation and beamline construction thus expanding the use of SR beyond the far-infrared into the THz gap. (page 49)

Together with eight other large scale research projects, the BESSY soft X-ray FEL has been evaluated by the German Science Council (Wissenschaftsrat). Our scientific case has been awarded a rating of 'excellent' and at the forefront of international research. We are encouraged to complete the technical design as planned by the end of 2003. (page 44)

The traditional users meeting in the beginning of December with some 250 participants, 100 posters and a large industrial exhibition was preceeded by an FEL-workshop focusing on experiments and beamline development. During the user meeting Fabrice Wilhelm (FU Berlin) and Tobias Lau (Universität Hamburg) were awarded the 'Ernst-Eckhard-Koch' Prize and Ralf Röhlsberger (Universität Rostock) received the BESSY Innovation Prize for his 'Nuclear Lighthouse Effect'.

In 2002, user services were improved substantially. Starting in August, BESSY now offers 24 hours user support for the more than 40 beamlines in operation. We are progressing in improving on laboratory facilities. To keep pace with the growing user community, a new guest house is now under construction and will be ready for occupancy by end of the year. User access to the experimental hall has been significantly simplified with the construction of cages around the first mirror boxes to the beamlines: The radiation safety authorities approved an almost complete elimination of the control area in the experimental hall. (page 61)

With the operational beamlines of the Protein Structure Factory, biology is becoming a more important research field at BESSY, offering already six experimental stations with several more to come. Two additional members from this community have been appointed to the beamtime committee to account for the raising numbers of biological proposals.

BESSY again has been a magnet for many visitors throughout the year with prominent guests such as the King and Queen of Jordan and the President of Malaysia. Events from 'breakfast lectures' to art exhibitions have caught visitor interest. At 'Berlins Long Night of Science' (Lange Nacht der Wissenschaft) about 6,000 people took the opportunity to obtain an inside view of the goings on here. BESSY was for a second time in sequence the institution with the largest number of visitors. (page 34)

The successful operation and further development of BESSY would not be possible without the excellent work of our users and the enthusiasm and competence of our staff. We would like to thank all people involved for their dedication and our funding agencies for their support.

Enjoy reading the Highlights

The BESSY Board of directors
Berlin, February 2003

Prof. Dr. Dr. h.c. Wolfgang Eberhardt

Prof. Dr. Eberhard Jaeschke

Thomas Frederking

2 Scientific Highlights

New concept to study magnetic behavior of early 3d elements

A. Scherz[1], H. Wende[1], C. Sorg[1], K. Baberschke[1], J. Minar[2], D. Benea[2], H. Ebert[2]

1
Freie Universität Berlin
2
Ludwig-Maximillians-Universität München

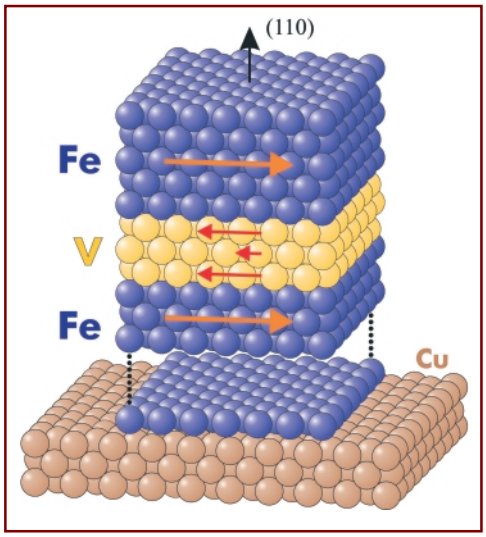

Fig. 1: Schematic view of the Fe/V/Fe(110) trilayers grown on Cu(100). The arrows indicate the layer-dependent magnetic moments of Fe and V.

Nearly everyone uses magnetic nanostructures similar to those we investigated here, for example as read-write heads of the hard disks in a computer. These nanostructures consist of a sandwich of magnetic layers with a non-magnetic layer in between (see Fig. 1). These structures exhibit new magnetic properties as compared to bulk magnets, e.g. the giant magneto resistance – the effect used nowadays to read data stored on hard disks. In the ongoing process of miniaturization only a few atomic layers of each material are used and therefore the importance of the interfacial properties increases dramatically. To study the magnetic properties of those nanostructures and especially their interfaces one needs an element-specific method to distinguish contributions of the various layers. X-ray magnetic circular dichroism (XMCD) is a method of choice since the energy positions of the X-ray absorption edges are characteristic for each element. If a magnetic sample is illuminated with circularly polarized synchrotron radiation, the absorption, especially close to certain absorption edges, will be significantly different whether left or right circular X-rays are used. The circular dichroism is defined as the difference of the corresponding absorption coefficients. Since the XMCD signal can be related to the difference of the spin-split densities of states close to Fermi-level, the direction and the size of the spin and orbital magnetic moments can be determined, based upon the application of sum rules for these spectroscopic data.

Up to now, the classical ferromagnets Fe, Co, and Ni were investigated. A systematic study of XMCD throughout especially the lighter 3d-transition-metals (TMs) series is lacking. There are several reasons for this: (i) In insulators the 3d-ions may carry a magnetic moment, however, e.g. ferromagnetic oxides are difficult to investigate because the energy ranges of the L edges (about 400-600 eV) and the O-K edge (532 eV and fine structures) coincide. (ii) The XMCD signals of the early 3d-TMs Ti, V, and Cr are expected to be much smaller than those of Fe, Co, and Ni, because these materials do not order ferromagnetically as bulk solids. (iii) The spin-orbit splitting of the core hole reduces towards the early 3d-TMs leading to considerable overlap of the L_3 with the L_2 edge. The latter is also related to the appearance of core-hole correlation effects [1] which strongly modify the relative intensities of the $L_{2,3}$ edges (see Fig. 2).

We have investigated Ti, V, and Cr layers sandwiched between two Fe layers (Fig. 1). The spectra are shown in Fig. 2. For the first time, we obtained nearly noise-free data with clear fine struc-ture, bridging the gap from classical ferro-magnets to early 3d elements. This was made possible by two technical developments: (i) optimized *in-situ* preparation guaranteed for flat interfaces and no oxygen contamination (ii) high photon fluxes together with a constant high polarization degree in the required energy range provided by the BESSY undulator beamline UE56/ 1-PGM using the gap-scan mode.
The presence of a XMCD signal itself demonstrates that the so-called non-magnetic layer of V indeed exhibits an induced moment at the interface [2]. The relative orientation of the magnetic moments of Ti, V, and Cr at the interface to Fe can be determined: As indicated in Fig. 1 the V spin moments are antiparallel aligned to the Fe moments as it is revealed from the *positive* sign of the V-XMCD onset at the L_3 edge in Fig. 2 (compared to the *negative* sign for Fe).

References:

[1] J. Schwitalla et. al., Phys. Rev. Lett. 80, 4586 (1998).

[2] A. Scherz et. al., J. Appl. Phys. 91, 8760 (2002).

[3] H. Ebert, Rep. Prog. Phys. 59, 1665 (1996).

[4] A. Scherz et. al., Phys. Rev. B 66, 184401 (2002).

[5] G. van der Laan et. al., Phys. Rev. B 43, 13401 (1991).

[6] I. Mirebeau et al., J. Phys. F: Met. Phys. 17, 191 (1987).

Supported by BMBF and DFG.

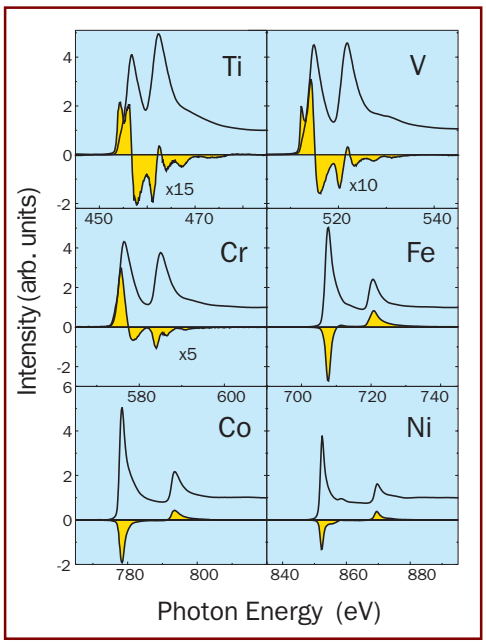

Fig. 2:
The isotropic XAS and XMCD spectra at the $L_{2,3}$ edges for part of the 3d-TMs. The spectra for the early 3d-TMs are determined from Fe/TM/Fe trilayers.

Even though the spectra reveal a large variety of different spectral features, the so-called integral sum rules are commonly applied to extract magnetic moments. In fact the application of sum rules is rather limited [3] in particular for the early 3d-TMs because of the considerable overlap of the $L_{2,3}$ edges. Hence, we used a new analysis concept, which compares the experimental fine structure to *ab inito* calculated XAS and XMCD spectra (for details see Ref. [4]). The calculations are based on a fully relativistic spin-polarized Korringa-Kohn-Rostoker (SPR-KKR) Greens-function method which is appropriate for itinerant magnetic systems as investigated here. In Fig. 3 the new concept is demonstrated for vanadium in a Fe/V trilayer and a Fe/V alloy serving as an experimental standard. Core-hole correlation effects were not included accounting for the deviation of the experimental branching ratio (close to 1:1) of the V-XAS (see top panels). Looking at the XMCD (bottom panels), we find that nearly all fine structures in the experimental data are reproduced by theory. The feature (S) in the experimental XAS spectra located at the high-energy side (~530 eV) can be falsely assigned to contamination with oxygen whereas the theory correlates the satellite to the vanadium band structure (Fig. 3, inset). The asymmetric contributions of the V-XMCD in Fig. 3 at the L_3 edge (B) and, less distinct, at the L_2 edge (C) are perfectly obtained by theory. In particular, the oscillatory fine structure (D) is elucidated as a contribution coming from the L_2 edge (red shaded in Fig. 3). Only the pre-edge feature (A) cannot be reproduced.

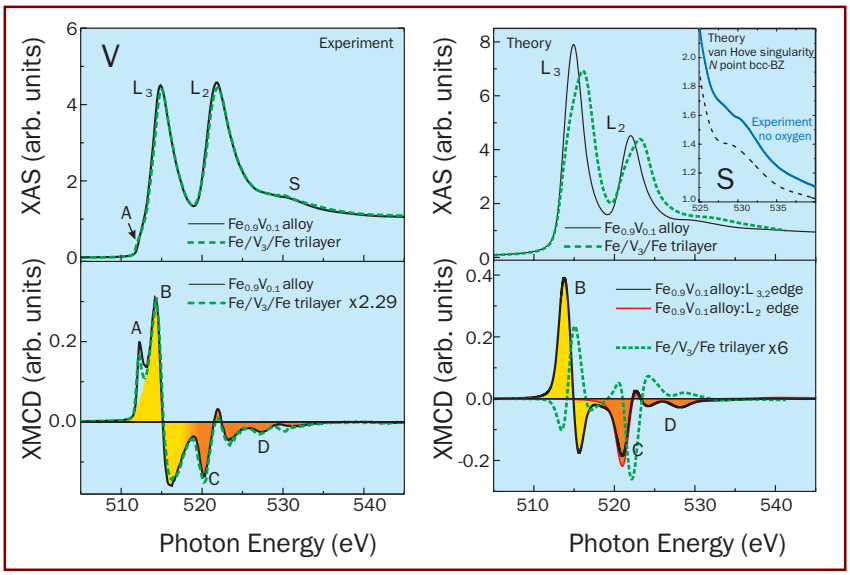

Fig. 3:
Comparison of the experimental XAS and corresponding XMCD at the V $L_{2,3}$ edges (left panel) to the SPR-KKR calculations (right panel) for a Fe/V alloy and a Fe/V layered structure.

It most likely stems from a multiplet feature. This is supported by comparable atomic-multiplet calculations of 3d-ions in a crystal field [5]. Therefore, similar to Ni, the inspection of the XAS and XMCD with the help of theory indicates some localized character of the 3d electrons.

For the experimental standard the band structure calculations provide the induced spin and orbital moments being $\mu_s = -1.01\ \mu_B$ and $\mu_l = 0.02\ \mu_B$ for V. The results are in agreement with an independent polarized neutron study [6]. For the Fe/V trilayers the deviations of the calculated XAS and XMCD is mostly related to differences in the band structure, see [4]. However, this allowed us to determine the vanadium moments in an absolute manner by using an experimental standard, avoiding the application of the "traditional" approaches like the sum rules, which lead to erroneous results for the early 3d TMs as demonstrated in [4].

Contact:
Andreas Scherz,
Institut für Experimentalphysik,
Freie Universität Berlin
babgroup@physik.fu-berlin.de

Heusler-Alloys: Novel Materials for Magnetoelectronics

C. Felser[1], B. Heitkamp[2], F. Kronast[2], D. Schmitz[4], S. Cramm[3], H. A. Dürr[2], H. J. Elmers[1], G. H. Fecher[1], S. Wurmehl[1], T. Block[1], D. Valdaitsev[1], S. A. Nepijko[1], A. Gloskovskii[1], G. Jakob[1], G. Schönhense[1], W. Eberhardt[2]

1 Johannes Gutenberg-Universität Mainz
2 BESSY
3 Forschungszentrum Jülich
4 Hahn-Meitner-Institut, Berlin

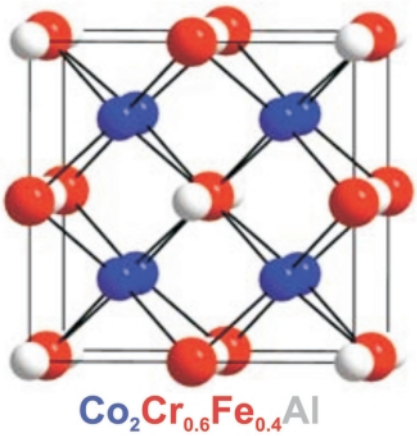

Heusler compounds are of the general formula X2YZ. X and Y usually are transition metals and Z is either a non-magnetic metal or a non-metal. Sometimes Y could be a rare earth element. The crystal structure of a Heusler compound is marked by four interpenetrating fcc-lattices. Ferromagnetic properties of Heusler alloys have been investigated experimentally and theoretically [3]. The Co-based Heusler alloys are of particular interest because they show comparatively high Curie temperature.

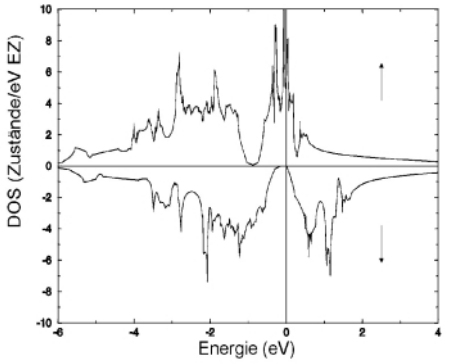

Fig. 1:
First principles calculation of spin resolved density of states of $Co_2Cr_{0.6}Fe_{0.4}Al$.

Materials, which display large changes in resistivity in response to an applied magnetic field (magneto-resistance) are currently of great interest due to their potential for applications in magnetic sensors, magnetic random access memories, and spintronics [1]. Precondition for large effects seems to be a high degree of spin polarisation at the Fermi level. A group of special compounds, the Heusler alloys, shows particular features in their electronic structure, which may cause a high magneto-resistance. Our band structure calculations predict that the ordered Heusler alloy $Co_2Cr_{0.6}Fe_{0.4}Al$ should show a hundred percent spin polarization at the Fermi level (Fig. 1).

We prepared $Co_2Cr_{0.6}Fe_{0.4}Al$ by arc melting the constituent elements under an argon atmosphere. The samples were cooled down to room temperature by rapidly shutting down the heating. Flat discs (8 mm diameter by 1 mm) were cut from the polycrystalline ingots and were mechanically polished. We obtained first evidence for the predicted high magneto-resistance by measuring a spin polarized transport at room temperature. In a small magnetic field of 0.1 Tesla, we observed a relatively high magneto-resistance effect up to 30% [2].

Neutron powder diffraction data of $Co_2Cr_{0.6}Fe_{0.4}Al$ reveal the well-ordered structure of a Heusler phase with a cubic lattice (Fm-3m) and a lattice constant of a = 5.737 Å. Using a SQUID magnetometer, we detected a saturation magnetic moment of 93 emu/g at T = 6.5 K and B = 1 T. The Curie temperature was determined to be 760 K and the remanence of 2 emu/g and coercitive field of 1 mT indicate that $Co_2Cr_{0.6}Fe_{0.4}Al$ is a soft magnet. This high magnetic moment corresponds to 3.3 μ_B per formula unit and is slightly reduced compared with the magnetic moment predicted by the first principle-band-structure calculation. This reduction is possibly due to the presence of paramagnetic clusters in the solid solution alloy observable in the Mößbauer spectra [2].

We studied the chemical composition and homogeneity as well as the magnetic properties of the Heusler alloy, particularly the behavior of the magnetic domains and

References

*[1] G. A. Prinz, Science **282**, 1660 (1998).*

[2] T. Block, Appl. Phys. Letters, submitted

*[3] P. J. Webster, J. Phys. Chem. Solids **32**, 1221-1231 (1971).*

[4] H. J. Elmers, Phys. Rev. B, accepted.

[5] C.T. Chen et al. Phys. Rev. Lett, 75, 152 (1995).

Supported by BMBF

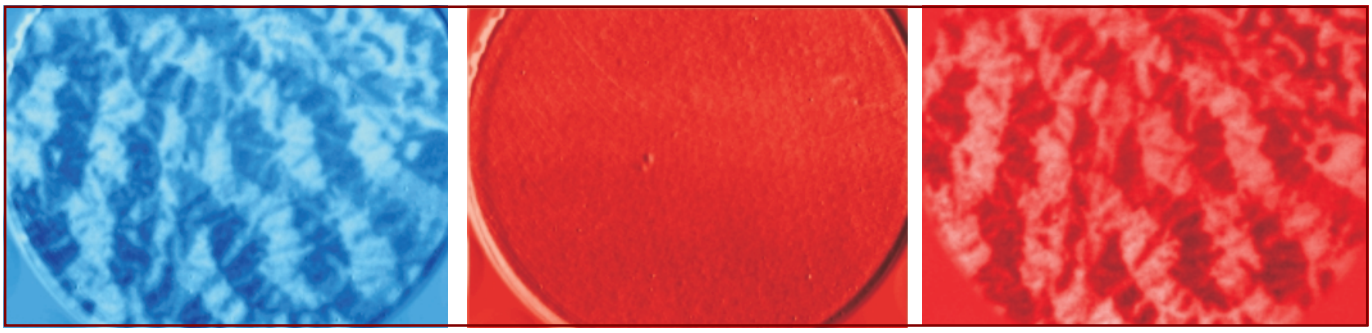

Fig. 2 shows magnetic contrast of $Co_2Cr_{0.6}Fe_{0.4}Al$ by photoelectron emission microsopy. A ferromagnetic coupling between Iron and Cobalt is seen by the similar magnetic contrast of the micrometer-sized domains measured at the corresponding absorption edges. At the Chromium Edge no contrast of magnetic origin is observed.

the element specific magnetic moments, in order to examine its suitability for magneto-electronical applications using photoelectron emission microscopy (PEEM) and X-ray magnetic circular dichroism (XMCD).

A PEEM magnifies the photoelectron distribution of the sample generated after excitation with synchrotron radiation. A spatial resolution of about 100 nm can be achieved without energy analysis of the photoelectrons. Sensitivity to the magnetic domain structure is obtained by subtracting the images for the opposite X-ray helicites. In Fig. 2, ferromagnetic coupling between iron and cobalt is seen by the similar magnetic contrast of the micrometer-sized domains measured at the corresponding absorption edges. At the chromium edge no contrast of magnetic origin is observed. However, on the nanometer-scale a more complicated domain pattern is resolved pointing to a small magnetic anisotropy energy. For these measurements the surface was cleaned by Ar-ion bombardment. Without cleaning, the magnetic contrast in the measurements was very weak but the micrometer-size magnetic domains were still clearly present.

X-ray magnetic circular dichroism (XMCD) of Cr, Fe and Co 2p -> 3d transitions [4] (Fig. 3) was measured at the undulator beamline U56/1-SGM with a resolution of 80 meV at 800 eV. The XAS spectrum was obtained by the total electron yield method, measuring directly the sample current while scanning the photon energy. The magnetic field applied to the sample (0.3 Tesla) during the measurement was aligned with the surface normal and at an angle of 30 degrees with respect to the incident photon direction. In our measurements we observed a strong selective oxidation of Cr when the sample surface was polished exposed to air. Consequently, the surfaces were scraped in situ in ultrahigh vacuum in order to remove the surface oxide layer.

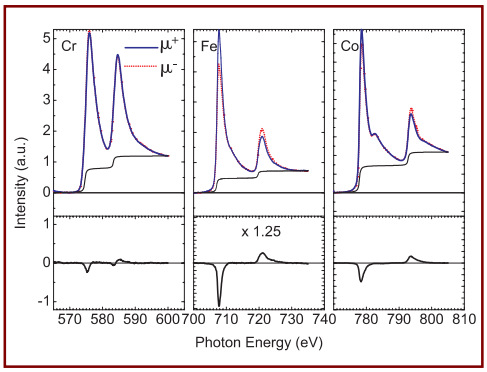

Fig. 3:
Cr, Fe and Co 2p –> 3d XAS-XMCD spectra in the quenched $Co_2Cr_{0.6}Fe_{0.4}Al$ compound. Solid (μ^-) and dashed (μ^+) lines show the XAS spectra measured with external field applied parallel and antiparallel to the surface normal. The bottom panels represents the XMCD spectra.

Using the XMCD data we have evaluated element specific magnetic moments by magneto-optical sum rules. Absolute values of spin and orbital moments were estimated using values of the total magnetic moments obtained by SQUID magnetometry. For quenched samples we obtained spin magnetic moments in agreement with the band structure calculations for Co and Fe atoms, whereas Cr possess a reduced magnetic moment. Orbital magnetic moments are 10% and 13% of the spin moment for Cr and Co, repectively. For Fe the orbital moment is 14% of the spin moment, corresponding to the absolute value of 0.33 μ_B, which is considerable larger then the Fe bulk value (0.09 μ_B [5]). We attribute the origin of the large orbital moment of Fe to the localization of the Fe 3d electrons. Annealing of $Co_2Cr_{0.6}Fe_{0.4}Al$ reduces magnetic moments at Fe and Cr drastically. We tentatively attribute this to increased atomic disorder, i.e. atomic disorder seems to play a major role for the magnetic properties of Heusler alloys.

Element specific magnetometry in combination with theoretical band structure calculations provides a key tool to understand the influence of disorder and the particular electronic properties of Heusler alloys. A careful preparation of the surface is necessary due to selective oxidation.

Contact:
Claudia Felser,
Institut für Anorganische und Analytische Chemie,
Johannes Gutenberg-Universität Mainz
felser@mail.uni-mainz.de

Crystallization atom by atom - GaAs surface kinetics studied by X-ray diffraction

W. Braun, B. Jenichen, V. Kaganer, L. Däweritz, K. H. Ploog

***Fig. 1:** Single crystals of Galliumarsenid (GaAs)*

The most basic way to study the growth of crystals is to assemble them one by one from their individual atoms. To avoid complications from chemical reactions or the use of solvents, this can be done by depositing atoms evaporated from ovens on a prefabricated crystal surface in a clean vacuum environment. We have combined this so-called molecular beam epitaxy method with X-ray diffraction, a technique that allows us to determine the positions of the atoms without disturbing the system. Si, the most commonly used semiconductor, consists of a single element. Most other semiconductors, however, are compound semiconductors consisting of two or more elements. These semiconductors are of increasing technological importance as they have special properties that allow new device applications. We are interested in how the growth of compound semiconductors differs from a single element system. We have therefore studied in real time the evolution of GaAs surfaces during growth using a dedicated beamline at BESSY by collecting X-ray diffraction data at crystals and surfaces.

The intensity of the diffracted signal is proportional to the number of atoms contributing to it (see insert). Surface diffraction intensities are therefore very much weaker than bulk reflection intensities. This is the main reason why high-brilliance synchrotron sources are required for surface diffraction. With our setup, we achieve a time resolution of around 1 s for GaAs.

During epitaxy, atoms are deposited on the surface (depostiton), move along the surface and form two-dimensional islands that eventually coalesce into continuous layers (recovery). A representative example is shown in Fig. 2. The red curves show the intensity variation during deposition and the subsequent recovery on a 2x4-reconstructed GaAs(001) surface. The damped oscillations during growth are characteristic of layer-by-layer growth with a slow coarsening of the surface. The layer coverages at the termination of deposition are determined as shown in Fig. 2b, where the upper panel shows the coverages obtained from the green line fit in the lower panel.

The recovery after growth proceeds in two phases: an initial fast recovery which is followed by a slow process (Fig. 2c). Similar to the analysis in Fig. 2b, the slow process can also be fitted (orange line in Fig. 2c), yielding a coverage value at the end of the fast recovery. Assuming that the almost completed layers are filled with material from the topmost incomplete layers during the fast recovery, we obtain a very accurate agreement between the coverage values before and after the fast recovery. Therefore, the initial fast recovery small islands and

Idealized crystals and their diffraction patterns

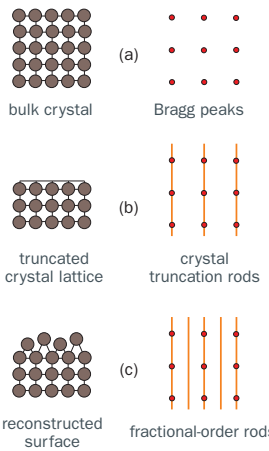

The top panel (a) displays the case of diffraction from a bulk crystal. The regularly spaced atoms in the single crystal produce a three-dimensional mesh of regularly spaced diffraction spots. A truncated crystal (b), where the surface is part of the diffraction volume, has redistributed intensity in the diffraction pattern with characteristic crystal truncation rods [1] that represent the crystal-vacuum interface between the bulk diffraction spots. A real surface is reconstructed, usually developing a surface mesh with a period that is a multiple of the underlying bulk. Such a superstructure causes additional, so-called reconstruction rods according to the superperiod to appear between the crystal truncation rods (c).

References:

[1] I. K. Robinson, Phys. Rev. B 33, 3830 (1986).

[2] V. M. Kaganer et al., Phys. Rev. Lett. 90, 016101 (2003).

[3] N. C. Bartelt et al., Phys. Rev. B 54, 11741 (1996).

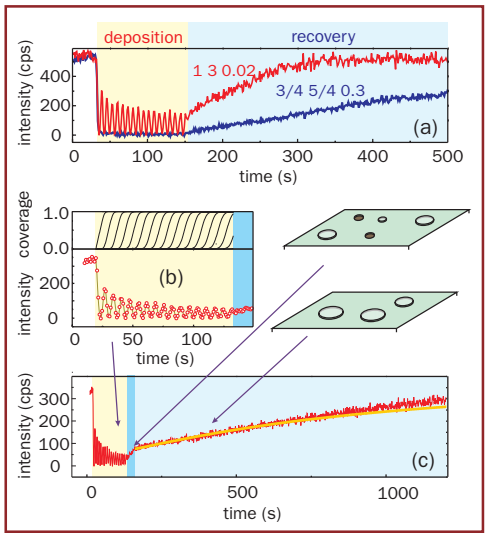

Fig. 2:
Diffraction signals from layer-by-layer growth: (a) comparison between crystal truncation rod and reconstruction rod (b) coverage analysis during growth and (c) two recovery regimes.

pits annihilate and the surface reduces to a two-level system. The remaining pits or islands coarsen during subsequent slow recovery process.

The formation of islands on the surface and their reconstruction can be studied by measuring on different rods. While the red curves in Fig. 2 are recorded on a crystal truncation rod, the blue curve in Fig. 2a is recorded on a reconstruction rod. This signal derives exclusively from atoms within the surface reconstruction. Measuring the intensity and width of the reconstruction streaks, we can determine the size of these surface reconstruction domains during recovery [2]. We deposit exactly one layer on a flat surface and follow the coarsening of the domains (Fig. 3b). The corresponding profiles across the reconstruction rod for one of the curves are shown in Fig. 3a. The results confirm the validity of domain coarsening theories in two dimensions, a problem for which only very few experimental studies are available. The correlation lengths of the domain size distribution l grow according to a power law $l(t) \approx t^n$ with exponents n between 0.15 and 0.5. We find that the different exponents and proportionality factors are due to different mobilities of the different types of domain walls in this multi-domain system, eventually leading to a dominance of the domain wall type with the highest energy when the domains are large. Discrete Monte Carlo computer simulations reproduce the main features of the experiment (Fig. 3c).

Repeating the same experiment on a crystal truncation rod which is sensitive to the islands on the surface, we deposit 0.5 layers and then follow the coarsening of the two-dimensional islands (Fig. 4).

Again, the intensity profile across the rod is monitored as a function of time (Fig. 4a). Surprisingly enough, this time the analysis yields *linear* coarsening of the islands. This exponent $n = 1$ contradicts the known theoretical models for two-dimensional systems which predict exponents of 0.5 or less. The corresponding elemental semiconductor system, Si(001), has been measured to have a coarsening exponent of 0.5 [3]. It is therefore likely that this large exponent is characteristic for the growth of compound semiconductors that consist of more than one element.

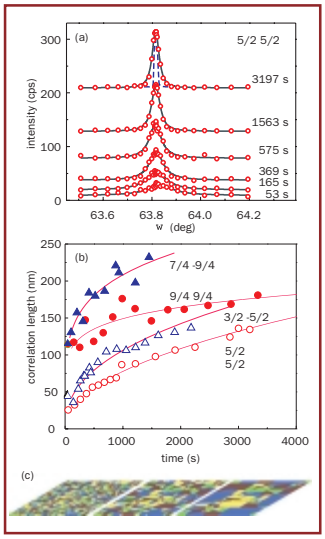

Fig. 3:
Coarsening kinetics of surface reconstruction domains after deposition of a complete layer: (a) diffraction profiles (b) domain size vs. time (c) computer simulation.

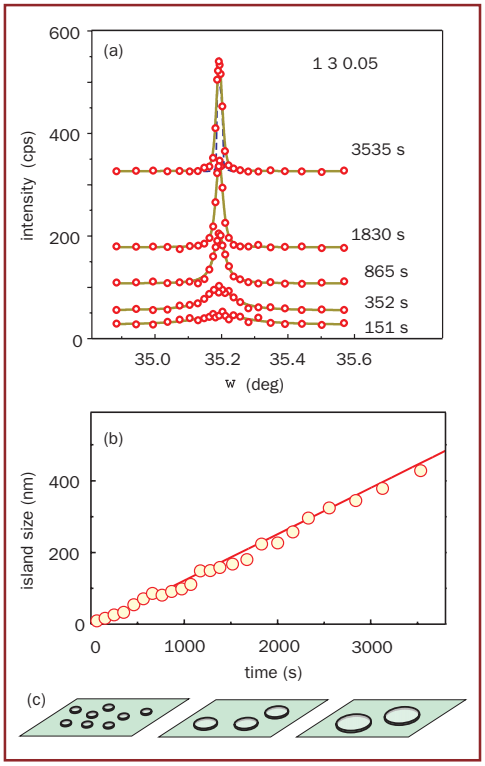

Fig. 4:
Coarsening kinetics of two-dimensional islands on GaAs(001) after deposition of half a layer: (a) diffraction profiles (b) island size vs. time (c) schematic representation. In contrast to established theories, the islands grow linearly in time

Contact:
Wolfgang Braun,
Paul-Drude-Institut für Festkörperelektronik, Berlin
braun@pdi-berlin.de

En route to Power Semiconductors: Surfaces and Interfaces of Silicon Carbide

Th. Seyller, N. Sieber, K. Gao, L. Ley

***Fig 1.:** High end switching mode power supply (SMPS) based on a commercially available SiC Schottky diode. The superior properties of the SiC Schottky diode allow a compact and cost effective design by reduction of the size of passive elements and cooling effort, thereby providing a high degree of reliability. SICED developed the basic technology which Infineon Technologies AG elaborated to high-volume products .*

On account of its physical properties, the wide bandgap semiconductor silicon carbide (SiC) is a promising material for electronic devices suitable for high-power, high-temperature and high-frequency applications. SiC-based electronics and sensors can operate in hostile environments and at higher temperatures (theoretically up to 600°C) than conventional silicon-based electronics. The new generation of electronic devices which recently began to emerge will exhibit higher compactness, improved reliability, higher voltage ratings, and higher efficiency than conventional Si based devices. Possible applications of such electronic devices would be beneficial for communication electronics, multimedia devices, server applications, transportation, engine sensors in cars or aircrafts, and many more. In some of these areas SiC devices are already in use.

Future development of SiC devices requires a surface preparation technique for clean, well ordered and chemically stable surfaces. In Si technology these demands are fulfilled by surface hydrogenation, which can be accomplished by wet-chemical methods involving hydrofluoric acid (HF) of buffered HF [1]. Considering the structural equivalence of hexagonal SiC(0001) (see Fig. 2) to Si(111) it was assumed that surface hydrogenation would be conducted similarly. However, this is not the case since HF-treated SiC(0001) surfaces are covered with a monolayer of hydroxyl groups [2].

Fig. 2: Crystal structure of 6H-SiC. The gray shaded area shows the bulk unit cell. The (0001) surface is equivalent to the Si(111) surface.

Eventually, H-terminated SiC surfaces were prepared by annealing in ultra-pure hydrogen at around 1000°C [3] and characterized by X-ray photoelectron spectroscopy (XPS), low-energy electron diffraction (LEED), and infrared absorption spectroscopy (FTIR). In order to improve on surface sensitivity and energy resolution we employed soft X-ray photoelectron spectroscopy (SXPS) with synchrotron radiation at BESSY.

The LEED patterns of hydrogenated SiC surfaces show a (1x1) symmetry and a remarkably low diffuse-elastic background, indicating well ordered surfaces. In addition, the sole presence of Si-H and C-H monohydrides on SiC(0001) and (000$\bar{1}$), respectively, was confirmed by FTIR [4-6].

The hydrogenated surfaces show an excellent chemical stability against oxidation in air [4], as determined by measuring the Si2p core level spectra after exposing the samples to air. Fig. 3 shows spectra of two different, H-terminated SiC(0001) samples taken with three different photon energies after exposure to air for 20 minutes and for 2 days. No significant variation of the line shape as a function of photon energy (and thus surface sensitivity) can be noticed implying that there are no chemically shifted components due to surface oxidation in air.

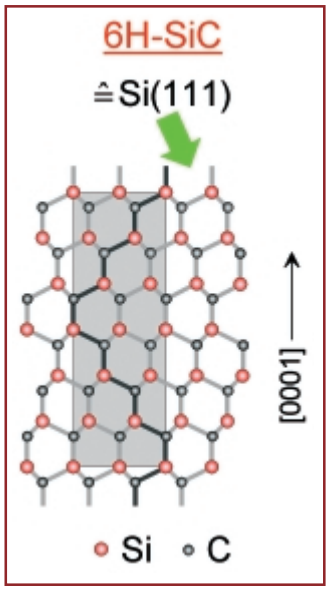

References:

[1]. W. Kern, Handbook of semiconductor wafer cleaning technology (Noyes Publications, Park Ridge, 1993).

[2]. N. Sieber et al., Mater. Sci. Forum 389-393, 717 (2002).

[3]. H. Tsuchida et al., Appl. Phys. Lett. 70, 3072 (1997).

[4]. N. Sieber et al., Appl. Phys. Lett. 78, 1216 (2001).

[5]. N. Sieber et al., Appl. Phys. Lett. 80, 4726 (2002).

[6]. N. Sieber et al., Phys. Rev. B (2003) submitted.

[7]. N. Sieber et al., Mater. Sci. Forum 389-393, 713 (2002).

[8]. T. Seyller et al., to be published

[9]. K.Y. Gao et al., to be published

Supported by DFG

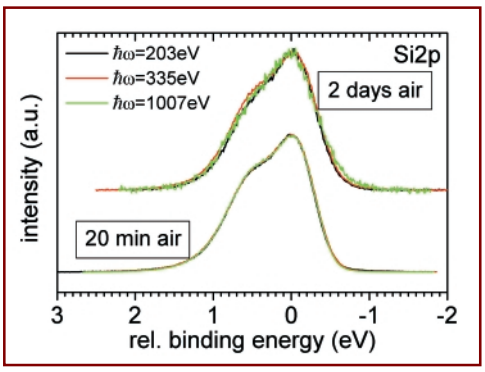

Fig. 3:
Si2p spectra of two different SiC(0001) samples taken after exposure to air for 20 min (lower spectra) and 2 days (upper spectra).

The chemical passivation is accompanied by an electronic passivation, i.e. removal of surface states from the bandgap. As a consequence, the surface Fermi level position of both, p-type and n-type SiC surfaces, was found to be equal to the bulk position. From the experimental uncertainties we estimate that the density of charged surface states must be below $7 \cdot 10^{10}$ cm^{-2} for p-type 6H-SiC(0001) and below $1.4 \cdot 10^{11}$ cm^{-2} for n-type 6H-SiC(000$\bar{1}$), respectively [4].

So-called a-planes of SiC, i.e. surfaces which are orientated with the surface plane parallel to the c-axis have recently drawn interest in crystal growth (micropipe suppression) and interface formation with SiO_2 (low density of interface states). Fig.4 shows the C1s spectrum and the FTIR spectrum of the Si-H stretch mode of a 4H-SiC(1$\bar{1}$00)-(1x1)-H surface. Only monohydrides and no di- or trihydrides are present, which is consistent with the model structure shown in the same figure [7].

Commercially available SiC devices are currently limited to Schottky diodes, which combine very fast switching with low (zero) forward bias and inverse voltages of up to 3,500 V. For example, Schottky diodes are currently used in high end switching mode power supplies for server applications (Fig. 1), where high reliability is demanded, or in video beamers, where the high operating temperature of SiC devices enables a compact design. The commercialization of a JFET – a 'normally on' device – is in sight. Ultimately it would be an advantage if SiC could be used in power MOSFET's, but unfortunately this is currently not possible due to the high density of electrically active interface states which are present at the SiC/SiO_2 interface. Whereas some researchers intend to improve this interface, we have started to investigate Al_2O_3 as an alternative gate oxide on SiC. Since it is known from Al_2O_3 on Si that there may be a Si suboxide (SiO_x) interface layer, we have inspected the interface between hydrogen terminated 6H-SiC(0001) and Al_2O_3 grown by Atomic Layer Chemical Vapor Depostition (ALCVD). Fig. 5 shows the Si2p core level measured on an ultra-thin (3.5Å) layer of Al_2O_3. The spectrum can be deconvoluted into a bulk contribution and a chemically shifted (0.47eV) component due to Si atoms with three carbon neighbors and one oxygen neighbor. The intensity of this component agrees well with what would be expected for a monolayer of Si-O bonds [2] and is therefore consistent with the structural model in Fig. 5. The formation of a significant SiO_x layer at the interface can be excluded. First electrical measurements show that the density of interface states is significantly lower than for thermal SiO_2 gate oxides [8].

After having demonstrated the exceptional properties of H-terminated SiC surfaces we now focus on their potential for application in electronic devices by exploring the structural, electronic and electrical properties of their interfaces with dielectrics.

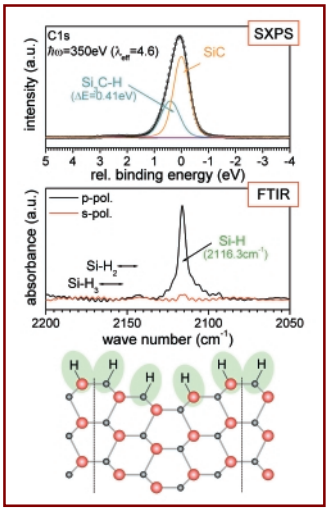

Fig. 4:
SXPS spectrum of the C1s core level and infrared absorption spectrum of the Si-H stretch mode of hydrogen terminated 4H-SiC(1$\bar{1}$00) together with the proposed model structure.

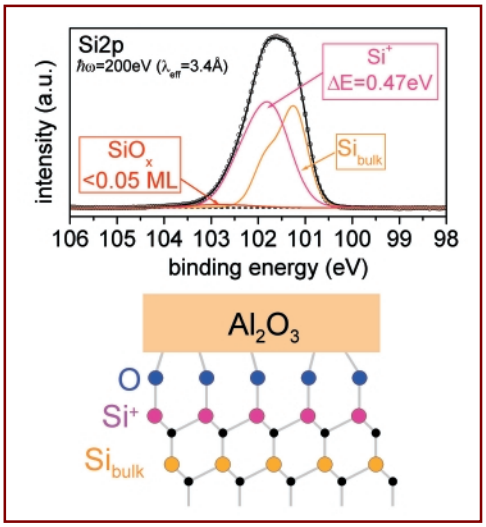

Fig. 5:
Si2p spectrum of 3.5Å Al_2O_3 deposited on SiC(0001) -(1x1)-H and sketch of the interface

Contact:
Thomas Seyller, Institut für Technische Physik II
thomas.seyller@physik.uni-erlangen.de

Ultra-trace analysis and speciation on silicon wafer surfaces

B. Beckhoff, G. Ulm

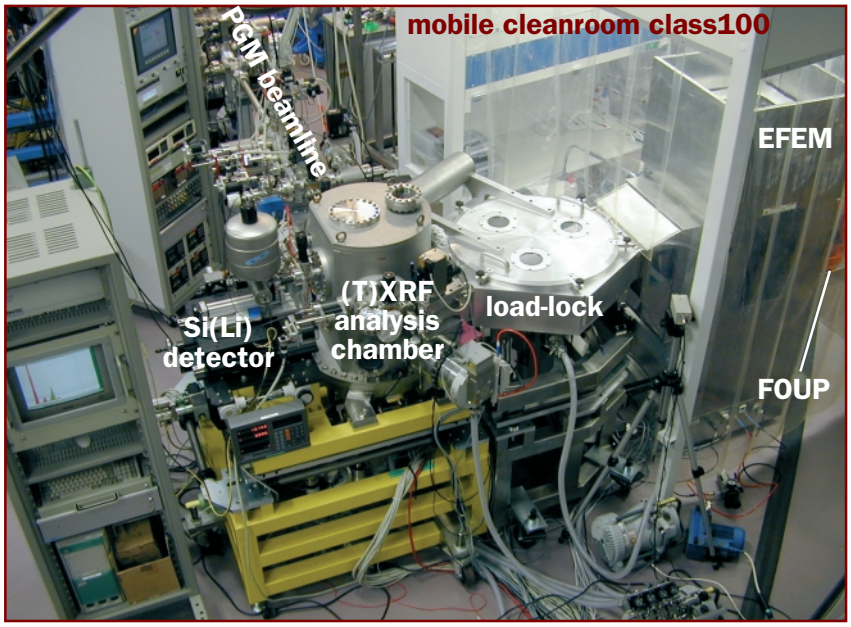

***Fig. 1:** Picture of the entire experimental (T)XRF facility.*

Quality control is of superior interest before and during the production of silicon-based microelectronic devices. Beside defects of fabrication in the lithographic process, metallic and non-metallic contamination can cause considerably reduced yields of structured semiconductors. The cleanliness requirements of initial materials such as silicon wafers range between 10^9 atoms/cm^2 and 10^{11} atoms/cm^2 (for comparison: an atomic monolayer consists of about 10^{14} to 10^{15} atoms/cm^2). These levels are steadily decreasing and are going to be extended to lower Z elements and organic compounds.

A standard inspection method for monitoring wafer cleanliness is total reflection X-ray fluorescence analysis (TXRF). Whole wafer surface control is achievable when using a vapor phase decomposition (VPD) preparation of the native silicon oxide. The combination of TXRF with VPD leads to improved limits of detection (LOD) of dissolved surface contamination. TXRF spectroscopy [1,2] using synchrotron radiation for the specimen excitation has been already employed at the SSRL and the ESRF for the analysis of minute amounts of transition metals and some lighter elements on silicon wafer surfaces. Complementarily the Physikalisch-Technische Bundesanstalt (PTB) at BESSY put emphasis on the methodological development of soft X-ray TXRF allowing for the analysis of low Z elements ranging from boron to aluminium.

At the plane grating monochromator (PGM) beamline [3] for undulator radiation within the PTB radiometry laboratory [4], the absolute LOD values of TXRF were determined for some low Z elements [5] such as C, N, Na, Mg and Al ranging between 0.3 pg and 1.3 pg, corresponding to VPD detection limits spanning from $2{\cdot}10^7$ atoms/cm^2 to about 10^8 atoms/cm^2 for Na, Mg and Al for a 200 mm wafer, thus fulfilling current analytical requirements of the semiconductor industry. Employing a deconvolution technique for XRF spectra [5] that uses experimental detector response functions instead of conventional peak fitting functions, it could even be shown that, in the very soft X-ray range, no relevant continuous scattering or Bremsstrahlung background exists when exciting the wafer samples with radiation of high spectral purity. A study concerning the resonant Raman scattering effect [6], which is a limiter for the determination of Al at ultra trace levels, could be performed with respect to both the energetic and the angular variation of the incident radiation. Additionally, a LOD [7] of B being 7 ng was found. Varying the angle of incidence, a soft X-ray TXRF investigation [7] of both a 1.6 nm C – 2.1 nm Ni – 1.6 nm C multilayered structure and a 5 nm thick C layer was performed confirming the respective layer thicknesses.

A novel instrumentation, recently designed and constructed by the PTB for the explicit purpose of the semiconductor industry, fully utilizes the excitation conditions at the PGM beamline: 300 mm Si wafers, as well as 200 mm wafers, are transported directly from their shipping cassettes (FOUP or SMIF) via a pre-aligner into a high vacuum load-lock by an adapted commercial equipment front end module (EFEM). After the pump down, a vacuum robot located inside the load-lock takes the wafer and places it inside the UHV irradiation chamber on an electrostatic chuck (ESC) mounted on an 8-axis manipulator. Fig. 1 shows the entire arrangement. To take advantage of the linear polarization of the

References:

[1] P. Pianetta et al., Rev. Sci. Instrum. 66, 1293 (1995).

[2] F. Comin et al., Nucl. Instr. Meth. B 150, 538 (1999).

[3] F. Senf et al., J. Synchr. Rad. 5, 780 (1998).

[4] B. Beckhoff et al., Nucl. Instrum. Meth. A 444, 480 (2000).

[5] B. Beckhoff et al., Spectrochim. Acta Part B 56, 2073 (2001).

[6] K. Baur et al., J. Appl. Phys. 88, 4642 (2000).

[7] C. Streli et al., Proc. TXRF 2002 Conf., Spectrochim. Acta Part B (2003), submitted

[8] B. Beckhoff et al., Proc. ICXOM XVI Conf., Spectrochim. Acta Part B (2003), in print

[9] G. Pepponi et al., Proc. TXRF 2002 Conf., Spectrochim. Acta Part B (2003), submitted

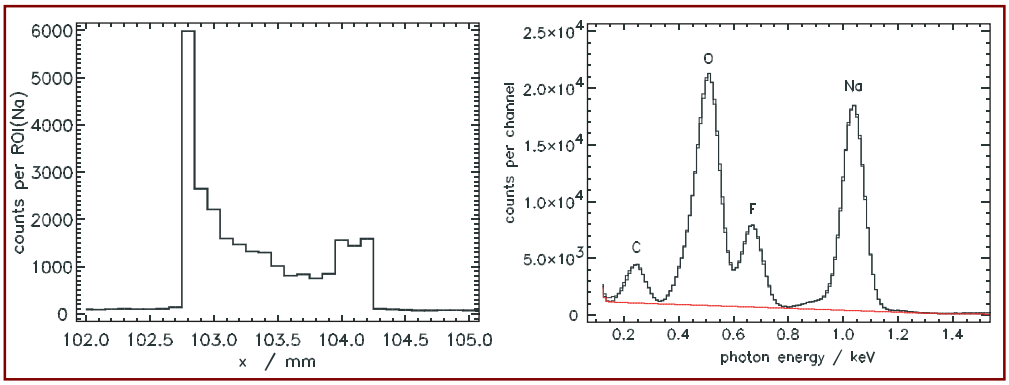

Fig. 2:
TXRF investigation of a 100 µl droplet containing 500 pg Na dried on a 200 mm silicon wafer. The figure to the left shows the lateral distribution of Na, deducted from the number of events in the corresponding region of interest (ROI) in 10 s spectra, using a 150 µm wide excitation beam. The TXRF spectrum to the right was recorded at the respective maximum Na position during 100 s real time.

exciting radiation, the ESC is moved into a vertical orientation during the measurements. The whole surface of a 200 mm or a 300 mm wafer can be scanned. To extend the capability of the system from the TXRF into the XRF regime, the angle of incidence can be increased from grazing incidence up to 45°, allowing for the analysis of thin multi-elemental, multi-layered structures. Both conventional Si(Li) detectors or superconducting tunnel junction (STJ) detectors [8] can be used. The EFEM, including a class 1 mini-environment, is surrounded by a mobile class 100 environment to further reduce the risk of unintentional cross-contaminations of the samples.

The commissioning of this arrangement was initiated in November 2002 with the investigation of a 200 mm silicon wafer, which was intentionally contaminated with 100 µl droplets containing metal and light element contamination in the pg range. The droplet depositions were prepared by the Central Analytical Laboratories of Wacker Siltronic. The first element of interest was Na, which was excited with monochromatic radiation having a photon energy of 1206 eV at an angle of incidence of one degree. The left part of Fig. 2 shows the lateral scan across the 500 pg Na droplet. The TXRF spectrum recorded at the maximum position of the lateral scans was deconvoluted by means of experimentally determined detector response functions. The remaining background (red line to the right in Fig. 2) was used to calculate the LOD value. For the accumulation time of 100 s, the conservative estimate of the LOD value for Na is 1.0 pg. Taking into account the ratio of the re-spective Na deposition present in the lateral maximum position to the total Na deposition in the droplet, the LOD value for Na is only 170 fg.

Organic contaminants are starting to play an important role in the production and quality control of silicon wafers.

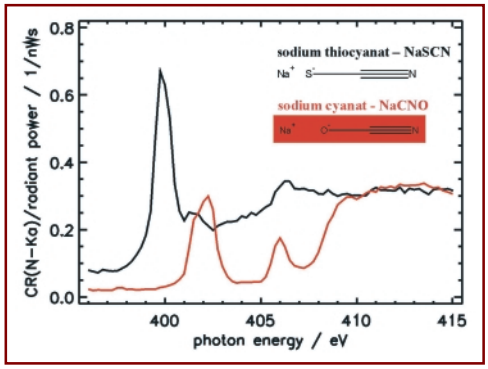

Fig. 3:
TXRF-NEXAFS spectra of minute amounts of two different compounds of light elements deposited as small droplets on a 200 mm silicon wafer surface. In these measurements, the energy of monochromatized undulator radiation is varied in the range around the K absorption edge of N in steps of 0.25 eV while recording the N-Kα fluorescence count rate normalized to the incident radiant power (/ nW).

A near-edge X-ray absorption fine structure (NEXAFS) investigation in conjunction with TXRF is able to contribute to the speciation. The PGM beamline is an appropriate source for TXRF-NEXAFS experiments, which require the tunability of the excitation radiation and a relatively high resolving power while ensuring both a sufficient photon flux and a high spectral purity. The contaminants were diluted and deposited as droplets on wafer surfaces. The K edges of C, N, O have been examined in initial experiments [9]. TXRF-NEXAFS spectra recorded from droplets containing 12 ng N deposited on a 200 mm silicon wafer are shown in Fig. 3. The reproducibility of these measurements at the N edge was good, whereas unintentional contaminations of the wafer at the C-K edge and the native oxide layer at the O-K edge can interfere considerably. Self-absorption effects and dependencies of the absorption on the adsorbate orientation will require further investigations.

The novel (T)XRF instrumentation for analyzing contamination and depositions on 200 mm and 300 mm silicon wafer surfaces offers off-line reference measurements to assess wafer cleaning procedures and multi-layered systems on wafers. Initial experiments demonstrate the promising prospects of this new instrument in soft X-ray TXRF for ultra-trace analysis of light elements and even their speciation by NEXAFS.

Acknowledgements:

The authors would like to thank G. Pepponi, C. Streli and P. Wobrauschek (Atominstitut Vienna, Austria), T. Ehmann, L. Fabry, C. Mantler and S. Pahlke (Central Analytical Laboratories of Wacker Siltronic), R. Fliegauf and J. Weser (PTB), B. Kanngießer and W. Malzer (Technical University Berlin) as well as W. Jark, (Elettra, Trieste, Italy).

Contact:
Burkhard Beckhoff,
Physikalisch-Technische Bundesanstalt, Berlin
beckhoff@ptb.de

Observations in the THz Gap: The Josephson-Plasma Resonance of $Bi_2Sr_2CaCu_2O_8$

E.J. Singley[1], M. Abo-Bakr[2], D.N: Basov[3], J. Feikes[2], K. Holldack[2], H.-W. Hübers[4], P. Kuske[2], M. C. Martin[1], W.B. Peatman[2], U. Schade[2], G. Wüstefeld[2]

1 Advanced Light Source, Berkeley, USA
2 BESSY
3 University of California, San Diego, USA
4 Deutsches Zentrum für Luft- und Raumfahrt, Berlin

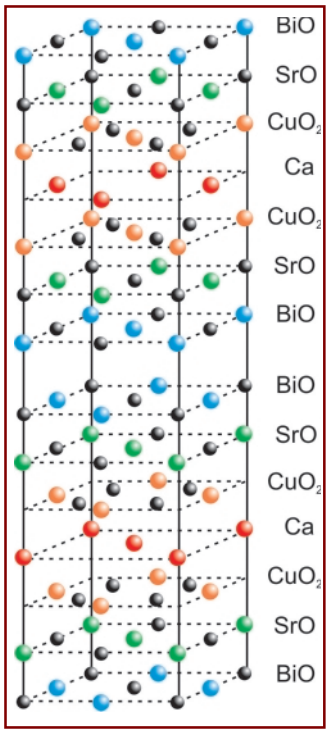

Fig. 1 : Multilayered structure of $Bi_2Sr_2CaCu_2O_8$

Superconductivity is a phenomenon of matter where below a defined temperature (T_c) the electrical resistance drops dramatically and the specific resistance is zero. Therefore, electric currents can propagate for many years without energy loss. "Classical" superconductors, with T_c between 4 - 23 K, require liquid helium for cooling which is not feasible for many technological applications. High-temperature superconductors with T_c of around 100 K would be far more suitable since liquid nitrogen can be used for cooling. However, the production of these compounds for technological applications is still unsolved since they are ceramic oxides which cannot be manufactured like metal wires.

Most high temperature superconductors are multilayer structures of metal oxides, like the cuprite $Bi_2Sr_2CaCu_2O_8$ (Fig.1). This compound consists of CuO_2 layers which are separated by insulating layers of Bi- and Sr-oxide or Ca. The assembly of conducting-insulating-conducting layers is termed as Josephson-junction. In the normal state (beyond T_c) $Bi_2Sr_2CaCu_2O_8$ behaves like a quasi 2-dimensional metal and electric current flows only along the CuO_2-layers. Below T_c these materials become 3-dimensional superconductors. Electric current flows perpendicular to the CuO_2 layers propagated by pairs of electrons (Cooper-pairs) which are tunneling the insulating interlayers. The entity of Cooper-pairs form an electron gas (Josephson-plasma) which can be described by a wave function with a specific frequency. For bilayer compounds (and hence two different Josephson-junctions) this results in two kinds of plasma frequencies. Their out-of phase oscillation gives rise to the so called Josephson-plasma resonance which has been assigned to the absorption peak that develops blow T_c.

The electronic properties perpendicular to the CuO_2 planes cover a broad spectrum, from marginally conducting overdoped $YBa_2Cu_3O_7$, to the essentially insulating character of $Bi_2Sr_2CaCu_2O_8$. The role of this varying degree of anisotropy in the CuO_2 intralayer and interlayer electronic properties in producing high temperature superconductivity is still unresolved [1]. Characterization of the Josephson-plasma resonance is of particular importance for the understanding the role of anisotropy and thus of high temperature superconductivity.

The energy scale of the Josephson-plasma edge is related to the degree of anisotropy of the material. In nearly all families of high temperature superconductors the plasma edge has been observed in the far infrared frequency range [2]. One exception is in the extremely anisotropic $Bi_2Sr_2CaCu_2O_8$ (Fig. 1) where at optimal doping (maximum T_c) the plasma edge has not been seen. By doping this compound with lead, and hence lowering the anisotropy (and T_c), the plasma edge is observed near 40 cm^{-1} [3]. Additionally, when reducing the carrier doping a resonance is observed in magneto-absorption experiments in the microwave region, usually attributed to the Josephson-plasma effect [4].

The energy range between microwave and far infrared, 3 – 33 cm^{-1} (0.1 – 1 THz), has proven to be challenging to access and is therefore referred to as the 'THz gap'. Using the stable coherent synchrotron radiation (CSR) recently provided at BESSY [5] (see page 49) we have been able to extend

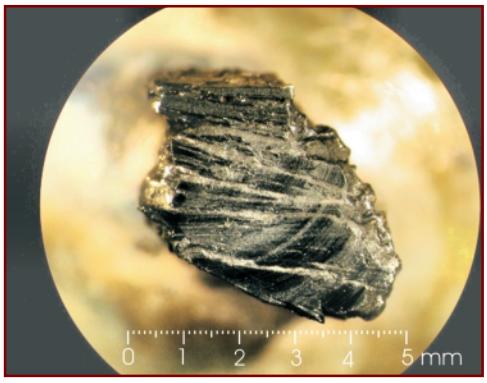

Fig. 2: The mosaic of the single $Bi_2Sr_2CaCu_2O_8$ crystals used in this investigation. To account the contribution to the measured reflectance the area of epoxy showing was estimated and the experimental reflectance was corrected accordingly.

References:

[1] P.W. Anderson, The theory of superconductivity in the high-Tc cuprates. Princeton Series in Physics. Princeton, N.J., Princeton University Press, 1997.

*[2] S.V. Dordevic, et al., Physical Review B, **65** (2002), 134511.*

*[3] T. Motohashi, et al., Physical Review B, **61** (2000), R9269-R9272.*

*[4] O.K.C. Tsui, et al., Physical Review Letters, **73** (1994), 724-727.*

*[5] Abo-Bakr M. et al, Physical Review Letters, **8825** (2002), 4801.*

*[6] Kakeshita, T., et al., Physical Review Letters, **86** (2001), 4140-4143.*

Supported by BMBF

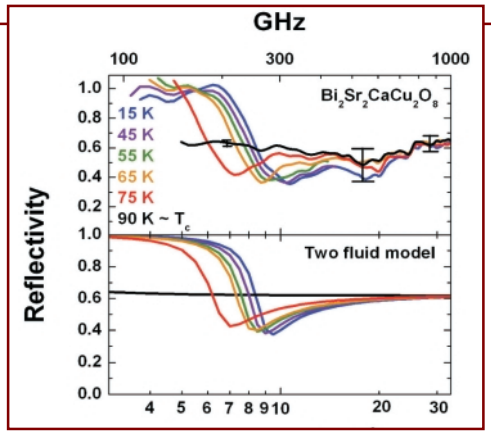

Fig. 3:
Measured c-axis polarized near-normal reflectivity of $Bi_2Sr_2CaCu_2O_8$ (upper panel) for various temperatures at or below the superconducting transition temperature, T_c. A resonance that shifts with temperature and disappears above T_c is clearly observed. The lower panel shows the calculated reflectivity of a superconductor with a shifting Josephson-plasma resonance.

traditional infrared measurements into sub-terahertz frequency range. Reflectivity measurements on optimally doped $Bi_2Sr_2CaCu_2O_8$ to 4 cm^{-1} show the Josephson-plasma resonance in the expected region.

In order to make specular reflectance measurements at wavelengths in excess of 1 mm it is necessary to have a sample larger than the wavelength of the probing radiation. Since it is difficult produce a single crystal of high temperature superconductors with c-axis dimension longer than 1 mm, a mosaic of several crystals was assembled with a net c-axis length of approx. 5 mm (Fig. 2). While this circumvents problems of diffraction effects, additional complications arise due to reflection from the conducting epoxy that binds the individual crystals together. Absolute values of the reflectivity were obtained by coating the sample in situ with a thin layer of gold and using the gold coated sample as a reference.

The top panel of Figure 3 shows the experimental reflectance in the sub-terahertz region on a logarithmic frequency scale. In contrast to the nearly flat and featureless spectrum at $T = T_c$ (black curve), the $R(\omega)$ spectra at $T < T_c$ shows a strong ω dependence. Below T_c the spectrum has a shallow minimum followed by a strong rise in the reflectivity. This reflectance edge and the minimum mark the onset of superconducting currents along the c-axis. Their position may be used to measure the superfluid density: As the temperature decreases in the superconducting state, both the minimum and reflectance edge shifs to higher frequencies. This shift nearly saturates at 15 K due to the increasing density of superfluid as the temperature is lowered.

In order to extract quantitative information from the spectrum we model the reflectance with a two fluid model. One component consists of the dissipationless supercurrents, while the other is an over damped plasmon. The second term is necessary to account for finite reflectivity at the plasma minimum and the rounding at the top of the reflectance edge. The bottom panel of Figure 3 shows the results of this modeling. The magnitude and both the frequency and temperature dependence of the data in the top panel are well accounted for.

Using the above modeling we are able to extract the value of the unscreened Josephson plasma frequency. At 15 K we obtain a value of $\omega_{ps} = 74$ cm^{-1}. This value corresponds to a c-axis penetration depth value of $\lambda_c = 21$ µm. The complete temperature dependence of the Josephson-plasma frequency is summarized in Fig. 4. The plasma frequency rises quickly below T_c, and is nearly saturated at the low temperature limit by $T_c/2$.

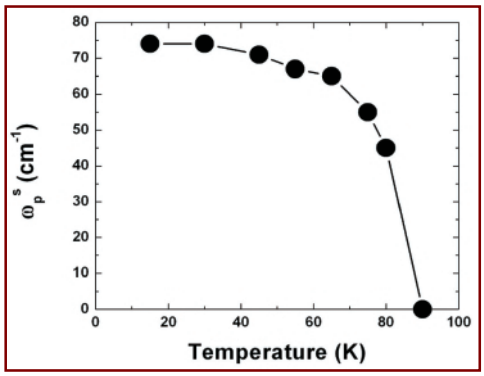

Fig. 4:
Superfluid plasma frequency as a function of temperature. Plasma frequency was determined from fitting the reflectance spectra with the two fluid model shown in the bottom panel of Fig. 3.

Another dip in our experimental data near 20 cm^{-1} might be a transverse Josephson-plasma mode [6] in $Bi_2Sr_2CaCu_2O_8$ caused by the two different distances between CuO_2 layers in the crystal structure. This feature in the data is however located right where our signal to noise is the worst due to interference from 50 Hz pickups, so for now this remains only a tantalizing prospect and should be investigated further.

The production of stable, high power, coherent synchrotron radiation at sub-terahertz frequency opens a new region in the electromagnetic spectrum to explore physical properties of materials. Just as conventional synchrotron radiation has been a boon to X-ray science, coherent synchrotron radiation may lead to many new innovations and discoveries in terahertz physics. As an initial feasibility test of using CSR in scientific applications, we have directly measured the Josephson plasma resonance in optimally doped $Bi_2Sr_2CaCu_2O_8$ for the first time. Our results provide a connection between the magneto-absorption experiments performed on underdoped $Bi_2Sr_2CaCu_2O_8$ and the infrared experiments in other families of high temperature superconductors.

Contact:
Ulrich Schade, BESSY GmbH
schade@bessy.de

Molecular Spectroscopy:

Investigating the Limitations of the Born-Oppenheimer Approximation

F. Burmeister[1], L. M. Andersson[1], G. Öhrwall[1], A. J. Yencha[2], T. Richter[3], P. Zimmermann[3], K. Godehusen[4], M. Martins[5], H. O. Karlsson[1], S. L. Sorensen[1], O. Björneholm[1], R. Feifel[1], K. Wiesner[1], O. Goscinski[1], L. Karlsson[1], S. Svensson[1]

1 Uppsala University, Sweden
2 State University of NY, Albany, USA
3 Technische Universität Berlin
4 BESSY
5 Universität Hamburg

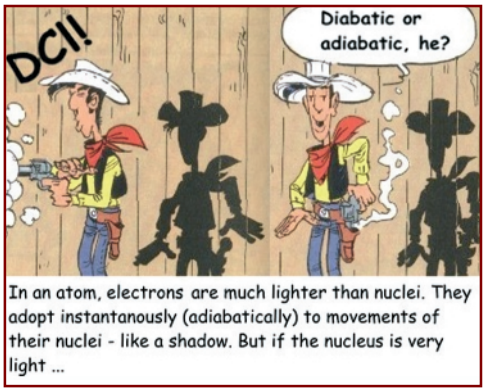

In an atom, electrons are much lighter than nuclei. They adopt instantanously (adiabatically) to movements of their nuclei - like a shadow. But if the nucleus is very light ...

On a microscopic scale, chemical reactions can be seen as movements of the atomic nuclei coupled with changes of the electronic structure. Such changes are especially important at internuclear distances for which two states of the same symmetry have nearly the same energy. We have studied a simple diatomic molecule, hydrogen chloride HCl, and its deuterated twin DCl, for which the first manifestation of such dynamic changes of the electronic structure is observed using photoelectron spectroscopy.

Matter is composed by positively charged nuclei and negatively charged electrons. The electrons are orders of magnitude lighter (mass relation $m_{proton}/m_{electron}$=1,836) and the movement of the electrons is typically so fast as compared to the nuclei, that they can be said to adapt instantaneously, "adiabatically", to the configurations of the nuclei (*adiabatic approximation*) Here we have probed a diatomic system (HCl and DCl), where the nuclei have been shown to move too fast, and the *adiabatic approximation* is violated.

In this project, photoelectron spectroscopy was used, a very sound scientific method. The outline of the experiment is shown in Fig. 1. An incoming photon γ of a well-defined energy $h\nu$, is used for probing a system, here HCl, in gas-phase, by exciting an electron and removing it from the molecule. This outgoing photoelectron is detected by a spectrometer, which is used for measuring the kinetic energy E_{kin} of the electron.

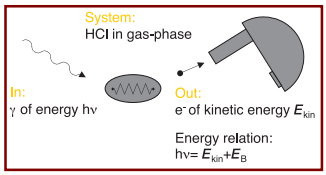

***Fig. 1:** Outline of our experiment at BESSY*

The difference between E_{kin} and the energy of the incoming photon determines the binding energy E_B of the electron, which is a measure of the energy difference between the initial and final state of the system (Fig. 2).

In the upper right-hand side of Fig. 2, four theoretical potential curves are shown for the HCl/DCl cation [1]. The black (diabatic) curves correspond to two electronic configurations, denoted 1h (for 1 hole, *i.e.* one electron missing) and 2h1p (2 holes 1particle, *i.e.* two electrons missing and one excited electron). The diabatic states have the same overall symmetry. The *adiabatic approximation* prohibits two potential curves of the same symmetry to be degenerate at any internuclear distance. The result is an *avoided crossing*. The resulting *adiabatic* potential curves (ϕ_1 and ϕ_2) are shown in yellow and blue.

A powerful method to understand our photoelectron spectra is the Franck-Condon projection scheme (also shown in Fig. 2). As the HCl molecule is in the bound ground state (at potential energy 0 eV in the right-hand potential curve plot), the molecule oscillates around the inter-nuclear equilibrium distance, shown as the Franck-Condon region in Fig. 2. The molecule is exposed to monochromatic light, energetic enough to ionize the molecule. Different final HCl^+ states can be populated. The transition, ground state -> final state can be regarded as instantaneous, so the nuclei do not have time to move. The final states of the cation can be either dissociative or bound, as shown in the potential curves in Fig. 2. The Franck-Condon projection of a dissociative (bound) state, *e. g.* the adiabatic ϕ_1 (ϕ_2) curve, results in a broad band (discrete vibrational states).

For the real HCl spectrum (Fig. 2, left panel), both broad bands and two vibrational progressions can be seen. The vibrational progression which starts at approximately 27 eV is associated with an electronic state, whose potential energy curve is not included in Fig. 2. This work focused on the main

References:

[1] M. Hiyama et al., Chem. Phys. Lett. ***210****, 187 (1993).*

[2] F. Burmeister et al., Phys. Rev. A ***65****, 012704 (2001).*

[3] L. M. Andersson et al., Phys. Rev. A ***65****, 012705 (2001).*

Funded by VR, SSR, TFR, Sweden

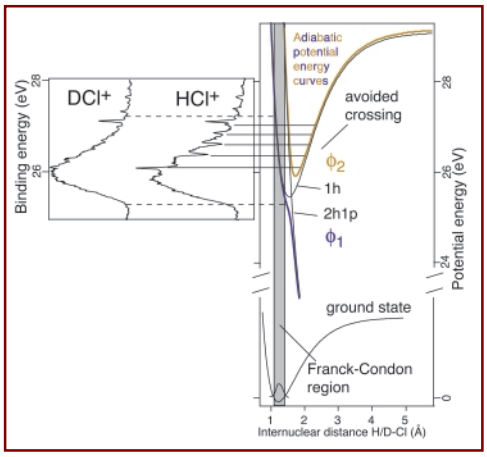

Fig. 2: Franck-Condon projections

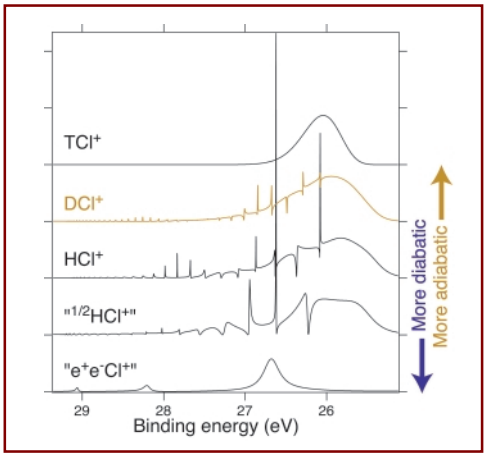

Fig. 3:
Simulated spectra: From one limiting case to another.

continuum band, associated with the dissociative adiabatic state ϕ_1. The Franck-Condon projection fits nicely, indicated by the dashed lines. On top of the broad band, a vibrational progression is seen, associated with the bound adiabatic ϕ_2 state. The Franck-Condon projection for this state is shown as solid lines. The peaks are clearly asymmetric, indicative of an interference phenomenon. In contrast, in the DCl spectrum, the same vibrational progression almost disappears. The continuum band, however, looks the same as for HCl^+. The spectra were recorded with 30 meV experimental resolution at MAX-lab in Lund, Sweden [2].

The explanation for the difference between the HCl and DCl spectra is the dynamics of the system. As mentioned above, the avoided crossing in Fig. 2 is based upon the assumption that the nuclei move infinitely slow compared to the electrons. However, in the case of HCl+, the *avoided crossing* is violated and the system jumps from the adiabatic electronic state ϕ_1 to ϕ_2. For DCl^+, the system develops slower due to larger reduced mass. The jump between the adiabatic states is less pronounced because the non-adiabatic coupling is smaller and the vibrational progression disappears.

This qualitative discussion was confirmed by simulations [3]. In Fig. 3, theory shows how the spectra would look for infinite experimental resolution, ranging from the hypothetical molecule "positronium chloride$^+$ ($e^+e^-Cl^+$)" to the tritium chloride cation (TCl^+). Here interesting information can be seen: For the heaviest system TCl^+, the adiabatic approximation is fully valid. The system develops exclusively on the adiabatic potential curve ϕ_1. For the other extreme "$e^+e^-Cl^+$", one has the "diabatic" (as the opposite to the "adiabatic") case, where only the diabatic bound potential curve associated with the 1h electronic state is populated.

But most importantly for the present project: the simulations show that if the resolution were to be enhanced to 10 meV, the vibrational progression (as seen for HCl^+) would also appear in the DCl^+ spectrum. This can be explained by the Heisenberg uncertainty relation, where the energy width of a predissociative state is inversely proportional to the lifetime. Since the coupling is smaller for DCl^+ as compared to HCl^+, the lifetime for a bound vibrational state in ϕ_2 is longer and the peaks get narrower.

In order to confirm the theoretical calculations experimentally measurements were performed at the BESSY beamline U125-2. Three reasons made one believe in the possibility to succeed: (i) We had lower photon energy available, 40 eV as compared to the 60 eV for the spectra shown in Fig. 2. This reduces the Doppler broadening (due to translation of the cation) of the peaks from 15 to around 7 meV, (ii) secondly, the Scienta electron spectrometer software has been updated, including a feature that now provides the possibility to correct for drifting potentials in the interaction region. (iii) And finally, the U125-2 has the best monochromator resolution worldwide.

Figure 4 (upper panel) shows the DCl^+ spectrum recorded at BESSY with 10 meV resolution together with simulations. For comparison, the HCl^+ spectrum (lower panel) was recorded at 23 meV resolution at ALS, Berkeley. Two vibrational progressions A and B are pointed out. Progression B is associated with an electronic state, which is not included in the theoretical discussion above. Vibrational progression A is associated with the bound electronic state ϕ_2 in Fig. 2. The DCl experiment at BESSY clearly confirms the theoretical prediction of the appearance of vibrational progression A for enhanced resolution.

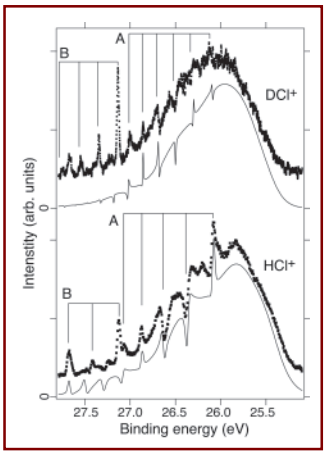

Fig. 4:
Experimental vs calculated spectra of HCl^+ and DCl^+.

Contact:
Florian Burmeister, Department of Physics, Uppsala University,
Florian.Burmeister@fysik.uu.se

Ping-pong with ions and electrons: O_2 can do

G. Prümper, O. Kugeler, U. Hergenhahn, S. Marburger, D. Rolles, F. Burmeister, J. Viefhaus, R. Hentges, S. Cvejanovic, U. Becker

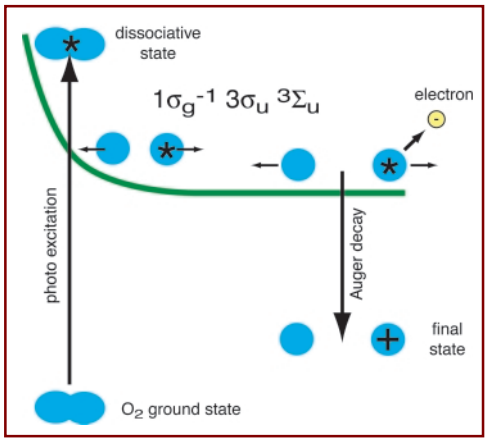

Fig. 1:
Schematic representation of the involved reaction

The properties of matter – e.g. chemical binding, electron transport in semiconductors, magnetism – are based on electrons surrounding the atomic nuclei as negatively charged clouds. The character and behaviour of the electron clouds account for the so-called electronic structure. Fundamental to a detailed description of complex electronic structures, is the understanding of the electron shell of single atoms or small molecules in gas-phase. However, all atoms except hydrogen possess more then one electron, which makes it impossible to find a physically exact description of their electron shell. Physicists use computational approximations instead. The comparison of these results with experimental data allows a step-by-step improvement of the computational models.

The electronic structure can be probed by using experimental methods like electron spectroscopy. But while spectroscopic methods yield information about electronic or geometrical structure, dynamic phenomena, like chemical reactions can only be investigated by time resolved or coincident methods. We have set up an experiment which involves elements of photoelectron diffraction and coincidence spectroscopy at the same time.

Photoelectrons emitted from molecules, adsorbates or bulk matter invariably are disturbed by the surroundings of the site, from which they have originated. Due to the wave nature of the electron, this influence will not simply lead to a mechanical scattering, but to a diffraction process, by which a pattern of scattered photoelectrons is produced [1]. Several investigation methods for the electronic or nuclear structure of matter employ an analysis of this scattering pattern.

At first thought it might be astounding that more elementary studies of photoelectron scattering have been performed for bulk matter than for simple free molecules, but a major problem in these studies is fixing a free (gas) molecule in space. This problem has only recently been overcome by several groups, who have developed techniques of determining the molecular orientation in retrospect from an analysis of the ionic fragment momenta. With these techniques it was possible for the first time to study the photoelectron diffraction pattern from a free molecule. Taking these studies one step further, in the example we present here, it is yet possible to separate the different contributions to the outgoing photoelectron wave, scattered and direct part, in an experiment.

The reaction we have studied is the fast dissociation of the free, core excited O_2 molecule. Recently, Björneholm et al. [2, 3] discovered that in this reaction a large number of molecules dissociate into two oxygen atoms before the core excited state can relax. Only after the two oxygen atoms have separated by several Angstroms, one of them emits an Auger electron (Fig. 1). Therefore, the part of these electrons which has been emitted in the direction of the fragment ion, or anti-parallel to it, shows a clear separation in energy, by the momentum acquired from the dissociating atom. This has also been termed a 'Doppler' shift.

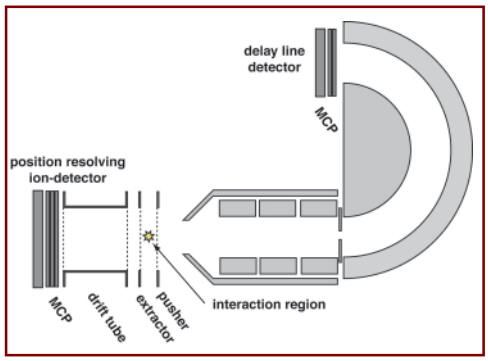

Fig. 2:
Experimental setup - A position-resolving ion spectrometer is mounted opposite to a time-resolving hemispherical electron analyser

References:

[1] D. P. Woodruff and A. M. Bradshaw, Rep. Prog. Phys. 57, 1029 (1994).

[2] O. Björneholm et al., Phys. Rev. Lett. 84, 2826 (2000).

[3] A. Baev et al., Phys. Rev. A 66, 022509 (2002).

[4] O. Kugeler et al., Rev.Sci.Instr. submitted

[5] A. Golovin et al., Phys. Rev. Lett. 79, 4554 (1997).

[6] P. Brühwiler et al., Rev. Mod. Phys. 74 (2002), p.708

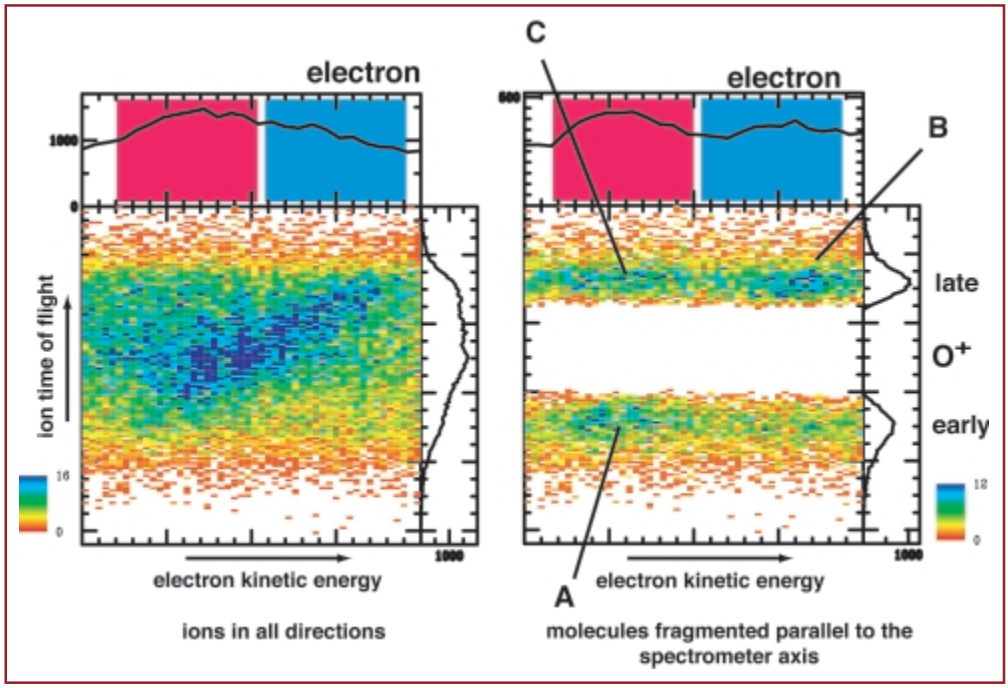

Fig. 3:
Coincidence maps - Left: ions in all directions, right: molecules fragmented parallel to the spectrometer axis

Yet, the experiments so far did not resolve whether the blue or red shifted Auger electron really travels along with the corresponding fragment ion. This can be revealed by a photoelectron - fragment ion coincidence experiment of the kind we have performed at the U49/2 beamline at BESSY using a coincidence set-up consisting of a SCIENTA SES 200 electron analyzer with delay line anode [4] and a pulsed ion time-of-flight spectrometer with a crossed wire position-sensitive anode placed directly opposite (Fig. 2). The novel arrangement makes high-resolution photoelectron-fragment ion coincidence experiments feasible for the first time and enabled us to distinguish between electrons emitted in different directions with respect to the molecular axis of the core-excited molecule.

Figure 3 shows the coincidence map between the Auger electrons and the corresponding fragment ions. The left map contains all ions, independent of the orientation of the molecular axis. The strong diagonal feature in the map shows that the Doppler shift of the electron is indeed a direct result of the ion momenta. Simply thinking, one could expect that the coincidences would exhibit blue-shifted electrons going along with the fragment ion and red-shifted electrons going into the opposite direction. These processes correspond to the reactions B and A in figure 4. Off-diagonal contributions do not belong to the directly emitted electrons but involve scattering processes, labelled reaction C in figure 4. In the right map only ions emitted parallel or anti-parallel to the spectrometer axis and the corresponding electrons are shown. Firstly, this selection reveals the Doppler splitting in the electron spectrum more clearly. Secondly the scattering process C can be observed as an intensity maximum in the area of red shifted electrons and late ions. This feature extends to even lower red-shifts, as the electron is scattered at an atom moving in the same direction. Naturally the blue shifted electrons are not scattered. This asymmetry is even exhibited in the left coincidence map representing all ions emitted in all directions. As a consequence the red shifted contribution in the electron spectrum is always larger than the blue shifted contribution. This asymmetry occurs also in the case of measurements which do not resolve the Doppler components. This has been seen for the auto-ionization of valence-excited dissociating states of molecular oxygen [5].

By choosing the appropriate directions of the molecular axis one can control the overlap of the red and blue shifted components of the Auger line. Such experiments open the window for a coherence control but also for time-dependent studies of the structure of dissociating molecules [6] and their dynamics in particular.

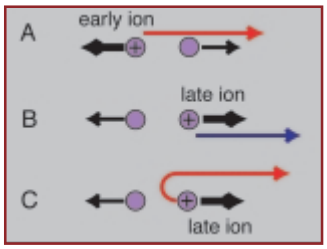

Fig. 4:
Schematic of the Auger emission from the dissociating molecule

Contact:
Uwe Becker, Fritz-Haber Institut
becker_u@fhi-berlin.mpg.de

1
Brandenburgische Technische Universität Cottbus
2
National Technical University of Athens, Greece

Preventing Corrosion of Aluminium Alloys by Polymeric Coatings

D. Schmeißer[1], J. Paloumpa[1], P. Hoffmann[1], Y. Burkov[1], A. Yfantis[2], D. Yfantis[2]

Fig. 1:
Schematic corrosion mechanism for aluminium surfaces. Pit formation is the main source of Al corrosion in the atmosphere or in natural waters.

Aluminium is a material of everyday use in many applications, like automobile, aerospace or cookware, due to its special properties (low density, low weight, strength, easy to form and cast, abundance etc). Although aluminium is a reactive metal, it also has a significant corrosion resistance because of a thin, protective oxide layer which is generally stable in air and aqueous solutions. However, pores within the oxide film and other defects caused from alloying elements can lead to local corrosion and the formation of pits.

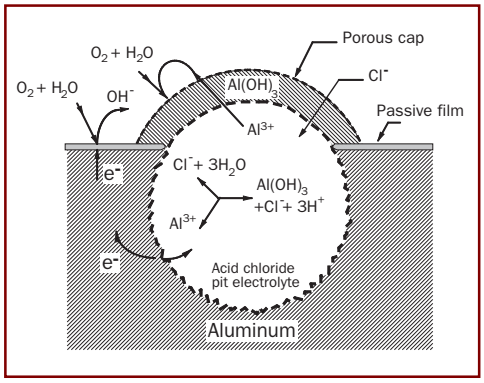

The corrosion of metals in general is an electrochemical process involving two half-cell reactions: an oxidation reaction at the anode and a reduction reaction at the cathode. In the case of aluminium the formation of pits is the main source of corrosion, since the pits work as microgalvanic cells (see Fig.1). Active metal dissolution proceeds in the crater of the pit (anode) and reduction reactions occur in the periphery (cathode).

The inhibition of corrosion is generally achieved by the deposition either of passive films (lacquers, ceramics etc.) or of active conversion coatings (e.g. chromates, noble metal coatings) on the surface which is to be protected. Both techniques are based on reducing the density of pores or causing surface chemical reactions to prevent oxidation. While in the former the inhibition depends on the thickness of the deposited film, the inhibition mechanisms are more complex for the latter systems.

The use of conducting polymers as corrosion protectives offers additional properties to those of inorganic conversion coatings due to the electrical and morphological characteristics of the polymer. Four mechanisms of corrosion inhibition by polymers are widely discussed. The conducting polymer ...

- ... acts as a barrier coating due to the repulsion of the negative ions from the negatively charged dopants surrounding the polymer chain,
- ... acts as an sacrificial anode (due to its conductivity) and provides cathodic protection to the metal surface,
- ... acts as a reservoir of ions, turning the corrosive anions into dopants or releasing the original dopants which subsequently act as inhibiting ions,
- ... stabilises a passive oxide layer.

In our studies we investigated the reactions of the dopants in a conducting polymer in order to obtain information on the inhibition process. We used TiF_6^{2-} and Zn^{2+} ions in an aqueous solution to dope polypyrrole (Ppy), which is one of the most stable, non-toxic conducting polymers. In this way we prepared active conversion coatings on alumini-

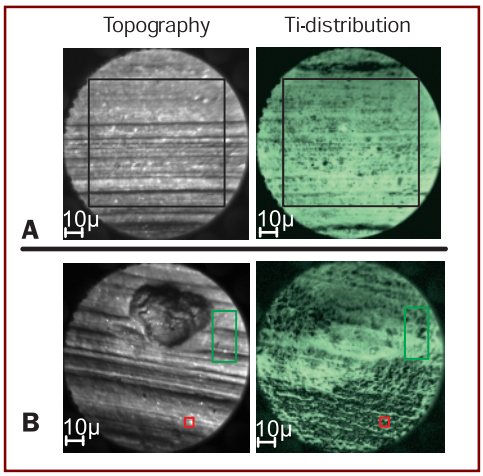

Fig. 2:
Topography (left images) and Ti distribution (right images) for sample A before (top) and for sample B (bottom) after the corrosion tests. The colored boxes indicate the sample sections of the spectra shown in Fig. 3 and Fig. 4.

References:

[1] F.M.F. de Groot et al., Phys.Rev.B 41, 928 (1990).

[2] J. Biener et al., Surf.Sci. 450, 12 (2000).

[3] D. Schmeißer et al., Phys.Rev.Lett. 83 (1999) 380; awarded by the Max-Grünebaum-Stiftung (2000).

[4] A. Yfantis, D. Schmeißer, Greek Industrial Property Org., Patent Nr. 100 37 63 (2002).

um by chemical oxidation / polymerisation of pyrrole monomers [4]. Accelerated corrosion tests were performed according to standard routines in a 5% NaCl solution by passing a constant current (100 mA/cm^2) for several minutes through the electrolyte.

We employed a Photo-Emission-Electron-Microscope (PEEM), an instrument which can deliver topographic contrast, elemental contrast, and chemical information with spatial resolution. Topographic contrast is obtained by imaging the secondary electrons. For elemental contrast we take two images, before and on the XAS resonance of a particular element, and build the difference. Chemical information is derived from the total PEEM image intensity of the imaged electrons as a function of the energy of the incoming photons (μ-NEXAFS). An excellent variable X-ray source for μ-NEXAFS is the BTU-Undulator beam line (U49/2-PGM2) at BESSY because of its tunability, high brilliance, and high energy resolution.

PEEM images of two Al samples coated with our polymeric conversion coating are shown in Fig. 2. Sample (A) is imaged before and sample (B) after accelerated corrosion tests. We studied the Ti distribution (difference image taken at the Ti2p absorption edge) in the same sample section. The two difference images on the right hand side of Fig. 2 revealed that the elemental distribution of Ti is not homogeneous. It is also not correlated to the sample topography caused by rolling lines and other irregularities seen in the topography images. Finally, there is no evidence for pitting corrosion. The elemental images of the other dopants show similar non-homogeneous behaviour. The difference images of Zinc qualitatively scale with the distribution of Titanium, while the behaviour of Fluorine is reversed.

Chemical information is obtained from the O1s and Ti2p NEXAFS data. In Fig. 3 we compare the O1s NEXAFS of the two samples. In the as deposited Ppy film we attribute the double peak structure with a characteristic splitting of 2.7 eV to the existence of TiO_2 particles. This is a first indication that the TiF_6^{2-} ions must have reacted upon film deposition. A possible explanation is that they link to defects in the native Al_2O_3 of the Al sample. Thereby the Ti-fluorides convert to TiO_2 nanoparticles [3]. The O1s spectrum of the sample B (after corrosion test) is significantly changed. Now, only a weak shoulder remains from the absorption doublet of the TiO_2 particles while a broad unstructured feature is indicative of other oxides, probably the native Al_2O_3.

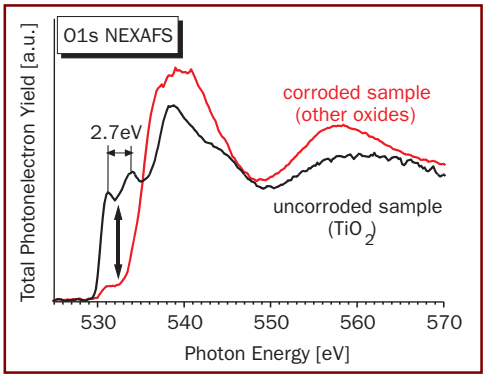

Fig. 3:
O1s-μNEXAFS spectra of the as deposited conversion coating (black) and after corrosion tests (red).

In the NEXAFS spectrum of the Ti2p signal we find our assignment of TiO_2 particles supported by the sharp features around 460 eV which reflects the transitions into the empty Ti3d states of TiO_2 (Fig. 4, black curve). After the corrosion tests the spectrum changes only subtle, there is a weak change in the relative intensities and a small increase in the width of the 3d-features. However, there is a much lower intensity. We show two spectra which are taken in the marked regions of the sample (Fig. 4, green and red curve) and indicate that the Ti concentration varies significantly and is almost completely disappeared in the lower spectrum. These data indicate that the TiO_2 particles may act as a sacrificial material in the conversion coating to getter oxidants and become washed out afterwards.

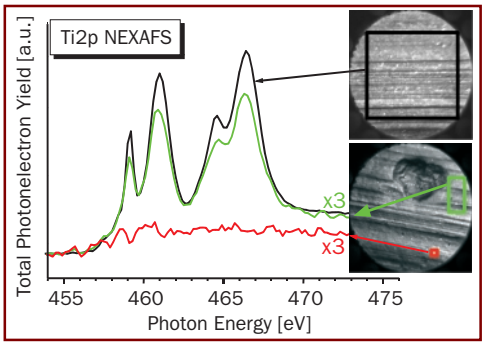

Fig. 4:
Ti2p-μNEXAFS spectra taken on the non corroded sample A (black) and on the marked sample sections of the corroded sample B (green and red, see also Fig. 2).

Our study demonstrates that local corrosion mechanisms are prevented by the Ppy conversion layers. Corrosion does not depend on topographic irregularities and does not proceed via etch pits. Instead there is an inhomogeneous distribution of TiO_2. Obviously, corrosion reduces the total intensity of the TiO_2. Our results indicate that our Ppy coating acts as a sacrificial anode rather than as a barrier coating or a reservoir of ions. Further details of the reactions occurring among the dopants within the Ppy film are currently investigated in order to understand the complex inhibition mechanisms.

Contact:

D. Schmeisser, Department of Applied Physics - Sensors, BTU - Cottbus,

dsch@TU-Cottbus.de

A. Yfantis, Department of Chemical Engineering, NTU - Athens, Greece.

yfantis@otenet.gr

Micro Harmonic Drive® gears made by direct-LIGA

R. Degen[1], G. Gruetzner[2], J. Goettert[3], B. Löchel[4]

1
Micromotion GmbH, Mainz

2
Micro Resist Technology GmbH, Berlin

3
CAMD, Louisiana State University, Baton Rouge, USA

4
BESSY

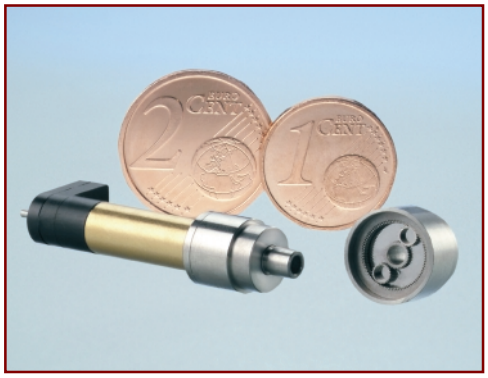

Fig. 1:
MHD-8 Micro Harmonic Drive® gear with Maxon EC6 motor

Dimensions	*8 x 1 mm*
Reductions	*160:1, 500:1, 1000:1*
Related torque	*3 - 20 mNm*
Peak torque	*10 - 40 mNm*
Momentary peak torque	*23 - 100 mNm*
Friction torque (with motor)	*40 - 50 µNm*
Efficiency (with motor)	*67 - 82 %*
Maximum input speed	*30,000 rpm*
Moment of inertia (with motor)	*$18 \cdot 10^{-4} – 23 \cdot 10^{-4}$ gcm²*
Weight (with motor)	*4.5 g*

©Micromotion GmbH, Mainz

The LIGA (Lithography and Galvanic Moulding) process is a widely established technology to produce micro-structured surfaces and components for micro-devices. The LIGA process consists of the three major fabrication steps X-ray lithography, electroforming of a high-precision mould insert, and cost-effective replication using injection moulding or hot embossing. Compared with the 'original' LIGA process the direct-LIGA approach also relies on the lithography and electroplating step but includes surface finishing and assembly of microstructures as further fabrication steps. Although the direct-LIGA production on a commercial scale was proposed more than 10 years ago, it is only due to the recent advent of ultra-sensitive SU-8 X-ray photoresists that the approach is coming closer to reality.

A collaboration of BESSY and the Center for Advanced Microstructures and Devices (CAMD) is now focussing on the direct-LIGA technology for micropart production. The collaboration is completed by Micro Resist Technology GmbH, a producer of advanced photoresists and semi-finished MEMS products, and by Micromotion GmbH, a manufacturer of micro-gears.

The object of the joint project is the development of a backslash-free micro-gear train consisting of only six toothed wheels for applications in manifold industrial products, such as for industrial robots, lens adjustment and optical switches in micro-optics, or micro-dosing pumps and surgical equipment in medicine.

Conventional methods of precision engineering for gear production can be used down to a module of 60 to 100 µm, depending on the tooth geometry. However, there are significant restrictions on an optimal tooth geometry if conventional techniques are applied to manufacture a gear with a module in this size. In order to achieve structures with heights up to several millimeters yet with tolerances better than 1 µm on horizontal dimensions it is necessary to use a lithographic process at a synchrotron X-ray source to pattern the resist. Using direct-LIGA technology, we manufactured the first prototypes of a new micro-harmonic drive gear design, ideally suited for precision positioning applications.

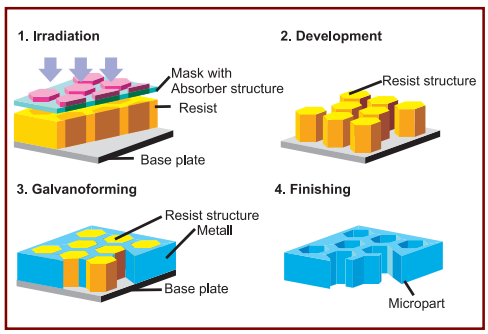

Fig. 2:
Direct-LIGA

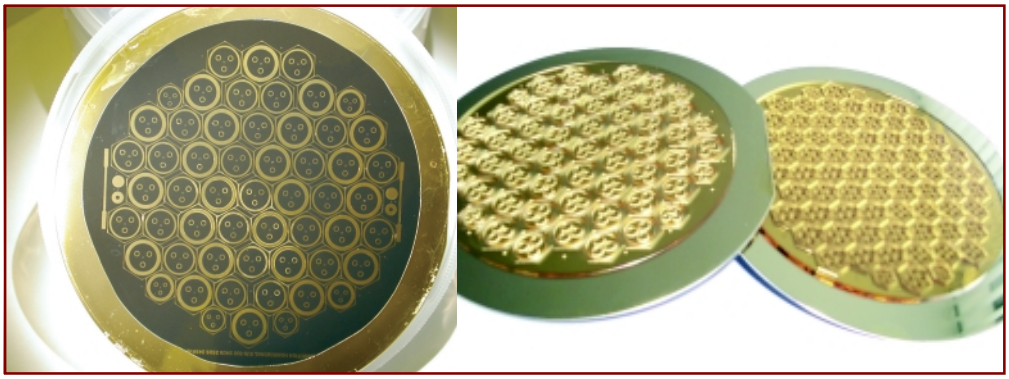

Fig. 3:
X-ray mask and patterned wafer

The main requirements for the realization of the direct-LIGA approach is the availability of a fabrication process for cost-effective X-ray masks and an X-ray lithographic process using highly sensitive resists. In order to meet the industrial demands, X-ray masks have to be available quickly and with an accuracy in the sub-micrometer range. The fast mask fabrication will improve the flexibility during production. New and promising mask membrane materials like graphite, vitreous carbon or glass are under investigation. Reduced costs of these materials will help to control costs for X-ray masks. An improved photoresist process on the base of SU-8 will also help to enhance the direct-LIGA process. The high sensitivity of SU-8 to synchrotron light permits a reduction of exposure times to about 1:100 as compared to the 'conventional' photoresists (PMMA standard). Both mask improvement as well as the resist process upgrade will help to reduce costs of fabrication.

A new market is developing for a new generation of compact lightweight machines and portable devices that can be manufactured with a minimal use of material and can operate precisely with high efficiency. Micro-motors with an outer diameter of just a few millimeters are already available on the market. However, many applications need reduction gears that can provide an increase in torque with minimal loss. Currently available micro-motors generate their maximum torque at high speeds, up to 100,000 rpm, thus demanding a high reduction ratio.

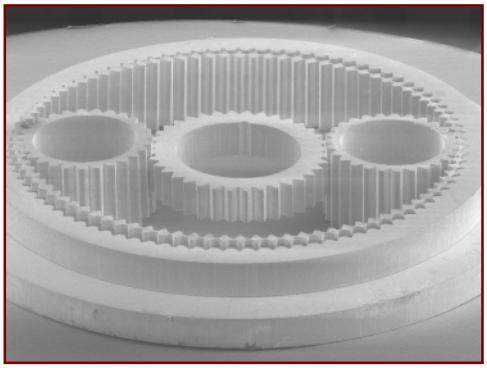

Fig. 4:
Detailed view of a Micro Harmonic Drive®

Many new applications also require high positioning accuracy and precise controlling, both not achieved with previous gear solutions. The new Micro Harmonic Drive® gear design is perfectly suited to precision positioning applications in a wide range of compact machines and portable devices and the fabricated prototypes fulfil the expectations. However, the transfer from ‘prototype development’ to ‘small and larger scale production’ remains a challenge, which will only be met within a close cooperation of all partners.

Contact:
Reinhard Degen,
Micromotion GmbH, Mainz
info@mikrogetriebe.de

Bernd Löchel, BESSY GmbH
bernd.loechel@bessy.de

1
Technische Universität Berlin
2
Staatliche Museen zu Berlin

Micro-XRF goes 3D: X-ray Insights into Indian Mughal Paintings

Birgit Kanngießer[1], Wolfgang Malzer[1], Ina Reiche[2]

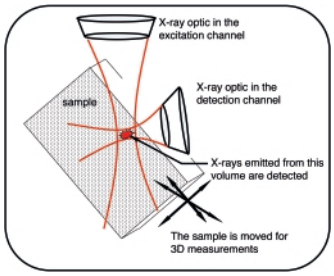

Fig. 1:
Scheme of the confocal set-up for the 3D Micro X-ray Fluorescence Analysis.

A well established, non-destructive method to investigate the composition of manifold materials is X-ray Fluorescence Analysis (XRF). The method relies on the fluorescence radiation after irradiation of the sample with an X-ray beam. The measured fluorescence is element specific and thus allows to determine elemental composition of a sample qualitatively and quantitatively. The spatial resolution is dependent on the excitation spot – size of the X-ray beam. Over a decade ago, the use of X-ray optics improved the spatial resolution to the micrometer range and the so called Micro-XRF has been developed since then very rapidly mainly due to the use of synchrotron radiation in combination with new types of X-ray optics. Micro-XRF already proved to be a versatile tool in a large variety of fields of application like materials science/quality control, environmental science, geology, life science and – since it is a non-destructive method – in archaeometry.

However, Micro-XRF did not allow depth profiling of a sample, which would be necessary to analyze different paint layers on a painting, for instance. Very recently, we improved the method capabilities towards a three dimensional Micro-XRF by realizing a confocal X-ray set-up (Fig. 1). The set-up consists of two X-ray optics: one in the excitation channel and the second in the detection channel. The overlap of the foci of both X-ray optics defines a micro-volume, which can be displaced by either moving the sample laterally or in perpendicular direction to its surface. Thus, depth information can also be obtained. In addition, a better peak-to-background ratio is achieved by restriction of the detector field of view.

The confocal set-up was first realized at the BAM*line*, at BESSY (Fig. 2). After passing through the ionization chamber the X-rays are focused by a polycapillary halflense having a focus FWHM of about 30 μm. The overlap with the focus of the polycapillary conical collimator (poly CCC) adjusted in front of the Si(Li) detector defines a micro-volume. A second detector, a driftchamber detector, monitors the radiation coming from the sample in order to get a global X-ray spectrum. The formed micro-volume was characterized by moving a 2 μm thick Cu foil through the beam. In the horizontal plane with respect to the storage ring the micro-volume had a FWHM of 55 μm, in the vertical direction a FWHM of 35 μm. In addition to the FWHM, the steepness of the slope is decisive for the evaluation of the spatial resolution of the method.

With the possibility to get three dimensional insights into the chemical composition of a sample we applied the new 3D Micro-Fluorescence Analysis method to investigate ancient Indian Mughal miniatures. Mughal miniatures, representations of sovereigns or other important personalities (16th – 19th century), were produced in spezialized workshops in India. These paintings consist of several well separated polished pigment layers on paper but until now, only scarce information is available on the painting technique and the artists pigment palette. Moreover, it is known that from the 18th century onwards there was an important production of miniatures copying master-pieces from the "classical" period, sometimes by overpainting old miniatures of low value. Using our new set-up, we investigated the multiple layers of two miniature and analysed their composition.

Fig. 3 shows a cantle of a classical Mughal miniature dated from the 18th c. (MIK 5004 (3), and the depth sensitive analysis of the represented red fence. The depth profile revealed a layered structure of a 10 μm thick cinnabar (HgS) layer, which was painted on a lead white ($PbCO_3 \cdot Pb(OH)_2$) ground layer

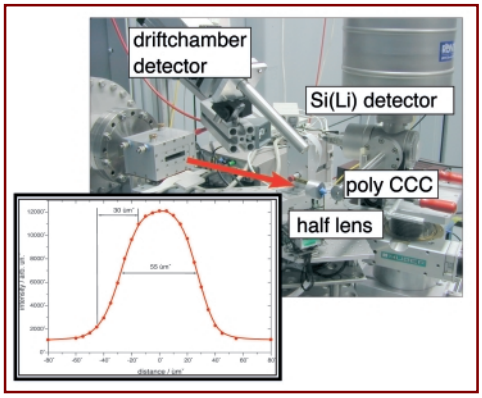

Fig. 2:
BAMline with confocal set-up at BESSY.

References:

[1] I. Reiche et al., "Röntgenanalyse in der Kunst" Physik in unserer Zeit 34(2), 80-86 (2003).

[2] B. Kanngießer et al., submitted for publication.

Supported by the DFG.

Shown miniatures are courtesy of Staatliche Museen Berlin, Museum für Indische Kunst.

Ina Reiche is now at the Laboratoire de recherche des musées de France - UMR 171 CNRS, Louvre, Paris, France

of the same thickness. These results confirm the use of classical pigments and a layered painting technique of Mughal miniatures.

Another investigated miniature, shown in Fig. 4 (MIK 5004 (10)), is dated from the second half of the 17th century, for stylistic reasons. The element depth profiles for the turquoise background clearly showed a single paint layer with Cu, Pb and Zn as the main components. These results are surprising as up to now there is no evidence of the use of Zn and Sn containing pigments in art before the beginning of the 19th century, at least in Europe. In addition, the investigation of the white dagger showed a three layered struc-ture which is in its succession inverted to the expected one. In the first layer on the paper, only Pb is detected. The second layer shows a mixture of mainly Pb, Zn, and Sn. And there seems to be a very thin third layer containing mainly Pb on the top. Thus, this painting represents either the first scientifically proved sample of an early use of zinc white in India or it is simply a copy manufactured in the 19th century. The analysis and comparison of ancient zinc white pigments from India will contribute to solve this problem, eventually.

The first archaeometric results show the potential of the new 3D Micro X-ray Fluorescence Analysis set-up. Successive paint layers were distinguished with a resolution of about 10 μm. Major and minor elements are detectable even if the same element occurs in different layers. This opens up the way for the non-destructive investigations of paint layers, underdrawings, metal surfaces, glass surfaces/glazes, inclusions in gemstones and many more, helping to answer questions in archaeology and art history. But the new 3D Micro XRF method is not restricted to archaeometry. It can make important contributions to all fields of application in material and environmental research. In life sciences, 3D Micro XRF analysis of histological samples emerges as an promising research field. A combination of 3D Micro-XRF with Micro-XAFS for chemical speciation and with Micro-XRD for phase information will be a unique tool at BESSY.

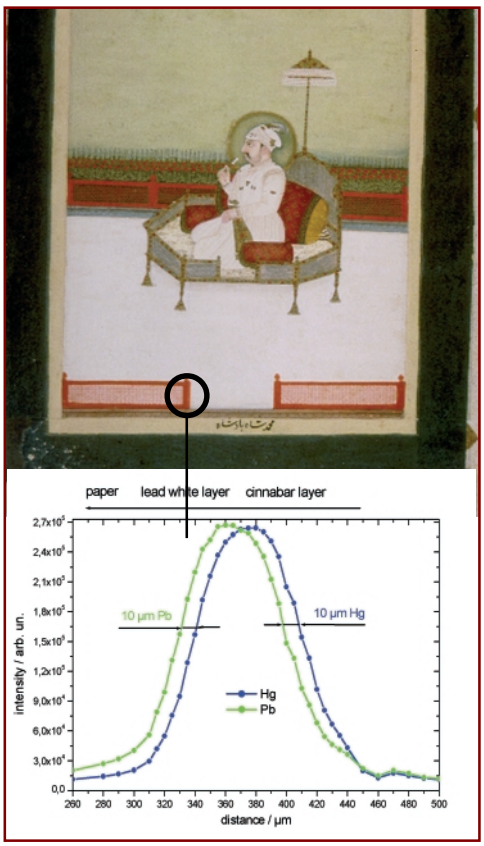

Fig. 3:
Micro-XRF depth profiling of a classical Mughal miniature MIK 5004 (3) dated to the 18th century.

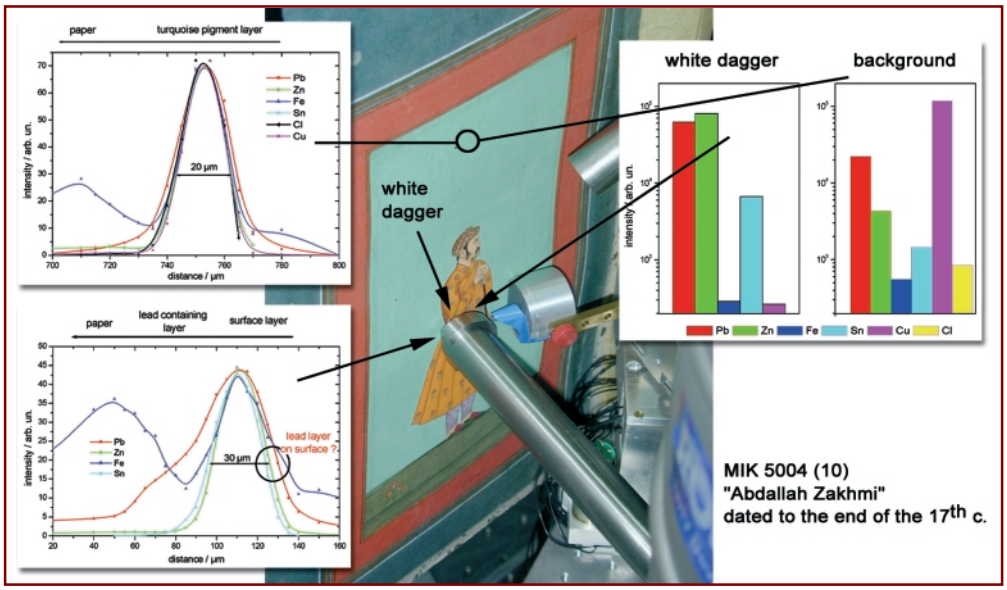

Fig. 4:
Micro-XRF depth profiling of a Mughal miniature MIK 5004 (10) "Abdallah Zakhmi" of doubtful origin (stylistically dated to the 17th century). Intensity curves are scaled to the same maximum height for a better comparison and bar graphs compare the maximum relative intensity of the elements detected.

Contact:
Birgit Kanngießer,
Institut für Atomare Physik und Fachdidaktik, Technische Universität Berlin
bk@atom.physik.tu-berlin.de

Structural Genomics at BESSY: From Gene to Protein Structure in Two Weeks

B. A. Manjasetty[1,2,7], H. Delbrück[1,3], P. Dinh-Trung[1,4], U. Mueller[1,3], M. Fieber-Erdmann[1,3], V. Sievert[1,5], K. Büssow[1,5], F. H. Niesen[1,6], W. Weihofen[3], B. Loll[3], W. Saenger[3], K. P. Hofmann[6], U. Heinemann[2,3]

1 Protein Structure Factory, Berlin

2 Max-Delbrück-Centrum für Molekulare Medizin, Berlin

3 Freie Universität Berlin

4 Alpha-Bioverfahrenstechnik GmbH, Kleinmachnow

5 Max-Planck-Institut für Molekulare Genetik, Berlin

6 Universitätsklinikum Charité, Berlin

7 On leave from: Government Science College, Bangalore, India

Investigations aimed at a complete understanding of the structure and function of genes and gene products in all life forms are rapidly progressing due to the availability of genome sequences. Structural genomics initiatives all around the world begun to develop and implement technologies that will permit to determine three-dimensional protein structures at high throughput in a automated fashion [1]. The Berlin Protein Structure Factory (PSF) is a structural genomics project which has set out to determine the three-dimensional structures of medically relevant human proteins by implementing and utilizing high-throughput technology. Within the PSF, the structure determination process incorporates in a factory-like production line all steps from gene target selection, protein purification and characterization, crystallization and structure solution.

The structure solution involves collecting multiple or single wavelength anomalous dispersion (MAD or SAD) data at a synchrotron beamline; solving the phase problem; tracing the electron density map and building the model; refining the structure and finally, drawing functional inferences from the solved structure. At this juncture, facilities for partial automation of all steps have been established at the BESSY electron storage ring, from crystal mounting to an interpretable initial electron density map, under the auspices of the PSF structural genomics project.

During 2002 the PSF facilities at BESSY have been completed and several structures have been solved using the PSF beamlines. We describe here the first protein structure which has been determined in 'factory style' from target selection to structure solution, taking only 2 weeks for completion.

Human protein hp14.5 is a member of the large protein family (Yjgf-like proteins) with unknown biological function. Although the molecular function of this protein family is not clear, previous studies suggest that it plays a role in the regulation of metabolic pathways and cell differentiation [2]. Recently, hp14.5 is identified as a tumor associated antigen derived from hepatocellular carcinoma [3]. The three-dimensional structures of hp14.5 homologs from *Bacillus subtilis* Yabj and *E. coli* Yjgf are known. These structures suggest that nine amino acid residues, which are also found in many other proteins of the Yjgf-like family, map to the narrow, deep cleft between the subunits [4, 5]. This conserved site has been proposed as substrate binding or catalytic site, but structures are unable to give a clue to the common biochemical mechanism for their variety of biological functions.

In order to elucidate the molecular mechanism of this protein family we have solved the crystal structure of human p14.5 by Hg-SAD methods. An Hg-derivative was prepared by soaking the crystals with 15 mM ethyl-Hg phosphate (EMP) for 30 min. A characteristic Hg L_{III} spectrum has been observed by scanning the crystals for fluorescent photons at the Hg lines. For data acquisition, the crystal was flash-cooled to 100 K. Single wavelength anomalous diffraction data at the Hg L_{III} edge to 2.3 Å resolution on a Hg derivative and high resolution 1.9 Å native data were collected on the MAR345 imaging plate detector at beamline PSF-ID14.2 (7TWLS/2-KMC2).

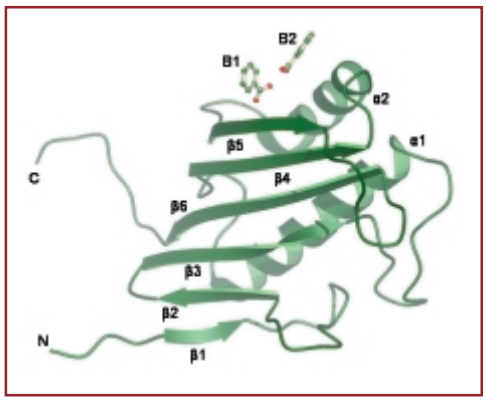

Fig. 1:
Ribbon diagram of human p14.5 monomer. The benzoate anions are also shown as ball-and-stick representation.

References:

[1] U. Heinemann et al., Acc. Chem. Res., (2003) in press.

*[2] J. M. Kim et al., Genes Cells **6**, 507-517 (2001).*

*[3] F. Stenner-Liewen et al., Cancer Epidemiol. Biomarkers Prev. **9**, 285-290 (2000).*

*[4] S. Sinha et al., Proc. Natl. Acad. Sci. USA **96**, 13074-13079 (1999).*

*[5] K. Volz, Protein Sci. **8**, 2428-2437 (1999).*

*[6] T. C. Terwilliger et al., Acta Crystallogr. D **55**, 849-861 (1999).*

*[7] T. C. Terwilliger, Acta Crystallogr. D **57**, 1755-1762 (2001).*

*[8] G. N. Murshudov et al., Acta Crystallogr. D **53**, 240-255 (1997).*

Funded by the BMBF

Fig. 2:
Human p14.5 trimer. The view is along the non-crystallographic threefold symmetry axis.

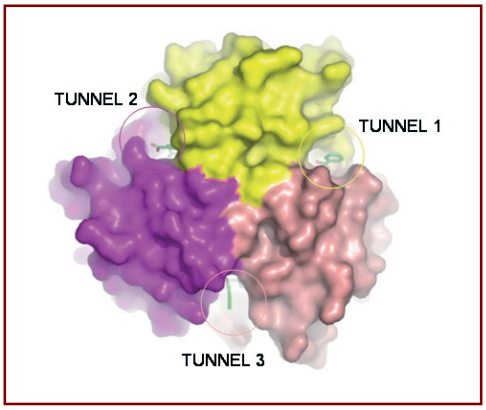

Fig. 3:
Molecular surface representation of the human p14.5 trimer. The surface was colored by chain. Three active tunnels are seen at the subunit interface.

Subsequent to data processing and location of the mercury atoms, anomalous phasing and refinement of the Hg locations were done with the program SOLVE [6]. The obtained experimental phases were subjected to solvent flattening and automatic model building with the program RESOLVE [7]. The program was able to automatically trace 682 out of 1233 residues. To this stage, our experiment at the BESSY site, including heavy atom derivatization, data collection and initial structure determination was finished within 24 hours.

The phases were further improved by nine-fold non-crystallographic symmetry averaging along with automatic model building and refinement with the program RESOLVE in combination with REFMAC [8] which yielded 925 out of 1233 residues. The final stages of model rebuilding and refinement with the program REFMAC (R_{free} = 25.6% and R = 20.6%) is underway.

The hp14.5 monomer chain, comprised of 137 residues, adopts a chorismate mutase-like fold (Fig. 1). Like homologous structures, hp14.5 is present as a symmetric trimer in crystals (Fig. 2). The hp14.5 trimers are related by non-crystallographic symmetry. There are three trimers (a total of nine hp14.5 molecules) in the asymmetric unit of the crystal. The most important finding in the structure is the binding of two benzoate molecules per hp14.5 protein subunit. The interface between two hp14.5 monomers forms an approximately 12 Å deep and 8 Å wide conserved cleft or tunnel on the surface of the trimer (Fig. 3). Two benzoate molecules are clearly visible within the tunnel (Fig. 4). One is deeply buried in the cleft and adopts a similar orientation in all clefts. The other benzoate molecule is found in two distinct orientations, seemingly either entering or leaving the binding site.

Sodium benzoate was present in the crystallization buffer at 35 mM concentration, indicating protein binding with a low dissociation constant. The nine invariant residues of the Yjgf-family proteins are arranged around the benzoate-binding cleft.

The localization and conformation of the bound benzoate molecules will help us to derive the common biochemical mechanism underlying the wide variety of biological functions of this protein family in order to understand its role in cell differentiation and hepatocellular carcinoma.

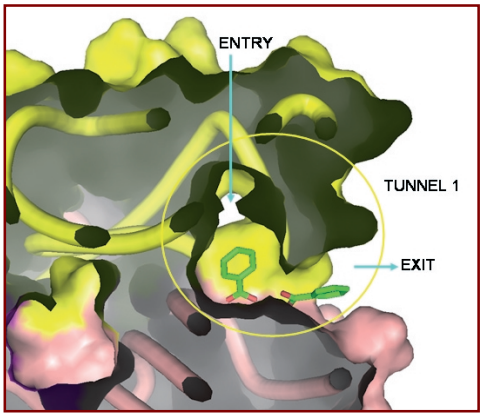

Fig. 4a:
Zoom view of the ligand bound at the tunnel 1.

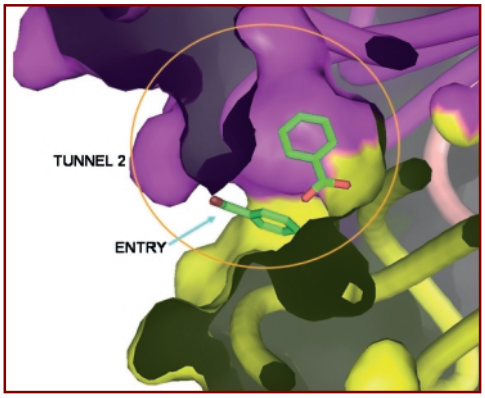

Fig. 4b:
Zoom view of the ligand bound at the tunnel 2.

Contact:
Udo Heinemann,
Forschungsgruppe Kristallographie, Max-Delbrück-Centrum für Molekulare Medizin, Berlin
heinemann@mdc-berlin.de

3 News & Events

Prof. Dr. Dr. h.c. Wolfgang Eberhardt awarded the honorary doctorate at Uppsala University.

The BESSY future project the design and construction of a soft X-ray FEL passed another milestone towards its completion in 2008. In the evaluation of nine large scale research projects, the German Science Council (Wissenschaftsrat) gave the scientific case of the soft X-ray FEL an excellent rating indicating the high international standard of the project. BESSY has been given the go-ahead to complete the technical design by the beginning of 2004 with the chance of becoming a leading european research center in the XUV spectral range.

BESSYs scientific director, Wolfgang Eberhardt, has been awarded an honorary doctorate at Uppsala University in recognition of his significant contributions in the field of Synchrotron Radiation Research. He has a long standing collaboration with researchers from Uppsala. These contacts will be increasingly important since the further development of the next generation synchrotron radiation sources, including Free Electron Lasers, will require even deeper international collaboration and coordination.

The 60th birthday of Gottfried Mülhaupt, the first BESSY technical director (1978 – 1986), was celebrated with a scientific colloquium on the topic of 'Synchrotron Radiation Sources – Past and Future'.

Among numerous scientific lectures and the new 'science on the fly' user talks, the contributions of Joachim Treusch (Chairman of the Supervisory Board) on the future of research caught particular interest.

Not only scientists from all over the world came to BESSY, non-scientists did as well. Almost 2000 people visited BESSY in 2002, among them, internationaly high ranking persons such as the King and the Queen of Jordan, the Prime Minister of Malaysia, and the Berlin Senator of Science, Research and Culture, Thomas Flierl. About a quarter of these visitors were pupils, even school children from Austria, Denmark and Norway.

And finally…

…a last farewell for BESSY I, which was shipped to Jordan in 2002, where it will form the core of the SESAME radiation source to be built close to Amman, a major UNESCO funded scientific research and training centre for Middle Eastern scientists in structural biology, environmental and materials science.

King Abdullah II. and Queen Rania of Jordan

Prime Minister of Malaysia on his tour at BESSY

Senator Dr. Flierl in discussion with Prof. Dr. Jaeschke

BESSY I on its way to Jordan

Events

As in the previous years, 'Berlins Long Night of Science' (Lange Nacht der Wissenschaften) was a major highlight in the BESSY calendar. On June the 15th, a new record number of 6,000 interested visitors populated the experimental hall and ring tunnel and enjoyed the Physics Show of the 'Physikanten', which was sold out on every one of their four performances. Groups of pupils from several schools explained physical experiments to children and adults. In addition, BESSY offered guided tours to families.

At the same time, BESSY presented the principle of a synchtrotron radiation source at the ScienceFair, which took place at the Breitscheidplatz in the Berlin city center.

During the summer holidays, BESSY scientists explored a new way to mix science and entertainment by inviting the public to a Sunday breakfast lecture on physics (Physik zum Frühstück) co-organized by the 'Schaustelle Berlin'. More than 120 people attended the two lectures. As a result of this success a similar event will be offered in 2003.

As a member of the Leibniz-Association, BESSY participated in two presentations of the Leibniz Research Institutes for members of the European and German Parliaments in Brussels and Berlin.

A synchrotron light source explained by model railroading: The President of the Bundestag Wolfgang Thierse visited BESSYs presentation at the ScienceFair.

Discussions during the IR Workshop

Workshops 2002

February, 4 – 8	*Course on Experimenting with Synchrotron Radiation*
May, 22 – 23	*EPICS Collaboration Meeting Spring 2002*
October, 8 – 9	*ISGO-Satellite Workshop: Automation of X-ray Structure Determination for Structural Genomics*
September, 3	*Workshop on Application of Microfocus X-Ray Sources in Material-, Environmental-, Life-Science and Archeometry*
September, 23 – 24	*ESF Workshop on Exploiting the Coherence of X-rays*
October, 21	*BESSY Forum*
November, 18 – 19	*IR-Workshop: Time Resolved, Coherent and Other Advanced IR-Experiments Using Synchrotron Radiation*
December, 4	*BESSY-FEL Workshop*
December, 5 – 6	*BESSY Users' Meeting*

Of several art exhibitions, the "LIGHT-objects" of the Berlin sculptor Micha Koch illuminated the BESSY foyer during the long winter nights.

Users' Meeting 2002

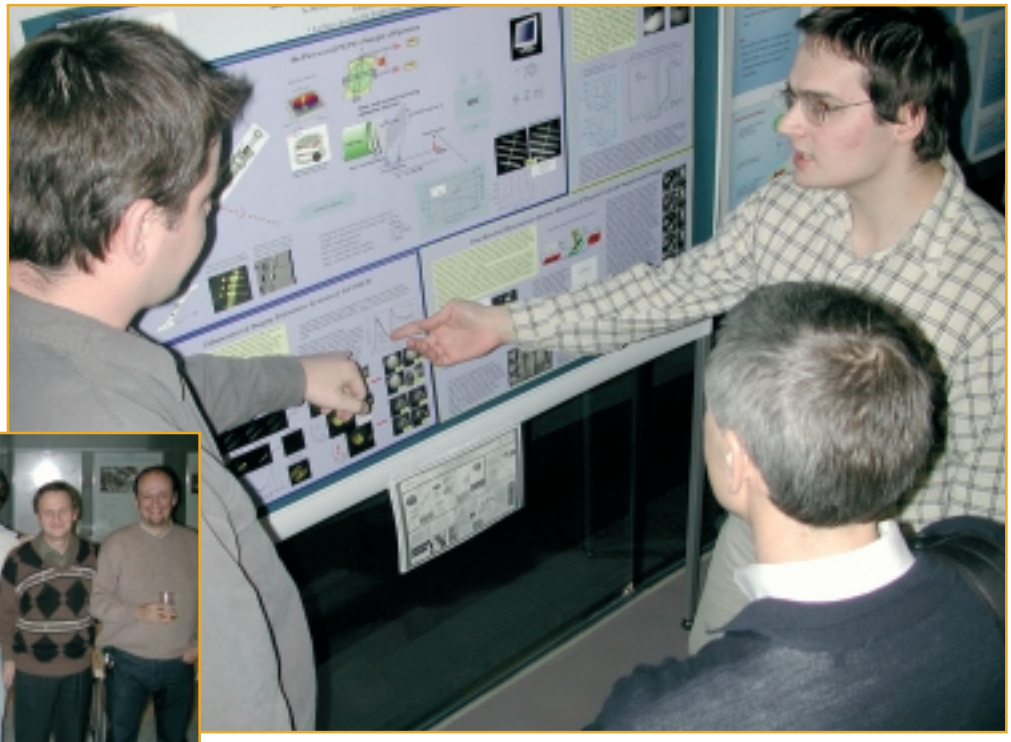

This years BESSY Users' Meeting in early December was frequented by almost 300 participants presenting their scientific work on some 100 posters in the experimental hall.

In the opening keynote lecture Jürgen Kirschner, executive dirctor of the MPI of Microstructure Physics, gave an intriguing overview of the developments in nanomagnetism. This topic was again addressed in the subsequent presentations, followed by talks on semiconductors, atomic physics, microengineering as well as microfocus applications in archeometry allowing a glimpse into the variety of research projects performed at BESSY. The recent results obtained with THz-radiation at BESSY have been especially highlighted. In the status reports of BESSY, Peter Kuske and William Peatman presented the ongoing developments of machine and beamlines, and Walter Braun summarized comments and suggestions from user beamtime reports.

The poster prize was awarded to Ina Reiche (Staaliche Museen zu Berlin), for bridging the gap between art and science by investigating silver pencil drawings with X-rays.

The vendor exhibition enabled the participants to keep in touch with suppliers of highly specialized components and recent technological developments for their research at BESSY.

Ernst Eckhard Koch Prize

Traditionally, the award of the Ernst-Eckhard-Koch Prize of the Society of Friends and Sponsors of BESSY takes place on the Users' Meeting. The prize is annually awarded for an outstanding PhD thesis using synchrotron radiation at BESSY or HASYLAB. This years' award was shared among Tobias Lau (Universität Hamburg) and Fabrice Wilhelm (Freie Universität Berlin) for their studies on the magnetic behaviour of clusters and thin magnetic multilayers by magnetic circular dichroism.

Tobias Lau focused on the evolution of magnetism of supported iron clusters with increasing size. He showed that for sub-nanoscale particles the magnetism depends strongly on the number of atoms in the particles and that every atom counts when it comes to understanding their magnetic properties. Fabrice Wilhelm investigated how magnetism is induced at the interfaces of two metallic (e.g. nickel/platinum) layers.

Drs. Fabrice Wilhelm (left) and Tobias Lau (right), laureates of the the Ernst-Eckhard-Koch Prize

Innovation Award on Synchrotron Radiation

Dr. Ralf Röhlsberger received the Innovation Award on Synchrotron Radiation 2002 from Prof. Dr. Wolfgang Gudat the chairman of Society of Friends and Sponsors of BESSY

For the second time, the Society of Friends and Sponsors of BESSY awarded the Innovation Award on Synchrotron Radiation for excellent achievements, which contributed significantly to the further development of techniques, methods or uses of synchrotron radiation. The award is announced europe-wide.

In 2002, Ralf Röhlsberger (Universität Rostock) received the Innovation Award for his pioneering work on nuclear resonance absorption of synchrotron radiation. The physicist developed a new method where the sample rotates 35,000 times per second while it is excited by synchrotron radiation.

The angle of the emitted radiation depends on the lifetime of the excited nuclear levels and on the momentum of the sample. This allows new and very exact spectroscopic studies to be made for example on magnetic samples, without changing the storage ring to a specific operation mode. The so-called 'Nuclear Lighthouse-Effect' is only a part of the exciting successful work of Ralf Röhlsberger.

4 Facility Report

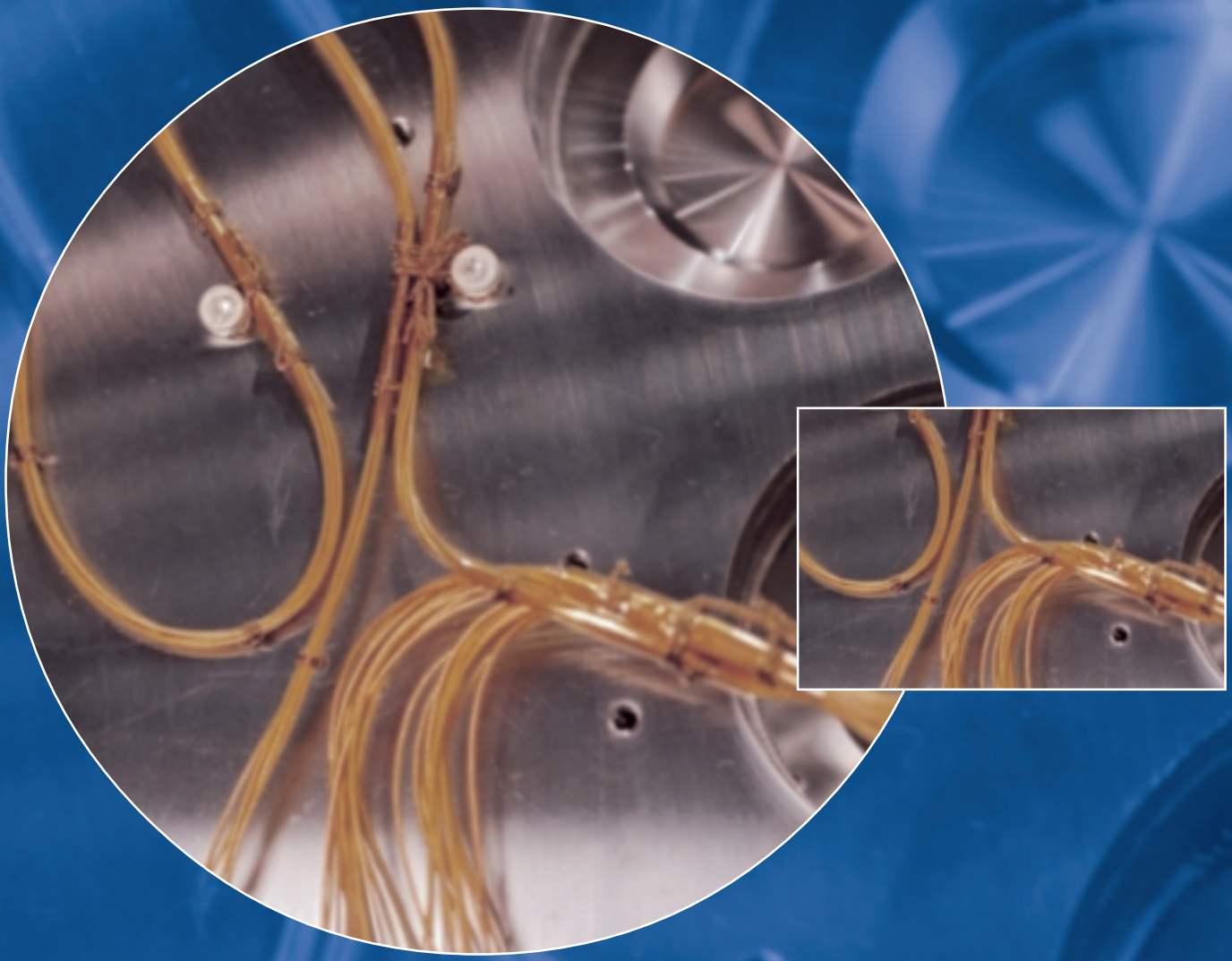

Machine Status

In 2002 the BESSY light source has been in user operation for 30 weeks and 4,167 h of beamtime were delivered. Five weeks of machine shifts were dedicated to further improvements of beam quality and to the creation of coherent synchrotron radiation by running the lattice in a special mode which produces very short bunches. During two shutdown periods, four new insertion devices and new hardware components have been installed in the storage ring in order to extend the spectral range and to enhance performance and reliability of the facility. In addition to the two APPLE-type undulators (UE 46 and UE 52), two 7 Tesla superconducting IDs, the wavelength shifter for the protein structure factory (Fig. 1) and the 7 Tesla HMI multi-pole wiggler have been inserted. After the first tests with beam the wiggler had to be removed again from the storage ring for mechanical modifications of the in-vacuum cold shield. The improved ID will be reinstalled during the spring shut down of 2003. Meanwhile, 13 out of 16 straight sections are already equipped with IDs and preparations started to clear part of the diagnostic straight section in order to install ID number 14 by the end of 2003.

Orbit Stability

The achieved long term orbit stability is well below the original target specifications of 10 % of the beam size. This year the attention was focused on the short term stability of the beam position since the recently installed IR-beamline (IRIS) is very sensitive not only to slow but also to faster orbit motions.

Careful investigations of the continuously monitored beam position in the storage ring gave valuable indications of sources of beam motion. For example repetitive vertical orbit distortion could be traced back to the cryogenic coolers of the superconducting insertion devices and occasionally to a strong switched magnet operated by a user group. When the central cryogenic plant will be available mid of 2003 operation of local closed cycle cryogenic coolers will be dispensable.

Fig. 1:
Installation of the 7 Tesla wavelength shifter for the protein structure factory.

Lifetime Improvements

Four modified 3rd harmonic cavities were installed in front of the BAM-WLS during the spring shut down (Fig. 2). These cavities are equipped with dampers for higher order modes and more reliable mechanical tuners. Above 150 mA the beam induced voltage can be kept constant by automatically tuning the cavities and a current independent bunch lengthening of 30 % is achieved. Under normal operating conditions the reduced particle density leads to an improvement of the lifetime by 20 %. The product of beam current and lifetime approaches 2 Ah.

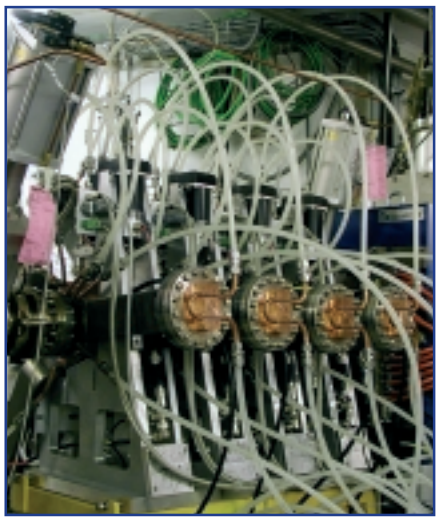

Fig. 2:
Photo of the four 1.5 GHz Landau cavities installed upstream of the BAM-WLS.

Low alpha-Mode

The BESSY II storage ring can be operated in a dedicated so called low α-mode.
The rms-bunch length in single bunch mode is a function of the beam current and ranges from 15 to 30 ps. By lowering the momentum compaction factor (α) – low α-mode – the bunch length can be reduced to 2 ps. These short bunches emit coherent radiation at wavelengths larger than the bunch length. Due to current dependent instabilities short bunches are restricted to low intensity (Fig. 3). For more information see SPECIAL (p. 48)

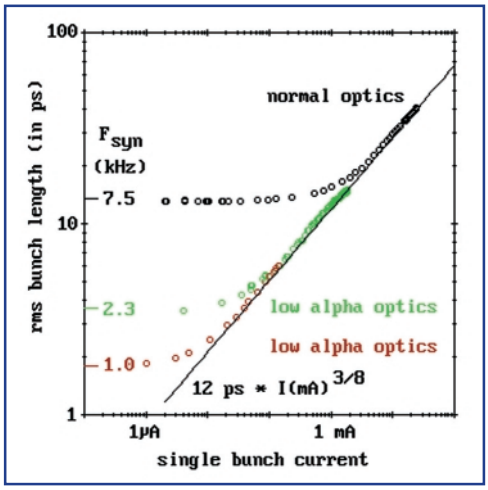

Fig. 3: Bunch length as a function of the beam current. Only at low current bunches are really as short as expected.

Future Activities

Activities during the forthcoming shut down periods will concentrate on required hardware improvements including reinstallation of the superconducting multi-pole wiggler, moving diagnostics components, and preparations for the bunch slicing project for producing femto second light pulses.

Currently, a superconducting 1.5 GHz cavity designed in cooperation with Cornell University is in production and expected to be ready for installation in 2003. With this cavity, bunch lengthening and shortening can be achieved even in single bunch mode. Work during the machine development shifts will be devoted to orbit stability and lifetime improvements. In addition, continuous efforts will be made to keep BESSY the leading facility for producing coherent synchrotron radiation.

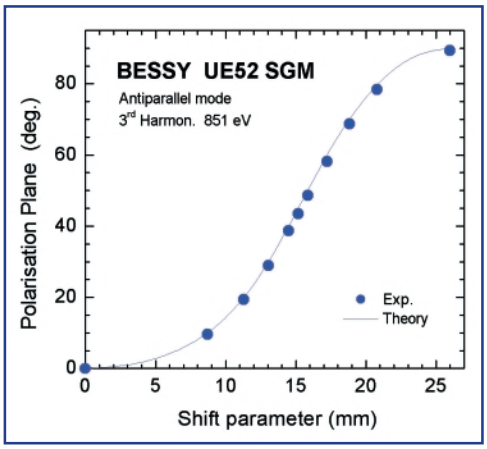

Fig. 4: Measured polarisation characteristics of the UE52-SGM. The polarisation plane can be continuously rotated from horizontal to vertical orientation whilst remaining the degree of polarisation and the intensity constant.

Beamline Developments

Maintenance Routines

Only four years after the first light, BESSY II is now a rather well developed SR-source, with the largest number of undulator and bending magnet systems of the European 3rd generation of soft X-ray facilities in operation. A major task of the optics group is the permanent maintenance and improvement of the beamlines. Weekly commissioning shifts for undulators and beamlines are absolutely inevitable to guarantee for the perfect operation of these complex systems at maximum performance.

Energy calibration, flux values, contamination effects, polarisation characterisation, focus position measurements, test and elimination of vibrational and thermal influences are only some aspects of these routine tasks. The optimised simultaneous scan of undulator harmonics and monochromator energy under full user control is a challenging task. User friendly computer software and proper adjustment of the drive tables have to be checked on a regular basis.

Undulator beamlines

Major highlights of 2002 were the start of two new APPLE II undulator systems. These insertion devices allow for a free choice of polarisation between right and left handed circular polarisation (parallel mode) and linear polarisation in any orientation between horizontal and vertical (antiparallel mode).

The great demand of beamlines with variable polarisation encouraged us to replace the planar ID U49/1 (which is now operated by the PTB alternatively to their U180) by an elliptical ID, the UE52. Both existing beamlines at this ID, a PGM and a SGM, could be continuously operated without any modification, thus allowing for first user runs only one week after installation of the new undulator. Nevertheless, some weeks for commissioning especially for characterization and optimization of the polarization features were essential. The variability of polarisation has been demonstrated for the 1st, 3rd and 5th harmonic by a full polarisation analysis using the BESSY polarimeter.

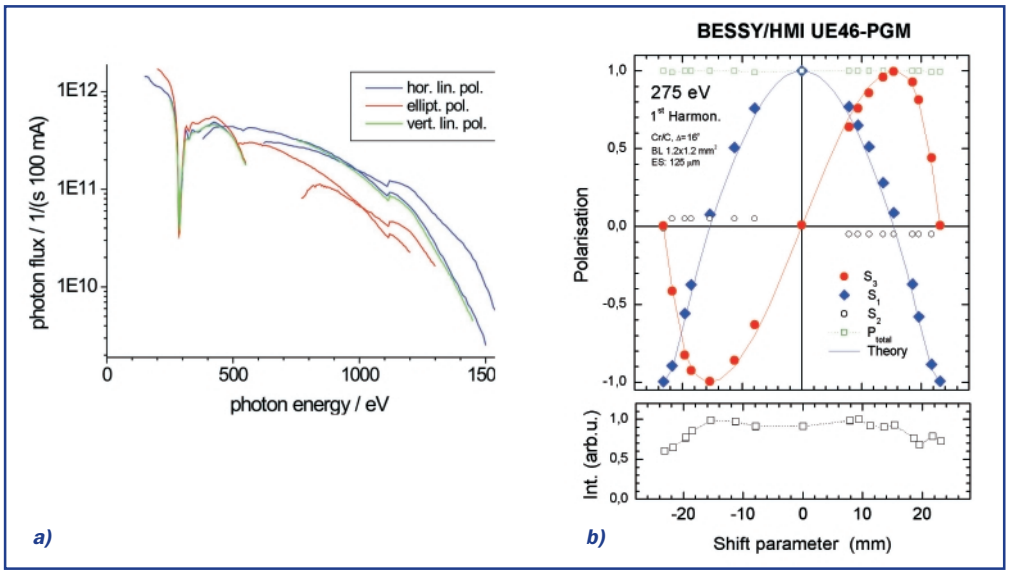

Fig. 5:
Photon flux and polarization at UE46 PGM

The degree of circular and linear polarisation as a function of the shift parameter shows the expected behaviour, known from the UE56. Fig. 4 shows the tuneability of the orientation of the polarisation plane from horizontally (shift 0 mm) to vertically (shift 26 mm) at 851 eV. While rotating the polarisation plane, the other radiation characteristics are maintained: the radiation is completely linearly polarised within 3%, the intensity variation is below 4%, the photon energy is stable as well as the focus position at the experiment. With this undulator, BESSY offers an experimental tool which will open up new avenues in basic and applied research of non isotropic systems. The mechanical rotation of the sample, i.e. its preferred axis, with respect to the polarisation plane, causing an essentially unavoidable shift of the light spot, is not needed anymore. Now, simply the polarisation plane can be rotated, probing always the same area. Investigations of the polarisation dependent angular photo-electron distribution in atomic physics will benefit as well as the spectroscopy and especially microscopy of antiferromagnets.

At UE46, the second ID of this type, a PGM beamline went into operation, a project realised by the HMI in co-operation with BESSY (Fig. 5). Polarisation measurements were performed with the newly developed miniaturised BESSY-polarimeter, which is now on loan to the Swiss Light Source for characterization of their first beamlines build according BESSY-PGM-designs.

Protein Structure Factory Beamlines at 7T Wavelength Shifter

The X-ray beamlines KMC-1 and KMC-2 of the PSF-7T-WLS started operation in 2002. These two tuneable energy beamlines provide photons in the range from 5 to 16 keV with typical spot size of 200 µm x 100 µm which are ideally suited for typical protein crystals (Fig. 6, left). The photon flux at the place of the sample was estimated to be $0.8 \cdot 10^{11}$ Ph/s at 12.65 keV with a slit diameter of 200 x 200 µm². The right panel of Fig. 6 shows the absorption of a Cu foil (d = 5 µm) measured with the ionisation chamber installed at the beamline.

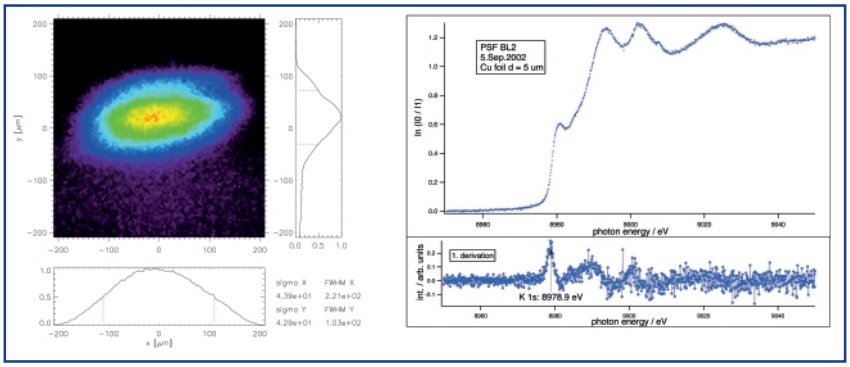

Fig. 6:
Typical spot size (left) and absorption of a Cu foil (right) at the 7T WLS/2-KMC-2

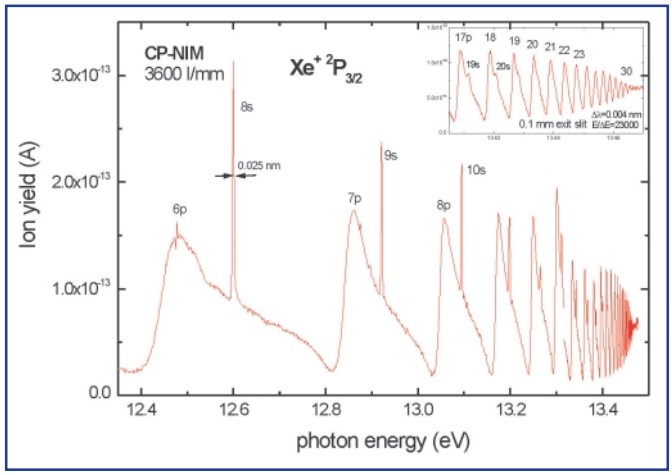

Fig. 7:
Autoionisation resonances of atomic Xenon between the $5p_{3/2}$ and $5p_{1/2}$ thresholds demonstrate the high resolution capabilities of the CP-NIM.

Bending Magnet Beamlines

The installation of field proven BESSY I beamlines went on successfully in 2002. As already seen with the Normal Incidence beamlines 3m-NIM-1 and -2, the superior quality of the source and the now available accuracy of optical components together with a careful set-up procedure make these refurbished beamlines attractive sources for a variety of experiments.

In order to fulfil the user demands for low energy circular polarized UV radiation two BESSY I monochromators have been reinstalled. The plane grating monochromator PM3, has been set-up at BESSY II with an improved optical design. The grating works now in vertically collimated light, allowing free variation of the c_{ff}-factor. Off-plane dipole radiation can be deflected onto the grating by a small tilt of the entrance mirror around its long axis.

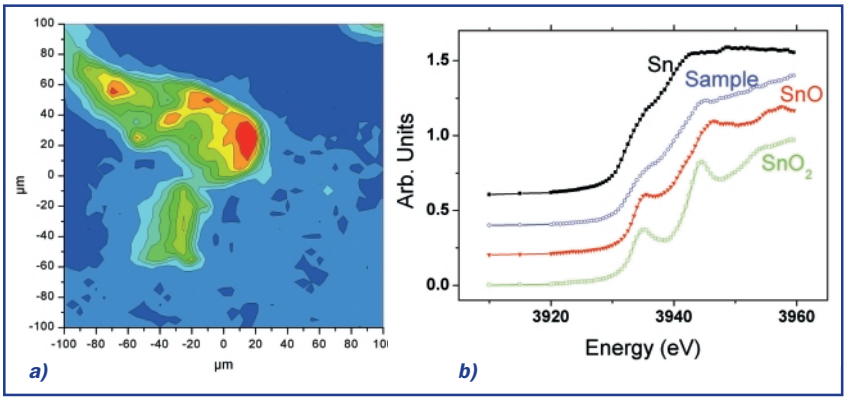

Fig. 8:
Amalgam mirror degradation. Hg forms small drops of about 10 μm in size. Micromap recorded at 12.4 keV (left).
XANES spectra at the Sn L_{III} edge in comparison with the reference materials (right).

The beamline covers the photon energy range 30 – 2,000 eV with adjustable polarization and is especially suited for long scan EXAFS type measurements. Standard value of the helicity at the Fe 2p edge is 92.5%.

6.5 m NIM has been re-set into operation as CP-NIM. The Monk-Gillieson type optical layout of a plane grating in a convergent light beam remained unchanged, but the focusing geometry had to be adapted to the new source. The radius of the pre-mirror is now 10.3 m making a 2:1 demagnification of the source on to the exit slit. Off-plane bending magnet radiation is used for creation of circular polarized radiation, which is horizontally dispersed to conserve the polarisation. The circular polarisation (left-right helicity) can be selected by vertical apertures.
The energy resolution has been determined using an ionisation chamber filled with Xe by recording the autoionisation range between the $5p_{3/2}$ and $5p_{1/2}$ photoionisation threshold (Fig. 7). The np series could be traced up to at least n = 30, corresponding to a resolving power of at least 0.004 nm at an exit slit of 0.1 mm and a resolution of $\lambda/\Delta\lambda$ of 23,000 exceeding the available BESSY I data by a factor of 50. Thus, this beamline has turned into a high resolution monochromator while keeping the flux in the range between 10^{10} and 10^{11} photons/second/100 mA ring current.

After adaptation to the new source, the HESGM monochromator (formerly HETGM2) successfully went into operation at DIP08.1A. Flux values in the 10^{10} - 10^{11} ph/(s·100mA) range were reached, meeting the design values, with considerably improved resolution as compared to the “old” HETGM2. The beamline was set up in cooperation with the Bundesanstalt für Materialforschung (BAM) and the universities of Bochum, Osnabrück and Heidelberg.

The crystal monochromator KMC-2 has been drastically improved by the installation of new crystals. It is the first middle-energy X-ray beamline with graded SiGe (111)-crystals. The beamline is operated at a bending magnet source in the energy range of 2.1 to 15 keV, reaching an energy resolution of 5,000. The KMC-2 is used for a wide

range of experiments, including EXAFS/XANES, diffractometry, fluorescence analysis, powder diffraction, standing-wave technique and X-ray optics tests. Recently a micro-focus add-on system based on elliptical glass mono-capillaries was successfully used for EXAFS/XANES and micro-fluorescence measurements of crystalline and amorphous samples. Fig. 8 shows the micro-map and XANES spectra, measured on a reference sample and a baroque Sn/Hg amalgam mirror with 5 µm spatial resolution.

Pushing the frontiers

In order to meet future demands either for the proposed FEL-beamlines or improved undulator beamlines BESSY has joined a cooperative research project called "Nanometer Optikkomponenten (NOK)". The NOK-project with its eleven partners from german industries and science was established with the goal to provide optical components for use in SR-research with an accuracy that exceeds the present technical limits of 0.1 arcsec rms for the slope error of mirrors and grating substrates.

At BESSY a measuring machine for determination of the slope deviation was developed (Fig. 9). The 'Nanometer Optikkomponenten Messmaschine' – NOM is able to acquire information about slope and height deviations of a sample of up to 1,200 mm in length (Fig. 10). By means of line scans in both dimensions surfaces of up to 600 cm^2 were inspected with an estimated measurement uncertainty <0.01 arcsec rms.

The industrial partners have taken the task to develop surface figuring and polishing techniques. A plane mirror of 510 mm length with a slope error of 0.04 arcsec rms was tested at BESSY. Additionally, a grating substrate of <0.04 arcsec rms illustrates the achieved level of accuracy.

In order to meet these excellent accuracies of optical components new drive mechanisms for monochromators have been exploited. A new generation of piezoelectric motors has been installed in the monochromator drive unit of the U125/2-10m-NIM.

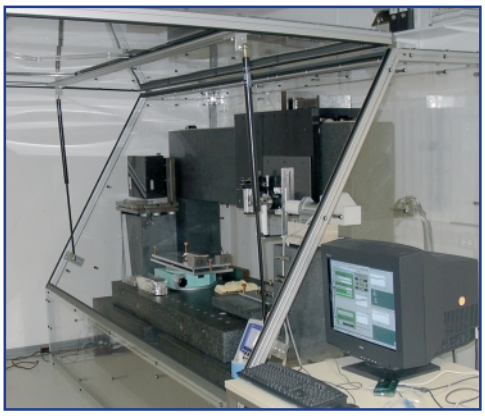

Fig. 9:
The Nanometer-Optical-Component-Measuring Machine - NOM – a development of BESSY.

These motors allow for large drive distances (only limited by the mechanical restrictions of the cooling pipes), amazing velocities (up to 250 mm/sec in servo-mode) and excellent resolution (<1 nm in DC-mode). In addition, this drive concept will enable us to reduce the vibrational sensitivity of the monochromator drive units.

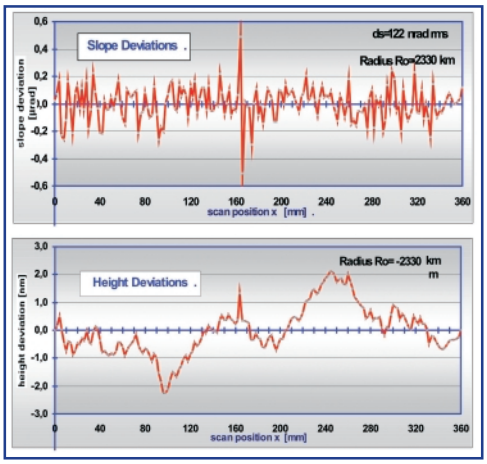

Fig. 10:
Measuring result of plane mirror over 360 mm length using the BESSY-NOM: slope error: 0.025 arcsec rms and height deviation 0.9 nm rms. The estimated measuring uncertainty is in the range of <0.01 arcsec rms or <0.2 nm rms.

FEL Status Report

In the year 2002, the work on the technical design of the BESSY Soft X-Ray FEL has made major progress. Funding of the design group by the 'Zukunftsfonds des Landes Berlin' allowed for a significant increase in man-power resulting in major advances in the design consideration. A consistent base line design has been worked out covering the features of the unique light source:

- three parallel operated, independently tunable FELs (see table)
- 1 kHz pulse sequence at each FEL
- GW peak power at a wavelength range 64 nm to 1.24 nm
- extremely flexible pulse pattern due to a superconducting cw linear accelerator
- option for external seeding, e.g. with external lasers, or using a 'two stage' undulator system providing mono-chromatic photon pulses and/or ultra short pulse duration of ≤35 fs.

Thus, simulation of the whole chain of components starting from the injector to the undulator output in a 'start-to-end' approach was adopted to achieve most realistic predictions on the FEL performance. Challenging components as rf-photoinjector, s.c. cavities, bunch compressors, beam transport and undulators as well as beamlines have been investigated and worked out.

A test bench for research and development work on superconducting cavities, tuners, couplers etc. was developed with the necessary components supplied by industry. In conjunction with the new He-liquifier at the BESSY storage ring, the HOBICAT test bench will be operational in the second half of 2003. Practical experience was gained in the 'Photo Injector Test Facility Zeuthen' (PITZ) and at TTF runs at DESY Hamburg.

The RF-Photoinjector

The superconducting cw LINAC to be used to accelerate the electron beam allows to operate most flexible bunch pattern according to the need of the experiments, e.g. generating single pulses or bunch trains at variable repetition frequencies. Present low emittance rf-photoguns are operating with normal conducting rf-cavities setting severe limits to the flexibility anticipated. Thus based on the 10 Hz injector at DESY Zeuthen a high duty cycle cavity is under construction to extend the repetition frequency to 1 kHz.

Table:
Parameters of photon beam and FEL-undulators

E_{Ph}:	photon energy
$\Delta\lambda/\lambda$:	energy spread
σ_τ:	pulse duration
σ:	beam size
σ':	divergence
λ_U:	undulator period length
L:	module length
L_{tot}:	total length of undulators

Parameter	FEL 1	FEL 2	FEL 3
$E_{Ph\,min}$ (eV)	20	270	500
$E_{Ph\,max}$ (eV)	300	550	1000
$\Delta\lambda/\lambda$ (%)	0.1	0.2	0.1 -0.8
σ_τ (fs) at λ_{min}	38	42	47
σ_τ (fs) at λ_{max}	50	37	40
σ (μm) at λ_{min}	108	78	73
σ (μm) at λ_{max}	234	80	84
σ' (μrad) at λ_{min}	12	11	9
σ' (μrad) at λ_{max}	107	15	14
λ_u (mm)	66	36.5	27.5
L (m)	3.4	3.5	3.6
L_{tot} (m)	58	59	60

Fig. 11:
Relative momentum distribution as function of the longitudinal bunch co-ordinate s (right figure) and transversely across the bunch radius r. The curved distribution in green is for the case no harmonic cavities are used.

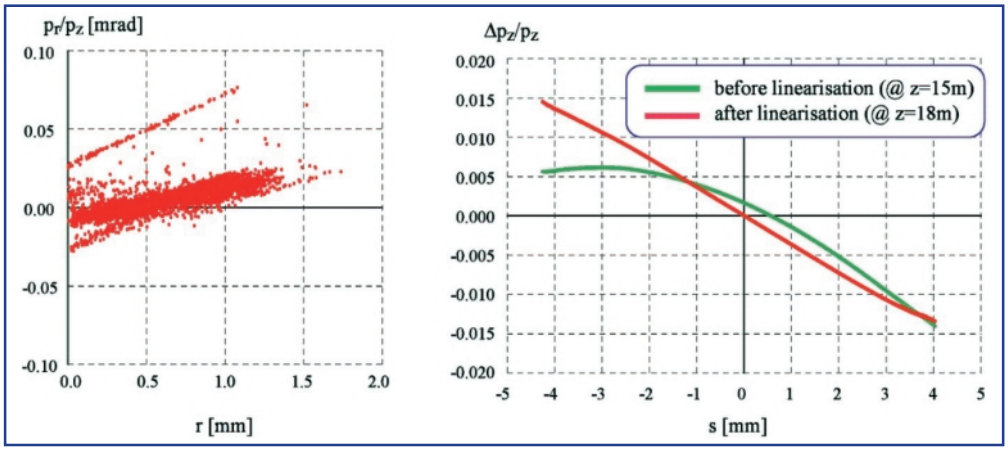

References:

[1] B. Flöttmann, http://www.desy.de/~mpyflo

[2] M.Borland, http://www.aps.anl.gov/asd/oag/oaghome.shtml

[3] S. Reiche, http://stout.physics.ucla.edu/genesis

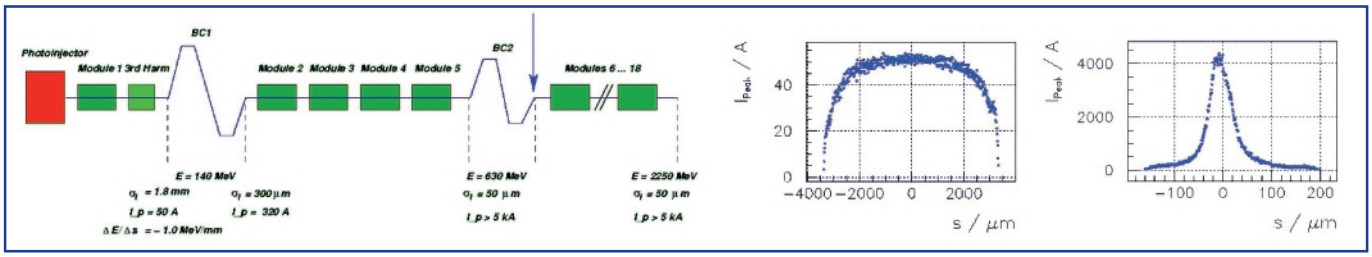

Fig. 12:
Schematics of bunch compression (left panel) and current distribution before and after bunch compression (right panel). Peak current is increased by a factor of more than 50.

A simulation of the photoinjector delivering a charge of 1 nC per pulse at a normalized emittance of 1 mm·mrad was computed using the ASTRA code [1]. The calculation includes the first accelerating sections and a set of 3rd harmonic cavities to minimize non-linearities, ending right at the first bunch compressor. To avoid emittance blow up the concept of invariant envelope matching is applied, e.g. by applying a solenoidal field near the cathode and suitable positioning of the first accelerator section. The resulting phase space distribution of the particles (Fig. 11) is used as the input for beam dynamical studies in the two bunch compressors and LINAC 2.

Bunch compression

Bunches from the injector are typically 1.8 mm long (σ_l) at a maximal current of 80 A. To achieve short electron bunches in the undulator at a high peak current to efficiently start the SASE process, the electrons are compressed in 2 stages to a final length of σ_l = 50 µm thus increasing the peak current to values of 4,500 A. Both compressors are of S-type with six dipole magnets each (Fig. 12). As coherent synchrotron radiation (CSR) is deteriorating the beam quality, simulations were performed using the code ELEGANT [2] to avoid emittance blow up in the bends. The right panel of Fig. 12 is showing the current distribution before com-pressor 1 and after passing compressor 2.

The Superconducting LINAC

For the LINAC cryo-modules of the TESLA design will be used. The modules house 8 cavities of 1.3 GHz 9-cell structures giving the cryostat a typical length of 12 m. A conservative value for the operation gradient of 15 MV/m is anticipated to keep the cryogenic losses at the 2 K level below 25 W/cavity; higher gradients are possible on the expense of a larger cryo-plant. To achieve an energy of 2.25 GeV, 18 TESLA modules will be used, adding up to a total number of 144 cavities that will be powered by individual rf-amplifiers. A detailled analysis of the cryostat showed that only minor changes arround the 2 K 2-phase return line are required to cope with the cw operation. The cryoplant to operate the LINAC has to be rated for 3.5 kW at 2K-He.

The Undulators

The pre-definition to operate three independent FEL-lines covering the photon energy ranges of 20-300 eV, 270-550 eV, and 500-1,000 eV and the intention to stay with the well proven technology of out-vacuum helical undulators as of BESSY II resulted in undulator parameters given in the table. Energy variation of the photon beam is enabled by variation of the undulator gap for FEL 1 and 2 whereas in case of FEL 3 the electron beam energy is changed. This is to allow independent operation of the lines as the electron beam energy is 1.875 GeV with FEL 3 having the possibility for further variation of the beam energy by ±375 MeV.

The RF-Test bench HOBICAT

Prior to finalizing the design parameters for the s.c. LINAC, e.g. mechanical layout of the cryostats, details of the cryo-plant etc., a number of challenges and unknowns have to be investigated. These include the demonstration of long-term, high-gradient cw-cavity and rf-coupler operation, the optimization of the input coupling, development of precise rf-regulation of very narrow bandwidth cavities as well as investigation of the optimal bath temperature and tests of prototype rf-power sources. To enable these systematic tests with rapid turn-around, a horizontal bi-cavity testfacility (HOBICAT) was constructed (Fig. 13). The set up will allow the off-line testing of TESLA 9-cell cavity pairs with all the ancillary devices needed for the final LINAC. All parts are ordered and first test will start in 2nd half of 2003.

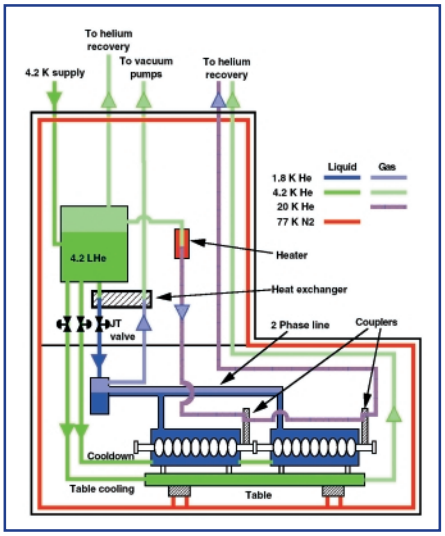

Fig. 13:
Schematics of the cavity test stand.

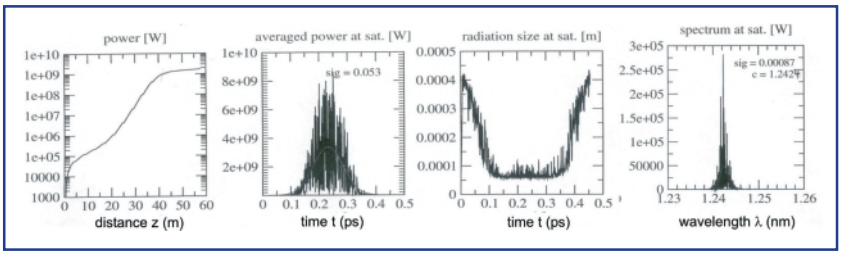

Fig. 14:
Typical results on output power, pulse duration, beam size and spectral distribution for the SASE-FELs.

Photon Beam Parameters

Detailed simulations of the SASE process in the undulator was performed with the code GENESIS [3]. In Fig. 14 typical results on the output power, photon pulse duration, photon beam radius and photon spectrum are displayed. Due to optimization of the overall electron beam parameters there is only marginal variation in the photon beam parameters within the energy range of the individual FEL-lines. Photon beam peak brilliance B and average flux F are in the range of $B = 7 \cdot 10^{31}$ ph/(s·mm²·mrad²·0.1% bw) and $F = 3 \cdot 10^{17}$ ph/s, respectively. Resulting parameters of the photon beam are listed in the table.

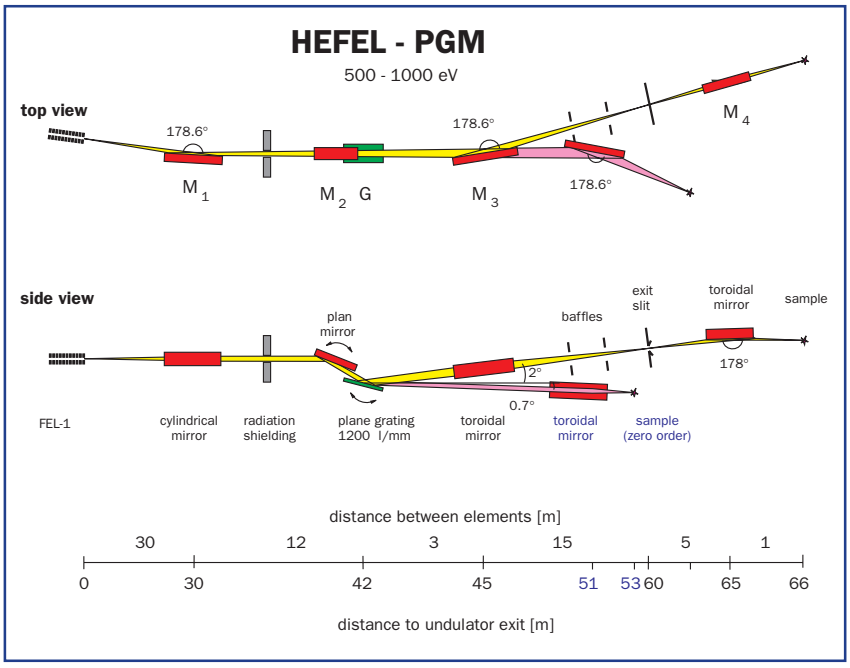

Fig. 15:
Optical layout of the high energy beamline optimized for high energy resolution.

Seeding Options

Seeding a SASE-FEL with an external generated electrical field from a laser or another undulator gives the possibility to control the photon pulse shape as well as shortening the pulse duration below the present 35 fs time scale. Thus further studies are in progress to simulate 2 stage self-seeding schemes and HGHG pre-stages to deliver ultra-short and low energy spread seeds to the SASE undulator.

Beamlines for the BESSY-FEL

Free electron lasers deliver high peak photon densities in beams with narrow cross section and small divergence. The beamline design has to cope with the extreme high photon densities and find configurations where damages of the optical surfaces are avoided. Moreover, the short pulse structure of the FEL should be preserved as well as possible. The latter requirement contradicts generally with the demand for high energy resolution. It seems therefore advisable to design beamlines either for high energy resolution or for short pulse preservation.

The three planned free electron lasers will produce VUV and soft X-ray light between 20 eV and 1,000 eV. Beamlines with high energy resolution have been designed for the low and high end of this spectrum. Both are based on plane grating monochromators operated in collimated light as shown in Fig. 15. At the highest photon energy of 1,000 eV the cross section of the laser beam has increased to 0.7 mm at a distance of 30 m where the first mirror is located. With an incidence angle of 0.7° the footprint of the beam is considerably enlarged and the peak power density on the mirror surface is reduced to 1 mJ/cm². This is well below the ablation threshold of approximate 50 mJ/cm². Taking into account, the reflectance and the exponential decay of the evanescent wave in the total external reflection regime, the average energy absorbed by a surface atom can be calculated. It is in the order of 2 meV per pulse. The pulse separation of 100 ns should be long enough to thermalize this energy deposit.

For most experiments the beamline operates in the high resolution mode with an energy resolution of more than 15,000 and a transmission of up to 5%. Furthermore, it is possible to operate the beamline in the onblaze mode where the zero and first diffraction order of the grating appear in fixed directions at all photon energies.

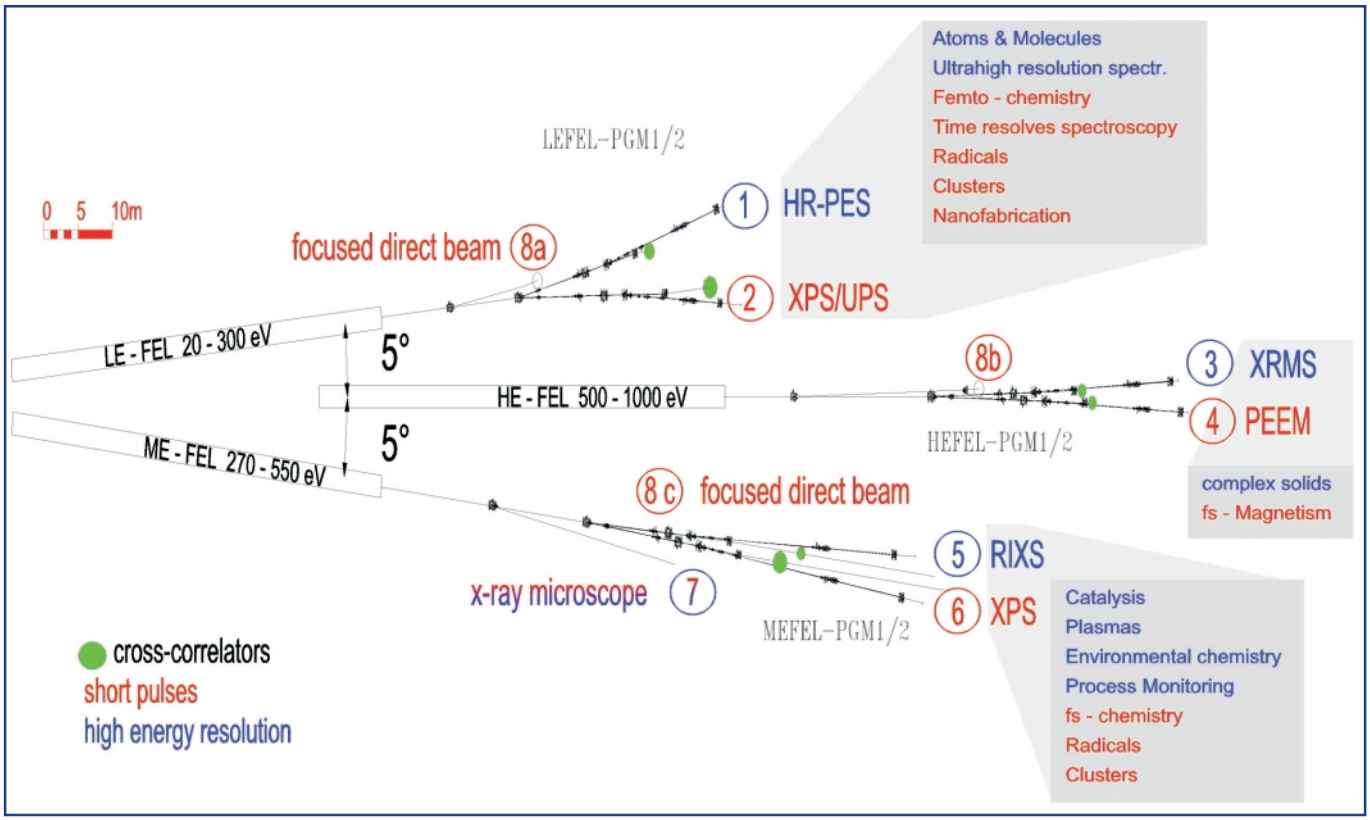

Fig. 16:
Floor plan of the experimental hall.

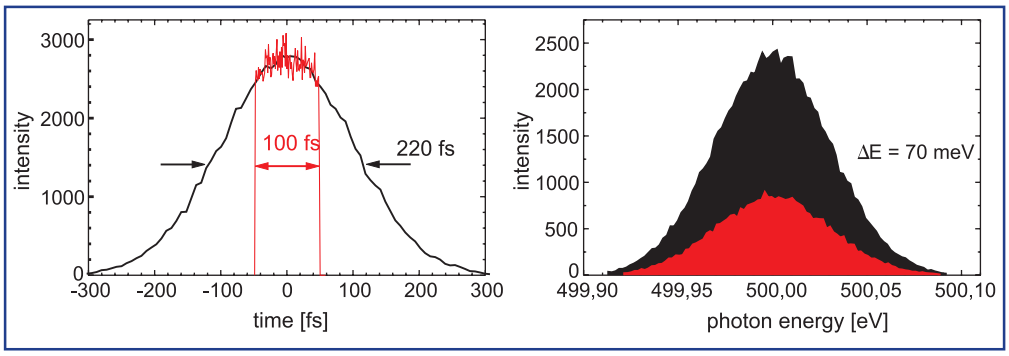

Fig. 17:
Energy distribution and pulse lengths in the onblaze mode at 500 eV of the high resolution beamline. The red area shows the effect of baffling the grating to a length of 10 mm.

This allows measurements with the original pulse structure in the zero order with a simultanous energy determination in the first diffraction order. Pulse lengths are between 400 and 900 fs in the high resolution mode but can be reduced down to 100 fs by baffling the grating in the onblaze mode (Fig. 17).

Based on the beamline designs a preliminary floor plan of the FEL experimental hall has been sketched (Fig. 16). Each of the three free electron lasers is fed to a high energy resolution beamline or alternatively into a beamline that conserves the short pulse structure. Additionally, a focused direct beam can be provided for experiments with ultimate demands on photon density.

The three lasers are separated by an angular offset of 5° with respect to each other to gain more space for the beamlines and experiments. Concerning floor space requirements the high energy laser is the most demanding. It operates at the highest electron energy, needs all accelerator modules and in turn produces the photon beam with the smallest divergence.
As space is limited in the straight line, this beamline design has the highest priority. With photon beam parameters obtained by the computer code GENESIS [3], the beamline and experiments extent to approximately 80 m from the end of the laser and fits well into the envisaged building of the experimental hall.

Contact:
Dieter Krämer,
Machine Status and FEL
kraemer@mail.bessy.de

Gerd Reichardt,
Beamline Developments
gerd.reichardt@bessy.de

Rolf Follath,
FEL Beamlines
rolf.follath@bessy.de

5 New Light at BESSY!

Brilliant, Coherent, Far-Infrared (THz) Synchrotron Radiation

The 'THz-Gap'

First reports on terahertz (THz) waves were published in Physical Review about 100 years ago by E. F. Nichols and H. Rubens from the University of Berlin. Similar to X-rays, THz-radiation can be used to 'x-ray' matter and detect hidden structures. Since engineers and researchers have recognized the potential of THz-radiation for imaging, spectroscopic and microscopic methods in solid state physics, biology, and medicine, interest in more powerful THz sources has grown.

THz-radiation is part of the electro-magnetic spectrum between electronically feasible microwaves and thermal black body radiation. Between these limits no powerful radiation has been available until recently. This region of the electromagnetic spectrum was therefore called the 'THz-gap'. The gap can be closed by thermal sources and more recently also by fs-table-top-lasers, but both sources are not particularly powerful. The only powerful sources so far have been free electron lasers or diodes. These sources, however, show a small bandwidth and hence are not useful for spectroscopic applications.

LINACs and Rings

Coherent synchrotron radiation (CSR) is a tool which overcomes these limitations. It offers powerful and broadband radiation in the THz-range. For the first time CSR was observed 1989 in Japan at Tohoku-300-MeV-LINAC. Recently an average power of 20 W was reported from the LINAC at Jefferson Laboratory, USA. CSR was also detected at some electron storage rings in the last years, but only as bursting radiation, indicating that bunch instabilities are involved in the emission process.

During the past few years, BESSY has developed a new technique to generate stable, coherent sub-THz and THz-radiation from the BESSY II electron storage ring in collaboration with the DLR [1]. THz-radiation is emitted by relativistic electrons radially accelerated by magnetic fields, as a part of the synchrotron radiation spectrum ranging from X-rays to THz-radiation. Normally, the phases of the electro-magnetic waves are not correlated and the power of the radiation is linearly increasing with the number of radiating electrons. In this incoherent radiation process the emitted THz power is low.

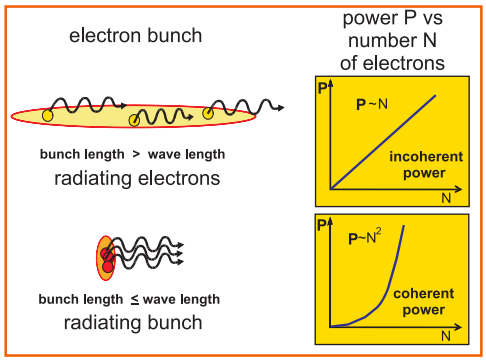

Fig. 1: Superposition of waves. Long bunches emit incoherent waves with random phase relation. Short bunches behave as a macroparticle and emit coherent waves at equal phase (left part of the figure). The resulting power grows linearly with the number of electrons for the incoherent case and the coherent intensity grows with the charge of the macroparticle (right part of the figure).

How to make Coherent Synchrotron Radiation

For the transition from incoherent to coherent emission process, three length parameters have to be considered: bunch length, radiation wavelength, and cutoff wavelength. For radiation with wavelength longer than the bunch, phases of the waves become independent of the emission point within the bunch and all phases become equal. The bunch can be considered as a single macroparticle, as sketched in Fig. 1. These waves add up coherently. Their field intensity grows linearly and their power quadratically with the number of electrons involved leading to a dramatic change in the emitted power since there are 10^8 to 10^9 electrons involved in this process. Fig. 2 shows the synchrotron radiation pattern with the coherent emission part included. The cutoff of the vacuum chamber sets a limit to this process.

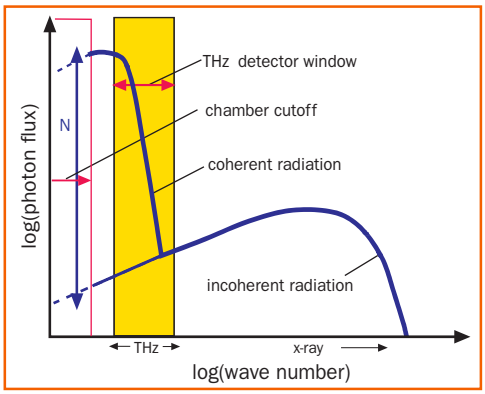

Fig. 2: Coherent and incoherent spectra.
The synchrotron radiation spectrum shows a dramatic increase of photon flux in the long wave length range, if the coherent radiation is no longer shielded by the vacuum chamber. This additional increase is proportional to the number N of electrons involved.

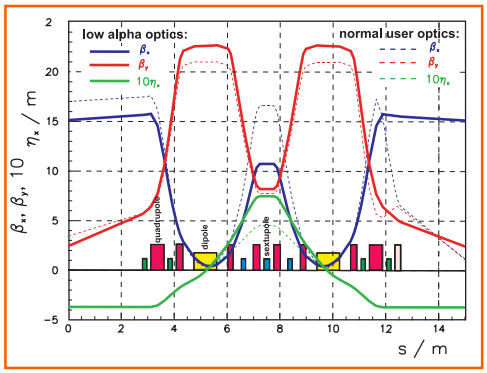

Fig. 3: 'Low alpha' optics. Comparison of the optical functions of 'low alpha' optics for bunch length manipulation and the normal user optics. The 'low alpha' optics changes the dispersion function (green) inside the dipoles in an appropriate way. α is defined as the change of the orbit length L per momentum p change ($\alpha = \delta L/L) / (\delta p/p$).

Only if the waves are shorter than the cut off wavelength they can propagate in the chamber demanding sufficiently short bunches.

At the BESSY storage ring a 'low alpha' optics is applied to compress the bunches and to generate CSR as a stable non-bursting process. A comparison between the normal user optics and the 'low alpha' optics is shown in Fig. 3. The differently tuned dispersion function inside the ring dipoles reduces the transverse machine optics parameter α, the 'momentum compaction factor'. With the reduced α the orbit length in the storage ring becomes nearly independent of the electron momenta. In the limit $\alpha = 0$, the orbit length is independent of the particle momentum. All particles circulate with the same revolution time and the optics becomes isochronous. Also with a reduced α, the longitudinal oscillation of the electrons around the bunch center takes longer and the oscillation amplitude becomes smaller. This leads to compressed bunches, where the length shrinks in proportion with $\sqrt{\alpha}$, i.e. a 25-times smaller α leads to 5 times shorter bunches (Fig. 4).

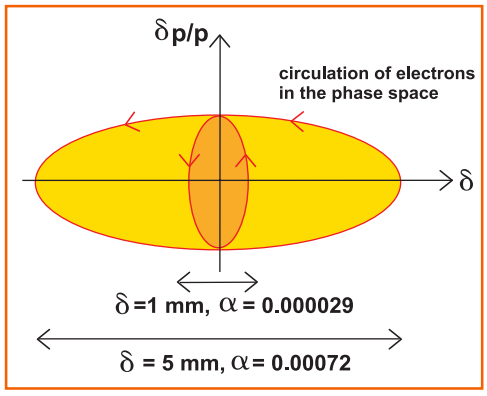

Fig. 4: Bunch compression. In a co-moving coordinate system electrons perform oscillations around the bunch center. In the 'low alpha' optics the oscillation amplitudes are reduced and the bunch is compressed. The momentum spread of $\delta p/p$ the electron beam stays unchanged.

The BESSY optics is very well suited for the required detuning of the beam optics to the 'low alpha mode'. The size of the radio frequency (rf-) buckets containing the electron bunches is defined by the rf-voltage, which has to be controlled very carefully during the detuning, because undersized buckets lead to the loss of electrons. These essential higher order optics corrections can be performed with the existing flexible sextupoles scheme.

In the normal user optics the rms (root mean square) value of the bunch length at low current is 5 mm and $\alpha = 7.2 \cdot 10^{-4}$. At approximately $\alpha = 6.5 \cdot 10^{-5}$ the bunch shrinks to an rms-length of 1.5 mm comparable to sub-THz wavelength and bunches become sufficiently shorter than the cutoff wavelength of the vacuum chamber. At this reduced bunch length a strong THz-power increase becomes detectable.

For CSR experiments typically a bunch length of about 1 mm and bunch currents of 50 µA are used. If all 400 buckets of the storage ring are filled the average current is about 20 mA and the life time of the stored beam is several hours. The radiation process is very stable. The emitted light is therefore very well suited for Fourier Transform spectroscopic applications.

Influence of the Ring Current

The bunch length is sensitive to the bunch current. Increased current leads to longer bunches but also to more CSR power. This indicates a bunch deformation away from a Gaussian shape, which results from an interaction of the bunch with its own CSR-field. Above a threshold current the interaction of the CSR-field with the bunch becomes so strong, that the emitted intensity is periodically modulated and finally changes into a chaotic bursting process. This unstable bunch dynamics and radiation process can be detected in the normal user and the 'low alpha optics', whereas the stable emission only occurs in 'the low alpha' mode.

The power of the emitted incoherent radiation is proportional to the average current, independent of α, whereas the coherent power scales completely differently. At the detection limit it grows nonlinear if α is further reduced and scales roughly with the square of the bunch current. However, due to bunch deforming and bunch lengthening effects the scaling is actually stronger than the square of the current. This nonlinear dependence on the beam current is a proof of the coherent emission process.

References:

[1] M. Abo-Bakr, et al., Phys. Rev. Lett. 88, 254801 (2002).

[2] M. Abo-Bakr, et al., Phys. Rev. Lett. (2003), accepted.

[3] W. C. Barry et al., Proceedings of the EPAC 2002, Paris, France.

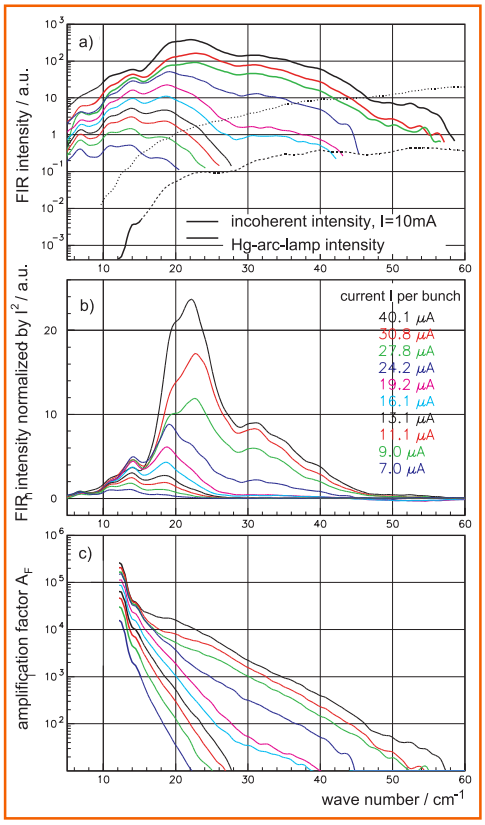

Fig. 5: CSR spectrum.
(a) The spectral content of the radiation measured by a Fourier transform spectrometer. The intensity is not corrected for transmission effects. In (b) the intensity is normalized by the square of the bunch current. The growth is stronger than the square of the bunch current, indicating bunch deformation effects.
(c) The amplification factor A_F is the ratio between coherent to incoherent intensity. The amplification by the coherent superposition of the waves becomes as large as 10^5. It is independent of the transmission efficiency of the setup.

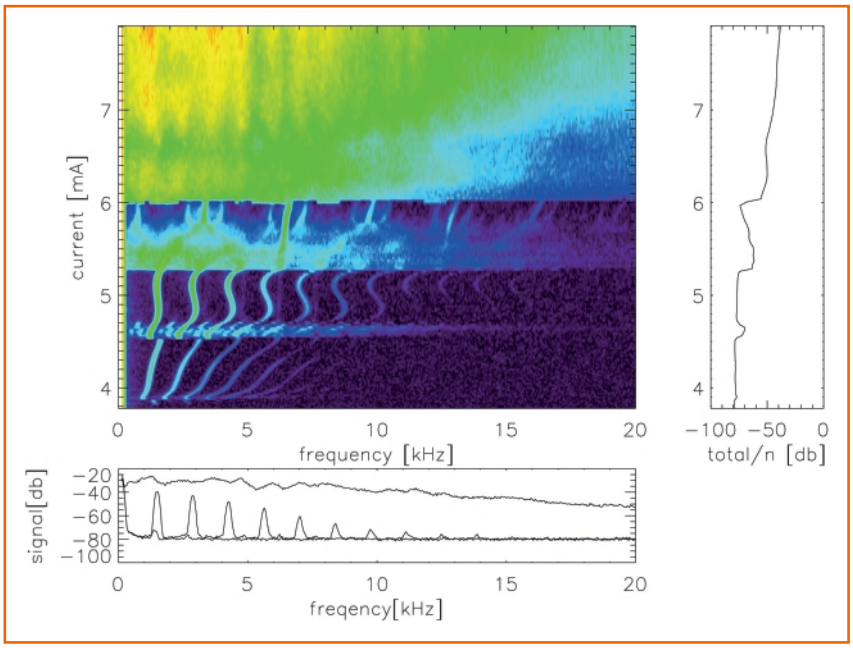

Fig. 6: THz-diagnostics of bunch instabilities.
Bunch instabilities are detected by the emitted THz radiation during single bunch shift with normal user optics. At about 4 mA, a periodic bursting is visible with frequencies of up to 5 kHz. With increasing current the periodic frequency pattern changes several times and eventually gives way to a chaotic pattern at 6 mA.
The panel shows the integrated intensity on the right. Cuts taken at three different currents show the frequency pattern as seen on the spectrum analyzer (lower figure).

New opportunities for BESSY User

The spectral quality of the CSR was characterized at the IRIS infrared beam line [2]. The detected power maximum is located between 10 to 20 cm^{-1} (0.5 to 1 mm wavelength). The intensity at larger wave numbers depends on the current per bunch. Additional current enhances the spectrum at larger wave numbers beyond 40 cm^{-1} at the expense of the stability of the emission process.

The incoherent spectrum in this frequency range, measured during the normal user optics shift shows very poor intensity and 10 times higher current is required to get reasonable signal strength. The ratio between coherent and incoherent spectra at the same average beam current is a measure of the power amplification due to the coherent emission process. The amplification factor is up to 10^5. This factor is used to estimate the strength of the coherent source, because the source intensity for the incoherent case can be calculated. In the wave number range from 12 to 50 cm^{-1} an average power of 1 mW is emitted into an angle of 60 x 40 $mrad^2$. During the unstable emission mode even more power is generated.

The THz radiation can also be used for diagnostics in beam dynamics. An example is shown in Fig. 6. During a single bunch shift and the normal user optics THz-radiation was applied to detect bunch instabilities. Depending on the bunch current, the emission process changes from a periodic to a chaotic busting process.

The technique applied to generate CSR offers new experimental opportunities in the THz range, to the scientific community. First THz experiments have already been performed at BESSY (see page 18). The technique might also be a starting point of a new class of dedicated storage rings for CSR [3] increasing the availability of powerful THz-radiation. Finally, the applied 'low alpha' optics is not only of interest for coherent radiation, it also offers the possibility of short bunches (at low current) for other applications, such as time resolved studies.

Contact:
Godehard Wüstefeld
wuestefeld@bessy.de

6 Facts & Figures

Status of BESSY

ID Beamlines at BESSY

(January 2003)

ID02-2 7TWLS/1-KMC1	BAM/PTB
ID03-1 U125/2-SGM	BUS
ID03-2 U125/2-KMC	PDI/HUB
ID05-1 UE56/2-PGM1	MPG
ID05-2 UE56/2-PGM2	MPG
ID06-1a 6T-LITHO	BESSY
ID06-1b 0.4T-LITHO	BESSY
ID07-1 13°	PTB
ID07-2 U49/U180-PGM	PTB
ID07-3 direct beam	PTB
ID09-1 UE52-SGM	BESSY
ID09-2 UE52-PGM	UFF-CRG
ID10-1 UE46-PGM	HMI
ID11-1 UE56/1-PGM	BESSY
ID11-2 UE56/1-SGM	FZ Jülich
ID12-1a U41-TXM	U Göttingen
ID12-1b U41-STXM	U Göttingen
ID12-2 U41-PGM	BESSY
ID13-1 U125/1-SGM	MBI
ID13-2 U125/1-ML	U Bielefeld
ID13-3 U125/1-PGM	BESSY
ID14-1 7TWLS/2-KMC1	PSF
ID14-2 7TWLS/2-KMC2	PSF
ID15-1 U49/2-PGM1	BESSY
ID15-2 U49/2-PGM2	BTUC

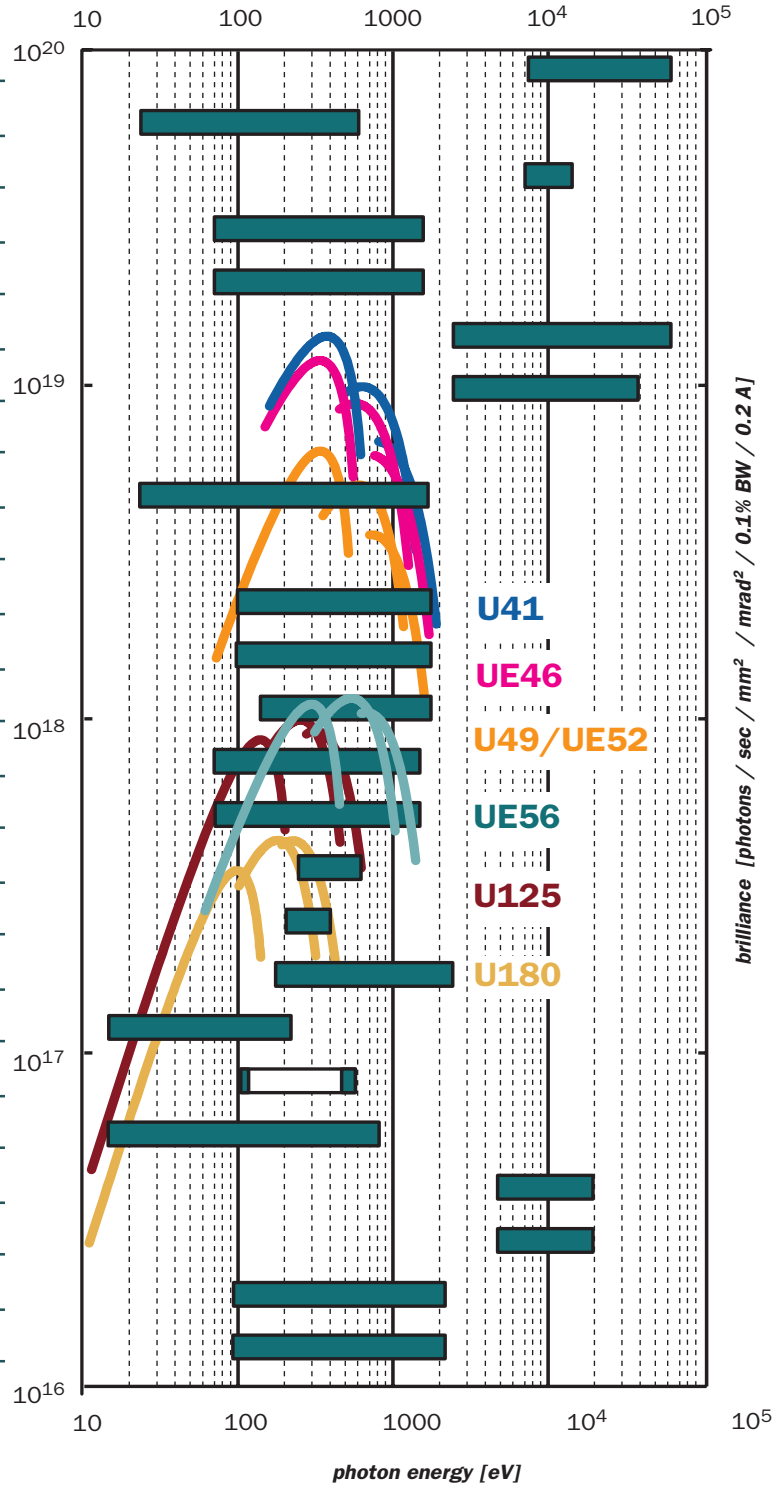

25 ID-BLs in operation

BESSY II,
1.7 GeV, 200 mA
coupling 1%

DIPOLE Beamlines at BESSY

(January 2003)

D01-1B KMC1	BESSY
D02-1A FT-IR	IRIS
D03-1B 3m NIM2	BESSY
D06-1A LITHO	BESSY
D06-1B 1m NIM1	PTB
D07-1A1 1m NIM2	PTB
D07-1A2 white beam	PTB
D07-1B KMC	PTB
D07-2 PM	PTB
D08-1B1 HESGM	CRG
D09-2 KMC2	BESSY
D11-1A PM3	BESSY
D12-1B 3m NIM1	BESSY
D13-2 EDR	U Potsdam
D15-1B TGM7	HMI
D16-1A RGBL-PGM	U Petersburg
D16-1B CP-NIM	BESSY

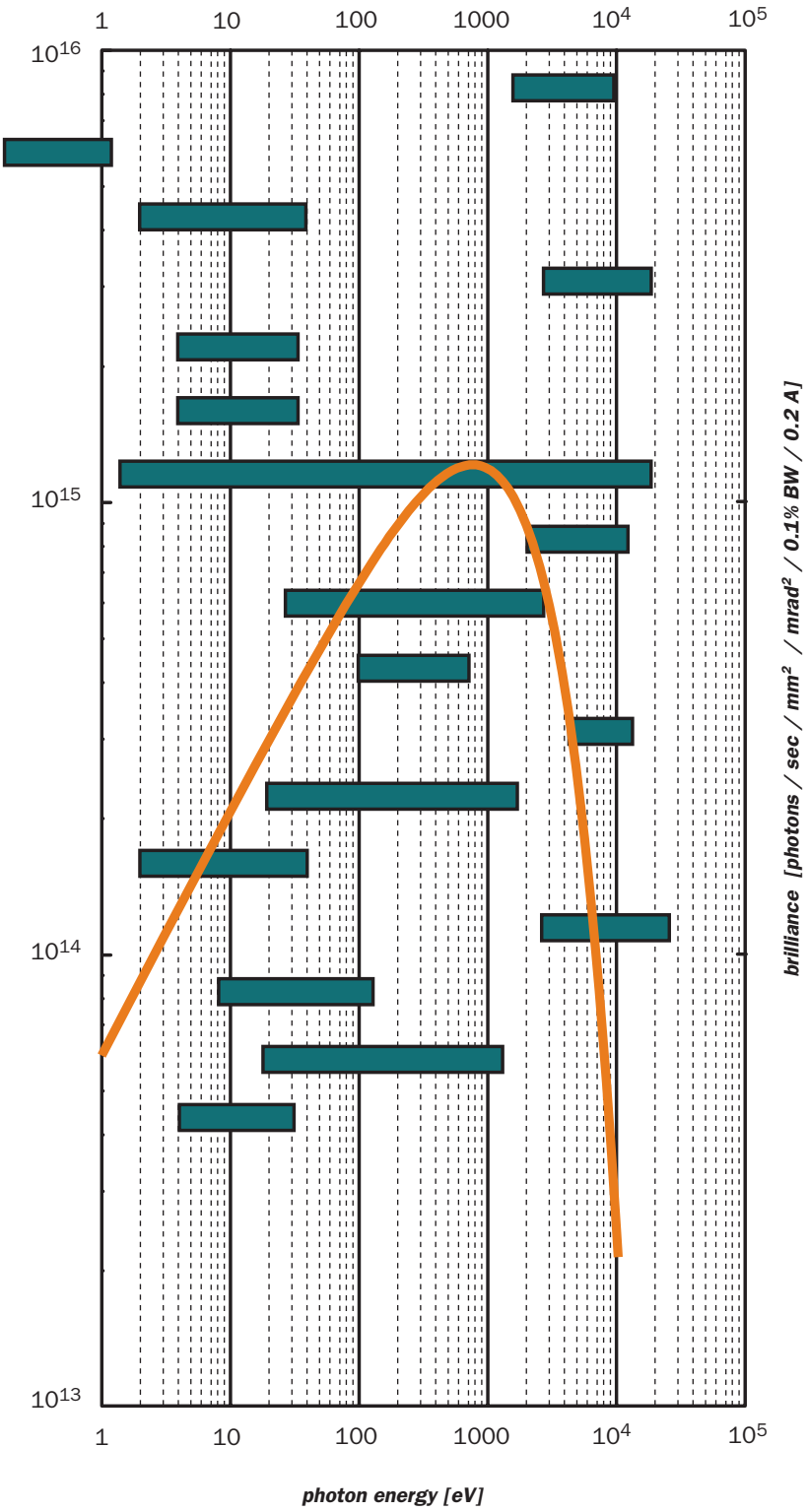

17 Dip-BLs in operation

BESSY II
1.7 GeV, 200 mA
coupling 1%

Beamlines on Insertion Devices

BAM
Bundesanstalt für Materialforschung und -prüfung

BTUC
Brandburgische Technische Universität Cottbus

FUB
Freie Universität Berlin

FZJ
Forschungszentrum Jülich

HMI
Hahn-Meitner-Institut

HUB
Humboldt-Universität zu Berlin

MPG
Max-Planck-Gesellschaft

PSF
Proteinstrukturfabrik

PTB
Physikalisch-Technische Bundesanstalt

TUB
Technische Universität Berlin

U Bi
Universität Bielefeld

TUD
Technische Universität Dresden

U Gö
Universität Göttingen

U Kl
Universität Kaiserslautern

U Po
Universität Potsdam

U Wü
Universität Würzburg

Insertion Device	*Monochromator*	*Energy Range (eV)*	*Contact Persons*	
7 T WLS/1	KMC-1	6 k – 50 k	H. Riesemeier (BAM) B. Müller (BAM)	A. Erko
U 125-2	KMC	6 k – 12 k	W. Braun (PDI) B. Jenichen (PDI)	A. Erko
U 125-2*	NIM	< 10 – 35	G. Reichardt	I. Packe P. Rotter
U 125-2	SGM	20 – 500	R. Püttner (FUB)	G. Reichardt
UE 56-2	PGM 1	60 – 1,300	W. Mahler (MPG) B. Zada (MPG)	H.-C. Mertins
UE 56-2	PGM 2	60 – 1,300	W. Mahler (MPG) B. Zada (MPG)	H.-C. Mertins
6 T WLS	LITHO	> 2,000	B. Löchel H. Köhrich	H.-U. Scheunemann M. Bednarzik
0.4 T	LITHO	> 2,000	B. Löchel H. Köhrich	H.-U. Scheunemann M. Bednarzik
U 180 / (U 49)	-	direct beam	R. Klein (PTB)	
U 180 / (U 49)	13°		R. Klein (PTB)	A. Gottwald (PTB)
U 180 / (U 49)	PGM	20 – 1,900	B. Beckhoff (PTB)	
UE 52	SGM	85 – 1,600	K. Godehusen F. Senf	T. Zeschke
UE 52	PGM	85 – 1,600	T. Schmidt (U Wü)	C. Jung
UE46	PGM	120 – 1,700	H. Rossner (HMI) D. Schmitz (HMI)	F. Senf
UE 56-1	PGM	60 – 1,300	H.- C. Mertins J. Schmidt	T. Zeschke
UE 56-1	SGM	60 – 1,300	S. Cramm (FZJ)	M. Freiwald
U 41	PGM	170 – 1,800	C. Jung	M. Mast
U 41	TXM	~ 250 – ~ 600	P. Guttmann (U Gö)	G. Schneider
U 41	STXM	~ 250 – ~ 600	P. Guttmann (U Gö)	G. Schneider
U 125-1	PGM	20 – 700	P. Bressler	F. Eggenstein
U 125-1	Multilayer	80 – 700	M. Pohl (U Bi)	
U 125-1	SGM	15 – 180	B. Winter (MBI) T. Gießel (MBI)	W. Widdra (MBI) R. Follath
7T WLS/2	KMC-1	4.5 k – 17.5 k	U. Müller (PSF)	M. Fieber-Erdmann (PSF)
7T WLS/2	KMC-2	4.5 k – 17.5 k	U. Müller (PSF)	M. Fieber-Erdmann (PSF)
7T WLS/2*	KMC-3	13.7	U. Müller (PSF)	M. Fieber-Erdmann (PSF)
U 49-2	PGM-1	85 – 1,600	O. Schwarzkopf R. Follath	J.-S. Schmidt
U 49-2	PGM-2	85 – 1,600	P. Hoffmann (BTUC)	D. Batchelor

**** under construction***

Beamlines on Dipole Magnets

Monochromator	*Energy Range (eV)*	*Contact Persons*	
KMC-1	1.7 k – 10 k	F. Schäfers F. Neißendorfer	M. Mertin
FT-IR	IR	N.N.	U. Schade
3m-NIM-2	4 – 35	T. Schroeter I. Packe	G. Reichardt
LITHO	direct beam	B. Löchel H.-U. Scheunemann	H. Köhrich M. Bednarzik
1m-NIM-1	3 – 35	M. Richter (PTB)	
1m-NIM-2	3 – 35	M. Richter (PTB)	
	direct beam	R. Thornagel (PTB)	
KMC	1.7 k – 10 k	M. Krumrey (PTB)	
PGM	30 – 1,800	F. Scholze (PTB)	
HE-SGM	200 – 700	A. Lippitz (BAM)	O. Schwarzkopf
KMC-2	4.5 k – 15 k	A. Erko	I. Packe
PGM-3	20 – 1,900	T. Kachel	F. Eggenstein
3m-NIM-1	4 – 35	T. Schroeter I. Packe	G. Reichardt
EDR	2 k – 12 k	W. Leitenberger (U Po) Y. Bodenthin (U Po)	A. Erko
TGM-4*	8 – 120	K. Godehusen	M. Mast
TGM-7	8 – 120	C. Pettenkofer (HMI) W. Bremsteller (HMI)	
PGM-RD-BL	30 – 1,500	D. Vyalikh (FUB) S. Molodtsov (TUD)	
CP-NIM	4 – 35	F. Neißendorfer F. Schäfers	M. Mertin
Litho EUV	95	H.-U. Scheunemann H. Köhrich	

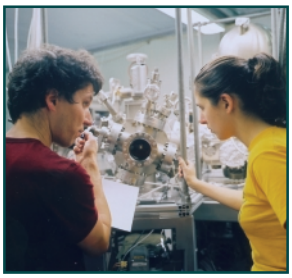

** under construction*

For general information on beamlines see BESSY website under www.bessy.de

Experimental stations

It is one of BESSYs objectives to give a wide user community access to a variety of experimental techniques. The following tables are intended to summarize the available experimental stations and techniques for common use. Researchers are invited to use these facilities. For planning an experiment or specific queries please contact the appropriate beamline scientist given in the table. Since biology is a growing research field at BESSY stations of interest for biological researchers are highlighted by BioSR.

More detailed information will be available on the BESSY website (www.bessy.de).

For further information on the experimental stations please contact W. Braun (braun@bessy.de) or Ch. Jung (jung@bessy.de).

Experimental systems available at BESSY	*UPS / XPS*	*Microscopy*	*Electron yield*	*Fluorescence*	*X-ray emission*	*Scattering*	*Contact*
HIRES – high resolution electron spectrometer	•		•				rader@bessy.de
PHOENEXS – photoemission and near edge X-ray spectroscopy	•		•	•			bressler@bessy.de
MUSTANG – multi-user stage for angular resolved photoemission	•		•	o			tepper@bessy.de
Fluorescence spectrometer			•	•			ruediger.mitdank@physik.hu-berlin.de
SAMIC – spectroscopy and microscopy integrating chamber	•	•					patrick.hoffmann@tu-cottbus.de
Two-photon-photoemission experiment	•						bwinter@mbi-berlin.de
XPEEM – photoemission microscopy		•					pohl@physik.uni-bielefeld.de
HIRE-PES – energy resolution photoemission	•						christoph.jannowitz@ physik.hu-berlin.de
Investigations on stored nano particles	•			•		•	ruehl@phys-chemie.uni-wuerzburg.de
Photoemission microscope for resolved spectroscopy in the ps-regime	•	•					schoenhe@mail.uni-mainz.de
High resolution spin-polarisation photoelectron spectroscopy	•						c.m.schneider@ifw-dresden.de
Soft X-ray emission spectrometer					•		eisebitt@bessy.de
CISSY – CIS-diagnostic using SYnchrotron radiation	•				•		cissy@hmi.de
ROSA – rotateable spectrometer apparatus	•				•		szargan@ rz.uni-leipzig.de
So-Li-AS – the solid-liquid-analysis system	•						mayerth@surface.tu-darmstadt.de
SMART – spectro-microscope with highest spatial resolution	•	•					thomas.schmidt@physik. uni-wuerzburg.de
XM – X-ray microscopy BioSR		•					guttmann@bessy.de

• available; o planned; BioSR suitable for biological samples

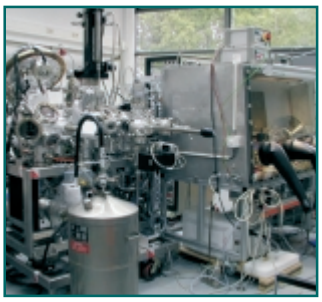

Experimental systems available at BESSY	*Contact*
IRIS – Infrared spectroscopy and microspectroscopy[BioSR] Infrared ellipsometry[BioSR]	schade@bessy.de hinrichs@isas-berlin.de
VUV / XUV ellipsometry	norbes@gift.physik.tu-berlin.de
Scattering experiments in the VUV / XUV range	eugen.weschke@physik.fu-berlin.de
X-ray diffraction micro-XANES[BioSR] micro-EXAFS[BioSR] micro-fluorescence experiments[BioSR]	erko@bessy.de
X-ray diffraction during molecular beam epitaxy	ploog@pdi-berlin.de
PSF – Protein crystallography[BioSR]	umue@chemie.fu-berlin.de
Reflectometry	schaefers@bessy.de
Polarimetry	mertins@bessy.de

Experiments under construction	*UPS / XPS*	*Microscopy*	*Electron yield*	*Fluorescence*	*X-ray emission*	*Absorption*	*Contact*
X-ray emission on organic substances and biomaterials[BioSR]			o		o		michael.grunze@urz.uni-heidelberg.de
UVIS – circular dichroism spectroscopy for biological investigations[BioSR]				o		o	sauerborn@bessy.de

• available; o planned; [BioSR] suitable for biological samples

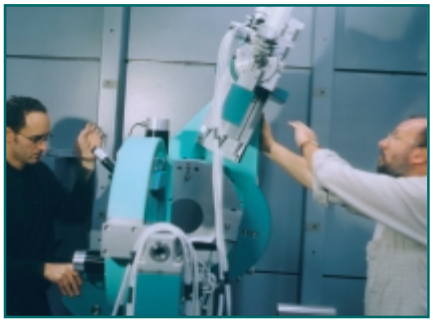

User operation

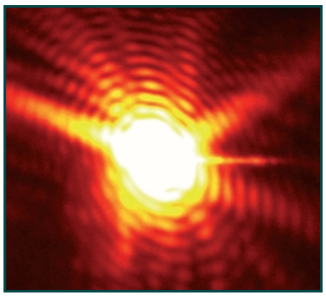

Operation statistics

During the last year the light source delivered photon beams to the experiments for 4,167 h, about 4% more than scheduled.

The storage ring was operated seven periods (30 weeks) in multibunch and 4 weeks single bunch mode. Together with additional 13 week dedicated to machine development as well as to insertion device and beamline commissioning this adds up to 47 weeks. The overall availability of the light source reached ~96 %.

Beam Time at BESSY

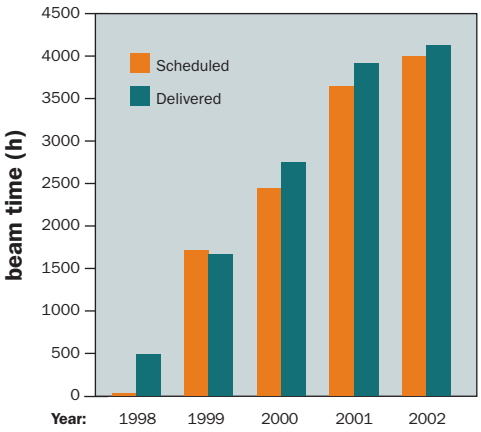

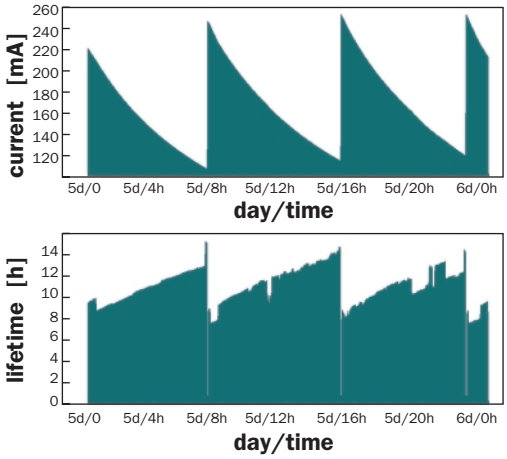

On a typical day at BESSY, the storage ring is operated at 1.7 GeV at beam currents between 250 and 110 mA. Three refills per 24 h shift are required for the beam lifetime of 6-14 h.

Number of User Runs: 348

Projects in the EU-HPP-Programme: 24

Average beam time per User Run: 18.7 shifts

MPG = Max-Planck-Gesellschaft

WGL = Leibnitz-Gemeinschaft

Grossforschung = Members of Helmholz Gemeinschaft

Bundesanstalten = BAM, PTB

Beam time allocation in 2002

Insertion Device Beamlines

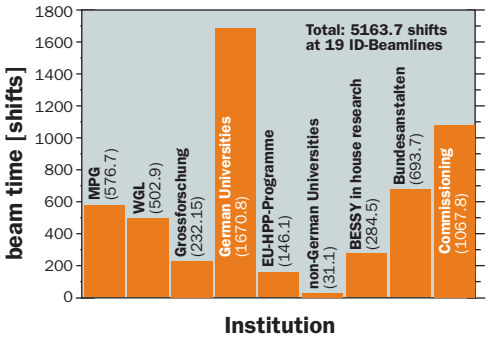

Bending Magnet Beamlines

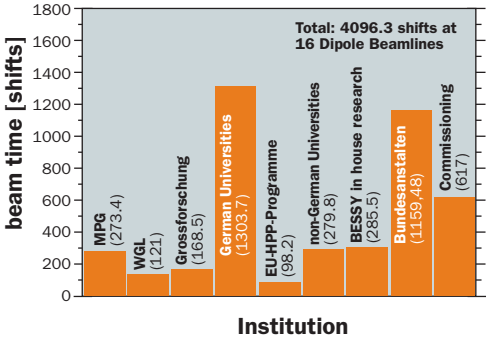

Improvements for Users

Starting in August, BESSY introduced 24 hour operations, seven days a week, allowing for more supported beamtime. The rate of increase in dedicated user beamtime over the past five years parallels that of the implementation of new beamlines yielding a quadratic increase in measuring station time for the users. Although this has momentarily reduced the pressure on fulfilling the user's requests for beamtime, it is expected that the pressure will soon return, on the basis of supply and demand!

The increasing number of users has exacerbated the situation regarding housing and subsistence on site. Fortunately, the planning of an additional building at the IBZ has been completed and the new building is expected to be inaugurated by the end of 2003. In addition, weekend-meals will be available in a nearby restaurant. Evening meals will be available until 22 h during the week at the 'Erwin-Schrödinger Zentrum' (IKA) of the Humboldt University (see map).

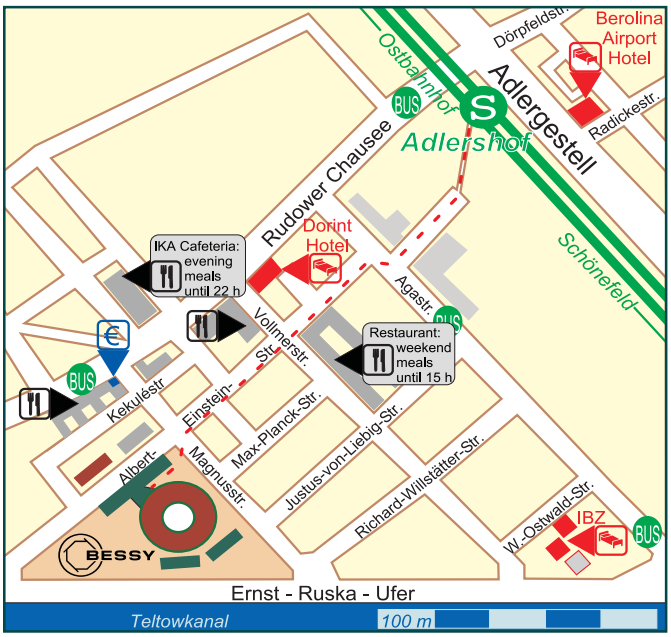

Several changes have taken place in the experimental hall. Immediately apparent is the elimination of the illuminated yellow 'radiation' signs at the entrances: the hall has the same status as the outside world. Nevertheless, we will continue to carry and evaluate personal dosimeters to document the safety of the hall.

Less visible are the changes in the network cabling and network software to the monochromators and measuring stations. Like a modern hotel, each possible work area has been provided with internet connections and there is now an active backup system, hard- and software, for all of the stations. In addition, the stability of the entire system has been improved. On the other hand, there is a tendency for user apparatus to produce noise, electrical, magnetic and mechanical, which is disturbing to others and/or to the operation of the storage ring. Switching magnetic fields and mechanical pumps are the two largest perpetrators of such noise.

The acoustical noise level at selected measuring stations has been measured differentially by the Department for Building Acoustics of the TU Berlin with the goal of reducing the acoustical noise level in the hall. Although the water pumps and generators for the RF system are noticeably loud, the local noise level at a given measuring station is often dominated by the user's own pumps, cryosystems, fans, etc. We want to encourage the users to include noise (of all varieties!) reduction in the design of their experiments. We will see what can be done to reduce noise level of the BESSY equipment.

Advisory Boards (January 2003)

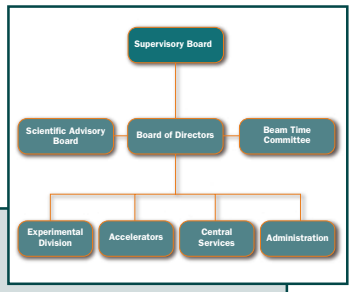

Supervisory Board

Prof. Dr. J. Treusch (Chairman)	Forschungszentrum Jülich
Prof. Dr. A. Goldmann (Vice-Chairman)	Gesamthochschule Kassel
Min.Dir. Dr. H.F. Wagner	Bundesministerium für Bildung und Forschung
Prof. Dr. E. O. Göbel	PTB Braunschweig
Prof. Dr. R. Maschuw	Forschungszentrum Karlsruhe
M. Meinecke	Max-Planck-Gesellschaft München
Dr. D.-M. Polter	FhG München
Prof. Dr. W. Saenger	Freie Universität Berlin
Prof. Dr. J. Schneider	DESY Hamburg
MinRat Dr. J. Schöttler	Bundesministerium für Wirtschaft und Technologie, Berlin
Prof. Dr. M. Steiner	HMI Berlin
Senatsdirig. W. Eckey	Senatsverwaltung für Wissenschaft, Forschung und Kultur Berlin

Scientific Advisory Board

Prof. Dr. M. Grunze (Chairman)	Universität Heidelberg
Dr. A. F. Wrulich (Vice-Chairman)	Paul-Scherrer-Institut Villigen
Prof. Dr. D. S. Chemla	ALS Berkeley
Prof. Dr. M. Eriksson	MAXLab Lund
Prof. Dr. K. C. Holmes	Max-Planck-Institut für medizinische Forschung Heidelberg
Prof. Dr. E. J. Nordgren	Universität Uppsala
Prof. Dr. V. Saile	Forschungszentrum Karlsruhe
Prof. Dr. W. Sandner	Max-Born-Institut Berlin
Prof. Dr. R. Schlögl	Fritz-Haber-Institut der MPG Berlin
Prof. Dr. G. Schütz	Max-Planck-Institut für Metallforschung Stuttgart
Prof. Dr. J. Stöhr	Stanford Synchrotron Radiation Laboratory (SSRL)

Permanent Guests:

Prof. Dr. J. Richter	BMBF
Prof. Dr. R. Gerhardt-Multhaupt	Universität Potsdam
Prof. Dr. J. Kirschner	MPI für Mikrostrukturphysik Halle
Dr. T. Möller	HASYLAB/DESY Hamburg
Dr. R. Schuchhardt	Senatsverwaltung für Wissenschaft, Forschung und Kultur Berlin

Financial Committee

Ass. jur. S. Lettow (Chairman)	Forschungszentrum Karlsruhe
R. Kellermann (Vice Chairman)	Forschungszentrum Jülich
Dr. W. Buck	PTB Berlin
OAR H. Diermann	BMBF
M. Schleier	Max-Planck-Gesellschaft München
Dr. R. Schuchhardt	Senatsverwaltung für Wissenschaft, Forschung und Kultur Berlin

Beam Time Committee

Prof. Dr. E. Rühl (Chairman)	Universität Würzburg
Prof. Dr. W. Wurth (Vice-Chairman)	Universität Hamburg
Dr. D. Arvanitis	Universität Uppsala
Prof. Dr. St. Blügel	Forschungszentrum Jülich
Prof. Dr. R. Ficner	Institut für Mikrobiologie und Genetik Göttingen
Prof. Dr. J. Fink	Institut für Festkörper- und Werkstofforschung e. V. Dresden
Prof. Dr. M. Grunze	Universität Heidelberg
Prof. Dr. K. Horn	Fritz-Haber Institut der MPG Berlin
Prof. Dr. K.-H. Schartner	Justus-Liebig-Universität Gießen
Prof. Dr. G. Schütz	Max-Planck-Institut für Metallforschung Stuttgart
Prof. Dr. L. Singheiser	Forschungszentrum Jülich
Dr. M. Wilmanns	EMBL Hamburg

Contact

Scientific Director
Prof. Dr. Dr. h.c. Wolfgang Eberhardt
Secretary: Ines Maupetit
phone +49 (0)30 / 6392 4633
fax +49 (0)30 / 6392 2989
eberhardt@bessy.de, maupetit@bessy.de

Technical Director
Prof. Dr. Eberhard Jaeschke
Secretary: Nikoline Hansen
phone +49 (0)30 / 6392 4651
fax +49 (0)30 / 6392 4632
jaeschke@bessy.de, hansen@bessy.de

Administration
Thomas Frederking
Secretary: Katrin Rosenblatt
phone +49 (0)30 / 6392 2901
fax +49 (0)30 / 6392 2920
frederking@bessy.de, rosenblatt@bessy.de

Beam Time Coordination
Dr. Walter Braun, Dr. Gerd Reichardt
Secretary: Stine Mallwitz
phone +49 (0)30 / 6392 2904
fax +49 (0)30 / 6392 4673
braun@bessy.de, reichardt@bessy.de,
mallwitz@bessy.de

User Office
Daniela Baum, Maha Krämer
phone +49 (0)30 / 6392 4734
fax +49 (0)30 / 6392 4746
baum@bessy.de,
mahakraemer@bessy.de

Public Relations
Dr. Heike Henneken, Dr. Markus Sauerborn
phone +49 (0)30 / 6392 4921
fax +49 (0)30 / 6392 4972
pr@bessy.de

Photo Credits:

For providing photographs and drawings we would like to thank:

IKZ, Arbeitsgruppe Verbindungshalbleiter, Dr. Neubert, Berlin

Egmont Ehapa Verlag, Berlin, Lizenz durch Agentur Fuchs, Stuttgart

Staatliche Museen Berlin, Museum für Indische Kunst

Bernhard Schurian, Berlin

Micromotion GmbH, Mainz

Infineon Technologies AG, München

Katja Bilo, Berlin